POLITECNICO DI MILANO

School of Industrial and Information Engineering

Department of Chemistry, Materials and Chemical Engineering "Giulio Natta"

Master's Degree Thesis in Materials Engineering and Nanotechnology

NANOPARTICLE-BASED DETECTION OF METALLOPROTEINASES

Nanyang Technological University, Singapore

Supervisor: Prof. Guglielmo Lanzani

Co-supervisor: Prof. Bo Liedberg

Ludovico Aloisio, 898404

Academic Year 2019/2020

Table of Contents

List of Figures

List of Tables

List of Equations

Abstract

Matrix metalloproteinases (MMPs) have attracted considerable attention in recent years because of their involvement in numerous pathological conditions, such as cancer and AIDS. In particular, Matrilysin (MMP-7) is an indicator of salivary gland cancer and is believed to contribute to invasive growth and metastasis of colon carcinoma and numerous other human cancers. The diagnosis techniques available today are not always suitable due to the need of sophisticated, bulky instrumentation and trained personnel. There is thus a great need for easy to use, rapid, specific and sensitive assays that allow detection of MMPs at clinically relevant concentrations for diagnostics.

The aim of this project is the production of a simple, cheap and remote kit for fast detection of cancer at its earliest stages and for remote field-testing in resource limited countries. A fluorometric and a colorimetric approach are described in this thesis: both exploiting the catalytic activity that MMPs have on peptide hydrolysis.

The colorimetric assay takes advantage of the plasmonic properties of gold nanoparticles. The particles are stabilized with a synthetic polypeptide, hydrolysis of the immobilized peptide by MMP-7 decreases its size and net charge, drastically reducing the colloidal stability of the suspension: the nanoparticles aggregate extensively upon exposure to MMP-7 resulting in a distinct concentration dependent Localized Surface Plasmon Resonance (LSPR) shift, sufficiently large to be detected by naked eye.

The fluorometric assay exploits the Förster Resonance Energy Transfer (FRET): a synthetic peptide sequence, labelled with a fluorophore and a quencher is immobilized on particles. Upon MMP-7 exposure, hydrolysis of the peptide cleaves the fluorophore tagged fragment in the solution, distancing it from the quencher and resulting in emission of light by fluorescence that can be detected by naked eye under UV light. This enables a quantitative monitoring of the protease activity.

The responses are obtained at clinically relevant concentrations in buffer and show promising activity in clinical sample matrices, thus going towards an application in early diagnosis of the disease.

Sommario

Le metalloproteasi (MMPs) hanno attratto una considerevole attenzione negli ultimi anni a causa del loro ruolo in numerose patologie, come cancro e AIDS. In particolare, la matrilisina (MMP-7) è un indicatore di tumore alle ghiandole salivari e si ritiene che contribuisca alla crescita invasiva e formazione di metastasi del carcinoma del colon e numerosi altri cancri. Le tecniche di diagnosi disponibili al giorno d'oggi non sono sempre adeguate, data la necessità di macchinari ingombranti, costosi e personale addestrato. Vi è quindi grande richiesta di test rapidi per identificare la MMP-7 a concentrazioni clinicamente rilevanti.

Lo scopo di questo progetto è la produzione di un kit semplice ed economico per effettuare diagnosi precoci e per condurre test anche in paesi con risorse limitate. In questa tesi vengono descritte due strategie per l'identificazione delle MMPs, sfruttando la loro attività catalitica sull'idrolisi di peptidi.

Il primo approccio sfrutta le proprietà plasmoniche delle nanoparticelle di oro. Le particelle vengono stabilizzate con un polipeptide sintetico, l'idrolisi di questo peptide causato dall'esposizione a MMP-7 riduce la sua dimensione e carica netta, destabilizzando drasticamente la soluzione colloidale e causando l'aggregazione delle nanoparticelle. Le proprietà ottiche delle nanoparticelle cambiano a causa della risonanza plasmonica di superficie, risultando in un cambio di colore della soluzione da rosso a blu visibile ad occhio nudo.

Il secondo biosensore è fluorimetrico: sfruttando il trasferimento di energia per risonanza è possibile individuare la proteasi usando un peptide marcato con un fluoroforo e un fluorocromo. L'idrolisi del peptide, immobilizzato su nanoparticelle, causa il rilascio in soluzione del frammento contenente il fluoroforo, risultando in un distanziamento dal fluorocromo e in una emissione di luce per fluorescenza quando illuminato con luce UV.

È stato possibile individuare matrilisina a concentrazioni rilevanti clinicamente in soluzioni tampone, mostrando inoltre una sensibilità promettente in campioni di plasma, avvicinandosi quindi all'applicazione del test per la diagnosi precoce di queste patologie.

Chapter 1: Introduction

1.1 Background and Significance

Cancer is a large group of diseases involving abnormal cell growth, starting in almost any tissue or organ and potentially spreading to other parts of the body [1].

A tumour is termed malignant, and therefore cancerous, when it acquires the ability to invade and destroy normal tissues. For invasion and metastasis to occur, the tumour cell must bypass a matrix barrier which holds normal cells in place. This is permitted by producing enzymes that destroy the barrier, allowing the tumour to invade surrounding tissues and metastasize to distant organs, passing through blood vessels and lymph nodes [2].

Matrix metalloproteinases are the perfect candidates for this role: when activated, they are collectively capable of degrading all the component of the extracellular matrix (ECM) and many other proteins, influencing tumour cells growth and their invasive behaviour [3]. In fact, active MMPs are upregulated in almost all cell tumour cells, correlating their expression to different stages of tumour progression and can serve as biomarkers for an assay to achieve early diagnosis [2].

Cancer is the second leading cause of death after heart disease: in 2018, an estimated 9.6 million people have died from cancer, with the most common cancers being lung, breast, colorectal and prostate cancer, according to the data published by WHO [4]. These numbers are continuously growing, contrarily to the decreasing trend of deaths by heart disease in the recent years [5].

As reported by WHO, cancer's survivability is significantly improved by detecting cancer early and promptly starting the treatment process, also leading to less expensive therapies.

Nowadays, early detections are achieved by promptly recognising symptoms of cancers or by population screening: tests capable to detect abnormalities suggestive of a specific cancer or pre-cancer are carried out on individuals who have not developed any symptoms. Example of these are colonoscopy, mammography, pap test, breast MRI and many others. The major available methods are costly and invasive, moreover, they require sophisticated and bulky equipment, which, at the same time, need

trained personnel and are time consuming. For this reason, they are rarely available in the public sector in low-income countries [4]. Therefore, there is great need for point of care assay capable to assist in the early diagnosis of these pathologies, characterized by low cost, fast response, while being highly selective and sensitive. In the recent years, many different biomarkers were individuated for cancer diagnostics: specific antigens (such as PSA), micro-RNA (miRNA), circulatory DNA [6] and matrix metalloproteases [2]. Many approaches were developed to detect cancer biomarkers such as matrix metalloproteinases at clinically relevant concentrations, including gel electrophoresis [7, 8], enzyme-linked immunosorbent assay (ELISA) [9], mass-spectroscopy and other optical methods [10], but these often require sophisticated instrumentation, trained personnel or tedious standard procedures. As a consequence, most of these diagnostic assays are not yet suitable for countries that are resource constrained, and with few trained technicians.

Point of care tests (POCT) are rapid detections assay that require small sample volumes and limited resources. These tests show good correlation with laboratory experiments and are therefore highly reliable [11]. The most common POCT are paper based: they are cost effective and easy to use, enabling diagnosis in resource limited settings. However, paper based assay sensitivity greatly depends on the properties of the materials involved in their manufacturing and on the complexity of the clinical samples employed: they often show very low sensitivity in clinical sample matrices such as saliva, blood or urine, and therefore require expensive, time consuming extraction or sample clean up before reaching a sufficient sensitivity, which has to be carried out by trained personnel.

Colorimetric assays have attracted significant attention due to their quick visual response that does not require sophisticated instrumentation to be detected, usually allowing detection by naked eye [12]. In recent years, many materials have been developed for transformation of the detection events into colour changes, these include gold nanoparticles [13], fluorophores [14], dyes [15], quantum dots, magnetic nanoparticles, carbon nanotubes, and conjugated polymers [16] and many others. Gold nanoparticles are particularly interesting for their plasmonic properties, such as Localized Surface Plasmon Resonance (LSPR): as described in Chapter 2 they have a particularly strong absorption band in the visible range, which gives colloidal solution of small gold nanoparticles a strong ruby red coloration, which slightly varies

when exposed to different surroundings. Interestingly, the aggregation of AuNPs can induce a LSPR shift, resulting in a change in colour from red to blue, easily visible by naked eye. For these reasons, AuNPs have been widely used for colorimetric biosensing.

Another interesting class of materials used in biosensing is fluorophore molecules, especially in the FRET (Förster, or Fluorescence, Resonance Energy Transfer) setup. FRET biosensors include a combination fluorophore (donor) and a quencher or fluorophore (acceptor), when the first gets excited, its energy is transferred to the second by a non-radiative dipole-dipole interaction, resulting in a dispersion of the excited state by heat or by light emission at the characteristic emission wavelength of the acceptor. Once the two molecules are distanced, the excitation of the donor molecules results in the emission of light at its the emission wavelength, without interaction with the acceptor. Thus, if the exposure to a biomarker (such as MMPs) leads to this distancing, it's concentration can easily be detected by a fluorescence signal [17, 18].

The previously described interaction between MMPs and proteins can be exploited for biosensing. Matrix metalloproteinases can be used as biomarkers since they also cleave peptide sequences in specific sites by proteolysis [19]. Peptides are sequences of amino acids that can be synthesized by the condensation reaction of the carboxyl group and amino group of two amino acids, therefore, synthetic peptides can be produced with specific recognition sites for different MMPs [20].

This thesis focuses on the development of a colorimetric assay for matrix metalloproteinases, exploiting their interaction with peptides, combined with the optical properties of nanoparticles and fluorophores.

1.2   Hypothesis

A point of care assay utilizing peptide functionalized nanoparticles can be developed for the visual detection of Matrilysin (MMP-7) activity at clinically relevant concentrations, minimizing sample handling and preparation. Peptides can be utilized for selective detection of matrix metalloproteinases. They can be combined with particles or other reporter molecules to give colorimetric response when cleaved.

Gold nanoparticles optical properties have been extensively used, both for POC tests [21] and food quality tests [22]. AuNPs can effectively translate the peptide interaction with proteases to an optical signal through an induced aggregation, causing a concentration dependent localized surface plasmon resonance (LSPR) shift [23]: the nanoparticles can be tailored with peptides bearing negative particles, rendering the colloidal solution highly stable, once these come in contact with active matrix metalloproteinases, the molecules cleavage reduces the charges kept on the particle surface, inducing aggregation and a colour change that can be clearly detected by naked eye. Moreover, the metal nanoparticles' composition can be varied in order to obtain a colour change more easily detectable by human eye.

Peptides can also be labelled with other reporter molecules such as dyes or fluorophores. FRET (Förster resonance energy transfer) peptides, including a fluorophore and a quencher, can be exploited to produce an alternative functional assay. In this case, distancing between the acceptor and donor molecules is induced by the peptide cleavage, leading to the interruption of the energy transfer by dipole-dipole interaction between the two and resulting in fluorescence emission when exposed to UV light [24].

1.3   Objective

Cancerous tumour cells produce matrix metalloproteinases to destroy the extracellular matrix that keeps normal cells confined. When active, these proteases contribute to cell growth and invasion to other tissues, also by entering the bloodstream and reaching organs in other parts of the body. For this reason, active MMPs are significantly upregulated in the case of cancerous cells [2] and can be used as biomarkers for an early diagnosis.

The overall objective of this thesis is to produce a simple and easy to use functional assay, capable of assisting in the early detection of cancer, through the quantitative detection of active MMP-7 in saliva or plasma, also giving an indication of the cancer stage depending on their concentration [3].

1.4   Scope

The final scope of this project it to finally develop a functional assay capable of detecting the activity of MMPs, associated to pathologies like cancer, AIDS and inflammation. This assay should allow to carry the detection with minimal sample handling and in short times, without the need for particularly trained personnel or sophisticated instruments. This is essential for early diagnosis of cancers and to increase survivability in resource-limited countries.

Chapter 2: Literature Review

2.1   Cancer

Cancer, or malignant tumour, is a large group of diseases that can affect any part of the body. It involves rapid creation of abnormal cells which can invade surrounding tissues or metastasize in other parts of the body, surviving even after being detached from the extracellular matrix (ECM) [25]. Metastasis are the major cause of death from cancer, accounting for about 90% of them [26].

Cancer burden in terms of incidence and death is continuously increasing: an estimated 10 million new cases and 6 million deaths were estimated globally in 2000 [27], which have increased to an estimated 18.1 million new cases and 9.6 million deaths in 2018 [4] and are estimated to increase to 29.5 million by 2040 [28]. Nowadays, 1 over 6 deaths in the world is due to cancer. Most of these deaths (approximately 70%) occur in resource-limited countries, due to absence of early detection and of access to treatments.

Only 5–10% of all cancer cases can be attributed to genetics, whereas the remaining 90–95% are caused by environmental (sun exposure, pollutants, infections) and lifestyle (alcohol, tobacco, diet, physical inactivity) aspects [5]. Smoking, alcohol use, overweight and obesity were the most important causes of cancer [29]. This is confirmed by Figure 2.1, which shows that areas where these lifestyles are more common, like Europe and North America, have the highest number of cancer cases per inhabitant.
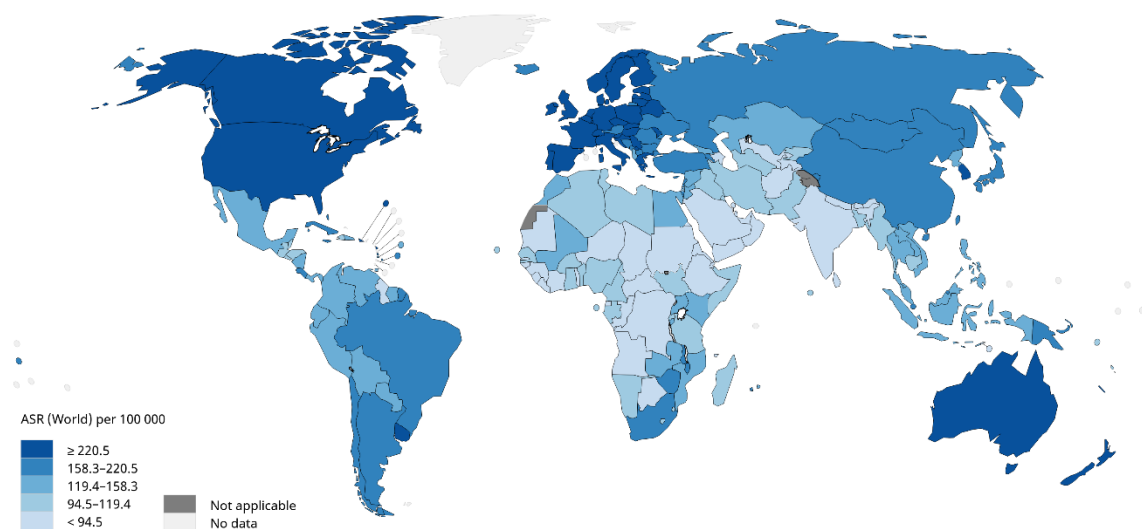
Figure 2.1: Estimated age-standardized incidence rates (World) in 2018, all cancers, both sexes, ages 0-74. [30]

However, death rates by cancer show a different situation (Figure 2.2): in the developed world, health care can provide everyone appropriate and timely care to patients, reducing mortality from cancer, whereas low to middle income countries usually do not have public and easy access to these treatments. Therefore, the cancer mortality rates increase drastically in resource-limited countries with respect to the incidence rates, with the main causes of death by cancer being smoking, alcohol use, and low fruit and vegetable intake. Moreover, infections due to papilloma virus is a leading risk factor for cervical cancer for cervical cancer for women in these countries [29].
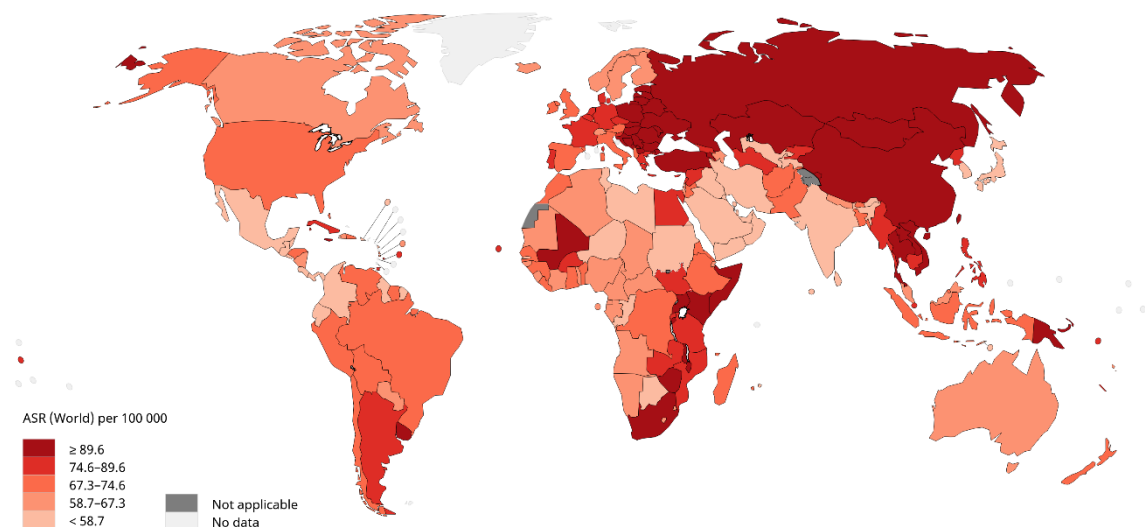
Figure 2.2: Estimated age-standardized mortality rates (World) in 2018, all cancers, both sexes, ages 0-74. [30]

In conclusion, more than one in every three of the 7 million deaths from cancer worldwide is caused by potentially modifiable risk factors, with smoking and alcohol use having particularly important roles in both high-income and low-and-middle-income countries. The importance of early diagnosis and adequate treatments is highlighted by the difference in incidence and deaths rates between developed countries and resource-limited ones, there is therefore great need for cheap, easy to use, selective and sensitive point of care tests capable of detecting cancer even in absence of sophisticated and expensive instrumentation.

2.2 Biomarkers

Biomarkers are molecules indicating a physiologic state that change during a disease process [31]. They are therefore considered useful tools in providing early detections of diseases and their progression, providing at the same time ease of detection [32]. Potential biomarkers are identified based on the biology of the tumours and its surrounding environment [33].

A series of potential biomarkers, which can be found in different samples, has been identified in the last years, as reported in Figure 2.3:
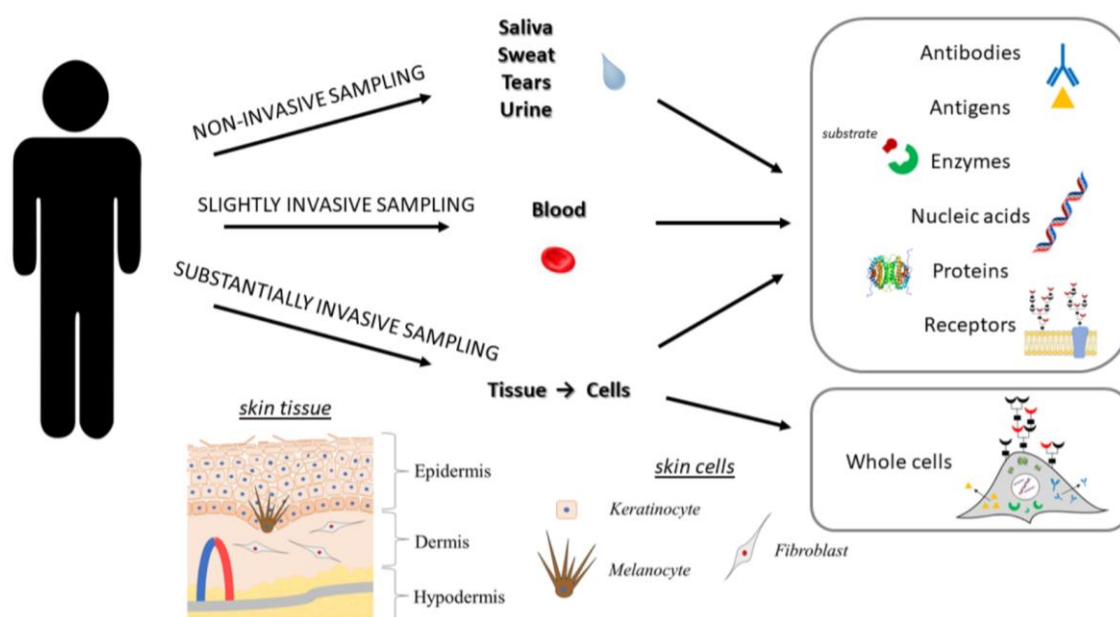
Figure 2.3: Schematic illustration of various biomarkers as targets for cancer detection with the biosensors methodology. [34]

As already mentioned, matrix metalloproteinases, which fall into the enzyme category in Figure 2.3, are produced by tumour cells and contribute to their growth and invasion. For this reason, they are upregulated in many cancerous cells, blood and serums and can serve as biomarkers for cancer detection and tumour stage determination [35].

2.2.1 Matrix Metalloproteinases

Matrix metalloproteinases are a group of 24 proteases [3] which have attracted considerable attention in recent years because of their large influence on cell behaviour: they are typically found in low levels,

but these grow in case of different pathological conditions, such as, inflammation, AIDS and cancer [36, 37, 38]

The MMPs are capable of digesting various components of the extracellular matrix and many other proteins, influencing cell growth and permitting invasion to the surrounding tissues, entry and exit from blood vessels and metastasize in distant organs.

A tumour is termed malignant when it acquires the ability to invade and destroy normal tissues. For invasion and metastasis to occur, the tumour cell must bypass the basement membrane. The basement membrane contains an extracellular matrix (ECM) composed of structural components such as collagens, proteoglycans and glycoproteins, [2, 39] which holds normal cells in place and must be degraded in order for tissues to change their form or function. Matrix metalloproteinases are particularly important for matrix degradation, in fact, excess matrix degradation is an indicator of cancer and an important contributor for the process of tumour progression [40]. For this reason, MMP levels affect the behaviour of tumour cells and their ability to metastasize, correlating their expression to different stages of tumour progression [3].

During invasion, the tumour cell penetrates the basement membranes around the cell, then, cleaving other non-matrix proteins, reaches blood vasculature, which are also surrounded by the basement membrane and enters the blood stream, or the lymphatic vessels (Figure 2.4). The process of entering the blood stream is named intravasation, while extravasation is the reverse process: the tumour cell crosses through the basement membrane once again and leaves the blood circulation, if it is able to survive in the new environment, metastases are formed in a distant site [2].
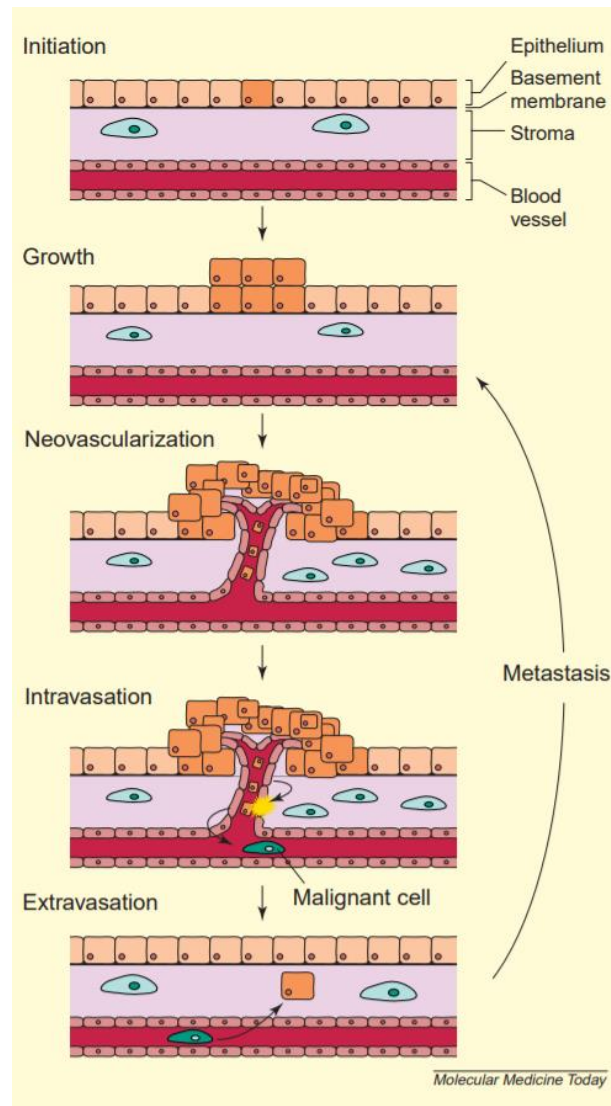
Figure 2.4: *Stages of tumour progression. Initiation occurs when a single cell becomes modified to exhibit a growth advantage over the surrounding tissue, which, at some point, requires neovascularization to supply nutrients for further growth. As the tumour becomes malignant, it acquires the ability to invade the surrounding normal tissue. Intravasation occurs when tumour cells cross the basement membrane and enter the circulation. Following the tumour cells' survival in the circulation, extravasation occurs when the tumour cells leave the circulation and penetrate the host tissue. Metastasis occurs if the tumour cells can establish and grow at this secondary site. [2]*

During the process of tumour progression, there are many ways in which cell behaviour is affected by matrix metalloproteinases, through matrix and non-matrix protein cleavage.

Cell proliferation is often regulated by the interaction of a growth-suppressive factor with its cell-surface receptor. Proteolysis of matrix proteins associated to this factor results in the solubilization of the latter, enhancing cell growth [41].

MMPs can also play a role in cell migration. This process requires coordinated regulation of cell-cell attachments, cell-matrix attachments and matrix remodelling: matrix metalloproteases affect cell-matrix and cell-cell adhesion by removing sites of adhesion or exposing them by cleavage of substrates. Moreover, cell migration is often initiated as a response to a chemotactic stimulus, which can be generated by MMPs in various systems [42].

In conclusion, it is interesting to note that these proteases show selectivity [43]: an individual MMP is able to degrade a limited subset of matrix proteins, therefore, matrix metalloproteinases play a complex role in tumour progression: the latter is the result of the combination of multiple MMPs, each playing a specific role [2].

MMPs general domain structure is shown below (Figure 2.5). The molecule can be divided into different domains, given their different roles.
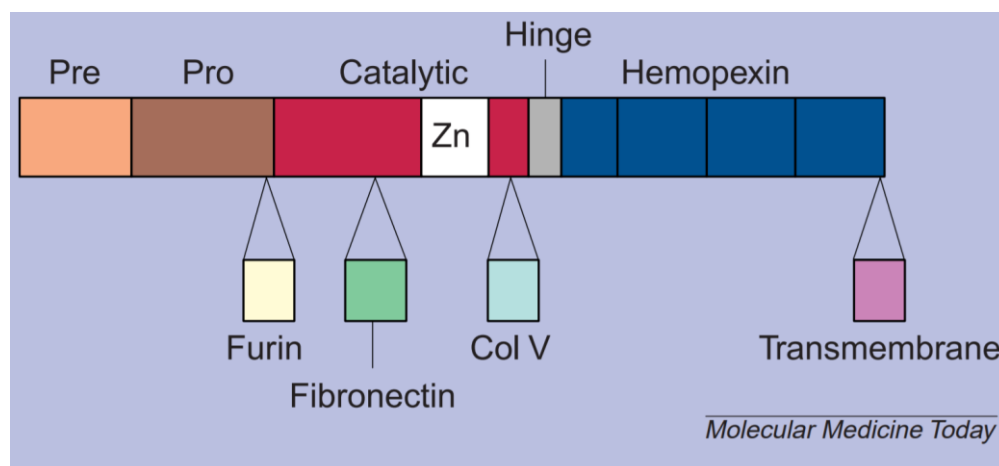
Figure 2.5: *MMP domain structures. There are three domain structures common to all MMPs: a pre-domain, which targets the MMP for extracellular secretion; a pro-domain, which maintains the MMP in an inactive state and whose removal is required for activation of the enzyme; and a catalytic domain, which contains the enzymatic core. Most MMPs also contain a hemopexin domain, which assists in substrate and inhibitor binding. Other domain structures provide regions for: alternative cleavage for activation of the MMP; transmembrane localization; or substrate recognition. [2]*

- Pre-domain: targets the protease for extracellular secretion

- Pro-domain: keeps the matrix metalloproteinase inactive. Once this domain gets cleaved, the MMP will be active

- Catalytic domain: has the protein-degrading ability and includes a site for the metal ion necessary for its activity. This domain is therefore responsible for proteolysis, both on proteins and peptides

- Other domain structures: offer the possibility for substrate recognition, transmembrane localization and alternative cleavage for MMP activation

Besides the important role in tumour growth and invasion, matrix metalloproteinases can also contribute to wound repair [44], cell death [45] and intracellular communication, especially during inflammatory responses [46].

2.2.2   Matrilysin

Matrix metalloproteinases are classified on the basis of their additional protein domains that contribute to their individual characteristics. The active form of Matrilysin for example (MMP-7) only contains the catalytic domain, lacking every other protein domain and both pre-domain and pro-domain since it has been activated.

MMPs expression show a large degree of heterogeneity across different cancer types. Figure 2.6 reports the differential gene expressions of 24 different matrix metalloproteinases found in different tumour tissues, with respect to control tissues. Differential gene expression is directly related to protease production since it is the process converting DNA instructions into a final functional product [47].

Gene	BLCA	BRCA	COAD	ESCA	HNSC	KICH	KIRC	KIRP	LIHC	LUAD	LUSC	PRAD	STAD	THCA	UCEC
MMP1	6.97	30.82	12.82	29.05	43.82	0.30	1.67	0.43	3.07	25.20	36.41	0.72	9.53	4.97	14.15
MMP8	1.72	1.45	3.51	3.10	2.63	0.89	1.20	1.35	0.74	1.84	1.96	1.04	3.14	1.33	1.47
MMP13	7.88	55.31	8.79	27.54	53.93	2.20	1.89	1.13	1.38	29.46	25.82	0.74	5.73	4.07	1.98
MMP7	3.19	0.44	141.85	14.07	4.14	0.07	0.26	2.48	0.31	2.13	1.65	0.96	13.11	5.01	1.84
MMP26	1.02	1.06	1.03	1.00	1.01	4.36	1.06	1.07	1.01	1.02	1.02	6.22	1.05	1.03	0.13
MMP12	2.19	2.29	2.36	38.96	15.58	1.76	1.32	1.08	4.24	17.07	52.46	1.55	8.93	1.83	19.18
MMP3	0.69	4.83	23.03	28.61	15.55	1.10	1.00	0.99	1.31	5.83	24.65	0.95	13.69	1.58	3.36
MMP10	2.21	5.72	6.17	20.48	11.38	1.04	1.17	0.90	2.15	5.13	34.32	4.24	6.21	2.13	5.10
MMP11	14.93	56.55	13.39	23.63	25.64	1.32	4.71	5.79	9.55	35.62	43.04	2.06	12.47	6.67	1.93
MMP2	0.34	0.78	0.89	1.08	2.58	0.70	1.07	0.44	0.80	1.06	0.77	0.60	1.11	0.95	0.30
MMP9	3.59	6.88	2.01	10.01	17.19	3.24	9.90	3.77	2.88	4.80	4.19	3.98	5.83	1.72	7.92
MMP20	1.11	0.73	1.35	1.46	1.25	1.47	0.72	0.49	1.16	1.09	1.82	1.00	1.06	1.01	1.17
MMP14	1.73	2.00	2.11	2.96	2.74	0.77	2.66	2.84	1.86	1.88	2.60	0.55	1.87	1.66	0.69
MMP15	1.89	1.17	0.61	0.74	1.30	2.28	0.80	1.89	0.89	1.78	0.63	1.14	1.42	0.69	3.05
MMP16	0.29	0.71	0.87	0.89	2.24	1.72	4.94	0.88	0.84	1.67	1.04	0.42	1.20	4.57	0.27
MMP17	0.74	1.43	0.96	1.85	2.36	0.70	2.09	1.60	1.25	4.40	2.02	0.80	0.92	0.80	0.44
MMP24	1.04	0.74	0.73	0.69	0.72	3.15	1.00	1.67	1.16	0.68	0.25	1.09	0.93	1.04	1.04
MMP25	1.04	1.56	0.33	1.80	1.60	0.88	3.61	1.74	0.78	0.58	0.39	1.23	1.12	0.81	1.37
MMP19	0.79	0.55	1.12	0.66	1.94	0.50	1.73	1.68	0.88	0.37	0.26	0.90	1.26	0.64	0.45
MMP21	0.89	0.85	0.97	0.61	0.97	0.61	1.24	0.85	1.30	0.89	0.83	0.93	0.82	0.67	0.78
MMP23A	0.61	0.93	0.96	0.88	1.20	0.78	1.10	0.78	0.99	0.83	0.42	0.92	1.30	1.10	0.74
MMP23B	0.19	0.59	0.53	0.64	1.47	0.18	0.70	0.54	0.52	0.51	0.27	0.78	0.73	1.04	0.45
MMP27	0.28	0.18	0.27	0.51	0.27	1.01	1.05	0.96	1.03	0.93	1.26	0.98	0.52	0.85	0.56
MMP28	0.57	0.25	0.09	0.60	1.91	0.14	0.86	0.87	1.29	0.16	0.08	0.53	0.30	0.70	0.10

Fold Change:
- > 4
- 2 - 4
- 0.5 - 2
- 0.5 - 0.25
- < 0.25
- pval > 0.05

MMP Subtype
- Collagenases
- Matrilysins
- Metalloelastase
- Stromelysins
- Gelatinases
- Enamelysin
- Membrane-Type
- Other

Figure 2.6: *Differential gene expression of 24 matrix metalloproteinases (MMPs) in 15 different cancer types. Fold change and p-values shown were obtained through comparison of unmatched control tissue (N between 11 and 114) to tumour tissue (N between 66 and 1097). Fold change was calculated as the median expression of a gene in tumour divided by the median gene expression in adjacent normal tissue. [48]*

Matrilysin (MMP-7) have high gene expression fold change in case of Colon adenocarcinoma (COAD), Esophageal Cancer (ESCA), Head and Neck Cancer (HNSC), Stomach Adenocarcinoma (STAD) and Thyroid Cancer (THCA), and it is therefore a perfect biomarker candidate for these types of cancer, especially for colon cancer. In fact, MMP-7 is closely associated with some prime factors in tumour genesis of colon cancer [48] and is believed to contribute to invasive growth and metastasis of colon carcinoma and numerous other human cancers [49, 50, 51].

2.3   Current Status of Analytical Techniques

The detection of matrix metalloproteinases has been studied with several analytical methods, such as enzyme immunoassays, western blotting, zymography, mass spectrometry and other optical methods [10]. These techniques are capable of detecting MMPs and their activity, however, they generally require sophisticated instrumentations, long incubation times and trained personnel.

2.3.1   Enzyme Immunoassays

Enzyme-linked immunosorbent assay (ELISA) is a plate-based assay technique designed for detecting and quantifying various types of biomarkers, including MMPs. In ELISA, an antigen must be immobilized

to a solid surface and then complexed with an antibody that is linked to an enzyme. Detection is accomplished by assessing the conjugated enzyme activity via incubation with a substrate to produce a measurable product. Different strategies were developed for the detection step:
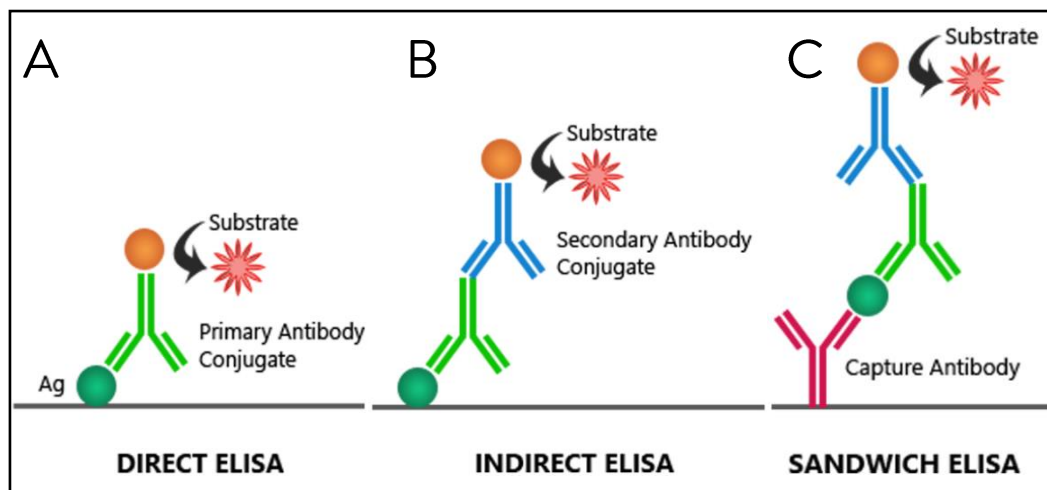
Figure 2.7: Schematic representation of ELISA detection methods: (A) direct ELISA, (B) indirect ELISA, (C) sandwich ELISA. [52]

- Direct ELISA, Figure 2.7 (A): the antigen immobilized on the surface is detected by an antibody that is directly linked to an enzyme.

- Indirect ELISA, Figure 2.7 (B): the detection of the coated antigen is detected in two stages. An unlabelled primary antibody, specific for the antigen, is applied, then a secondary antibody, which is labelled with an enzyme, is added and bound to the first antibody.

- Sandwich ELISA, Figure 2.7 (C): first "capture" antibody is coated to the surface, then, the sample solution is added, and the antigen is immobilized on the antibody layer. A second "detection" antibody is added in order to measure the concentration of the sample.

- Competitive ELISA: The sample and enzyme conjugated recombinant protein (the competing molecule) are added to the wells coated with a capture antibody. The amount of enzyme conjugated molecule in each well is constant, therefore the concentration of sample molecule will determine the binding ratio of enzyme conjugated molecule vs. sample molecule. After an incubation period, any unbound antibody is washed off. The enzyme substrate is added to each wall and an amount of yellow precipitate (maximum absorbance at 450nm) is created

proportionally to the amount of enzyme in the well. The absorbance is then studied to determine
the amount of sample molecule present in the wells.

In general, ELISA does not offer the possibility to distinguish between active and latent forms of MMPs
[53]. Moreover, methods like indirect ELISA may be sensitive to cross-reactivity with the secondary
antibody, resulting in nonspecific signal. Sandwich or competitive ELISA offer more sensitivity [54], but
the multiple steps involved when carried out makes them time consuming assays.

2.3.2   Western Blotting

Western blotting goes a step forward with respect to ELISA: the sample first undergoes electrophoresis,
separating the molecules by size, then, the separated molecules are transferred to a solid support,
maintaining their position. The coated support is then exposed to a primary antibody and a secondary
antibody, similarly to what is done in indirect ELISA [55].

This technique offers the possibility of separating molecules by size, allowing to distinguish false positives
from specific signals. However, this technique is still not able to distinguish between active and inactive
MMPs, since no substrate cleavage is involved for the analysed protease. Moreover, this assaying is
characterized by multiple steps with varying incubation times, that have to be performed by trained
personnel.

2.3.3   Zymography

Similarly to Western blotting, zymography exploits electrophoresis to distinguish matrix
metalloproteinases by their molecular weight. The MMPs are separated by electrophoresis while inactive
(in the presence of sodium dodecyl sulphate, SDS) in a polyacrylamide gel that contains a specific
substrate for the analysed MMP. After electrophoresis, the gel is washed to remove SDS, following which
the MMPs partially recovers its activity. The gel is blue, therefore the MMPs are visible as clear bands
against the blue substrate in the background and can be measured by densitometry [56].

Zymography can be carried out both in situ or on substrate, allowing detection both in serums and on
tissues. This technique is capable of distinguishing active MMPs from ProMMPs (inactive since Pro-

domain is still present), even if both get activated, because of their different molecular weight. However, it is not able to distinguish between matrix metalloproteases and MMPs complexed with their inhibitor (TIMP-MMP complexes) which are inactive in the human body but gets separated by SDS and therefore activated, once the latter is removed [57]. Other main limitations of these technique are the long incubation times and the possible interferences of other MMPs. Moreover, the activity of some proteases is much more difficult to detect in clinical samples matrices like plasma [58].

2.3.4 Mass Spectrometry

Mass spectrometry permits identification of MMPs based on their activity: using site−directed probes to report on the functional state of enzymes in complex biological systems. Activity-based protein profiling (ABPP) probes have been shown to selectively label active enzymes but not their inactive precursor or inhibitor complexes [59]. The specific digestion of proteins by proteases releases digested products that can be then analysed by liquid chromatography mass spectroscopy (LC-MS) [60, 61].

Also MALDI (Matrix-Assisted Laser Desorption/Ionization)-TOF (Time of Flight) Mass Spectrometry can be used to detect the activity of MMPs [62]. A peptide including a recognition site for the studied protease is deposited on a microplate. The peptide is then exposed to the MMP and the plate analysed through MALDI-TOF MS. This technique evaporates the solution and ionizes its molecules, which are driven towards a detector by an electric field. The molecular weight of the ionized species is calculated considering the time of flight needed for the molecules to reach the detector after desorption from the surface. In this way, it is possible to identify the peptide and also the two peptide fragments (all with known MW) obtained after hydrolysis by the enzyme, confirming the molecules cleavage and the protease activity.

These techniques can be very precise but are very time consuming and require sophisticated and expensive instrumentation, that must be run by trained personnel in laboratories.

2.3.5 Other Optical Methods

Other optical methods have been used to detect matrix metalloproteinases.

Near-IR optical imaging of MMPs was carried out directly on tumour tissue, using an optical contrast agent that was highly activatable by the protease. [63] However, since this technique is carried out directly on tumour tissue, it is invasive and not always practicable.

A combination of capillary gel electrophoresis (CGE) and laser-induced fluorescence (LIF) was used to measure MMPs activity [64]. Employing a dynamic fluorescent labelling, it is possible to measure fragments produced by cleavage by a specific matrix metalloproteinase (in this case collagen fragments, cleaved by collagenase), which are separated by CGE and emit light by fluorescence. Also in this case, the technique requires laboratory instrumentation and its sensitivity can be significantly reduced in clinical sample matrices.

2.4 Introduction to Point of Care Diagnostics

Point of Care (POC) diagnostics can play a key role in healthcare for assessing a person's condition. Nowadays, people in the developed world have access to health care capable of providing appropriate and timely care to patients. However, in developing countries, laboratories are not well equipped, lacking essential equipment, consumables, trained staff, water supply and power supply. This majorly affects the diagnostics in low resource settings. For these reasons, Point of Care (POC) can be an alternative to laboratory procedures to make an initial assessment and to monitor a patient health remotely [65]. POC devices are usually cheap, fast, portable and require small sample volume, making them a perfect fit as a diagnosis tool for resource-limited areas. These devices find a role also in the developed world, where they are used for tests that have become common nowadays, such as pregnancy tests [66] or HIV tests [67]. They can be beneficial for emergency responses and to allow patients to be involved in their own disease management, as happens with diabetes monitoring through glycaemic control [68].

According to the World Health Organization (WHO), an idea POC diagnostic device should follow "ASSURED": Affordable, Sensitive, Specific, User-friendly, Rapid and robust, Equipment-free, Derivable to the end-user.

The ideal structure of a POC device is shown in Figure 2.8.
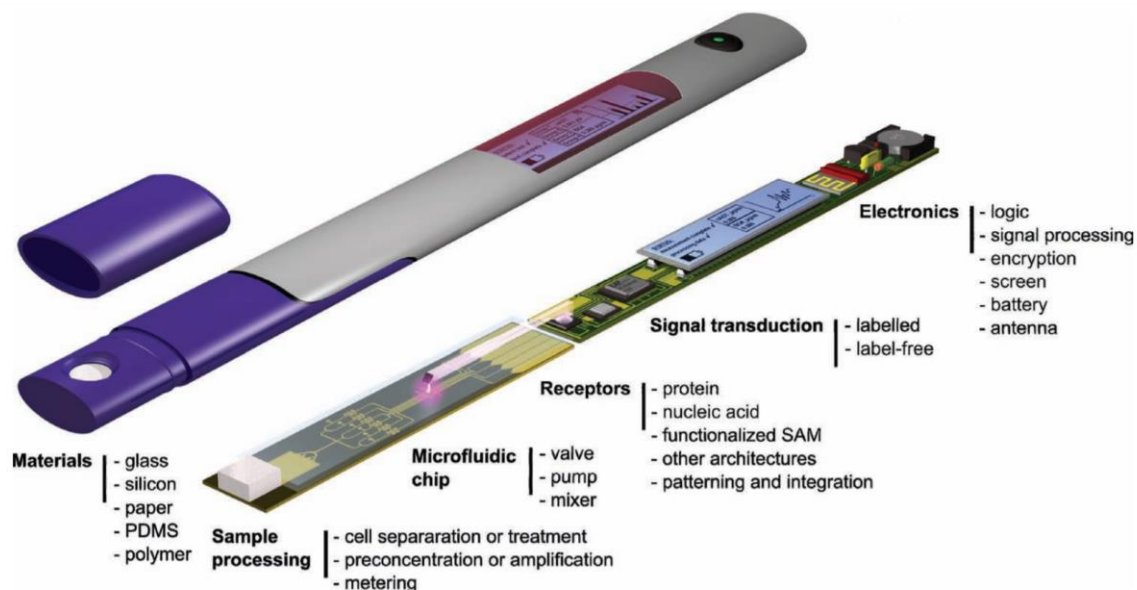
Figure 2.8: The ideal POC diagnostic device. [69]

Figure 2.8 represent a Chip based device, which is usually manufactured with polymers, silicon or glass; the sample is pushed through the device by a pump and a screen is needed for reporting the outcome of the analysis. In recent years, Paper-based devices are getting more attention, since they are cheaper, driven by capillary forces and allow visual detection, without the need of a screen or battery [70].

Paper based assays are widely used for their versatility, sensitivity, abundance, biodegradability, hydrophilicity, and biocompatibility. Paper-based POC tests are classified into different types: dipstick assay, lateral flow assay (LFA), vertical flow assay (VFA) and microfluidic paper-based analytical device (μPAD), each with determined characteristics [70]. The mechanism of detection and the detection limits depend on the target analytes, materials used, fabrication protocols and the detection labels used. They can be quantitative, semi-quantitative and qualitative, depending on the assay techniques. The ideal Paper-based POC test (in this case a lateral flow assay) is represented in Figure 2.9.
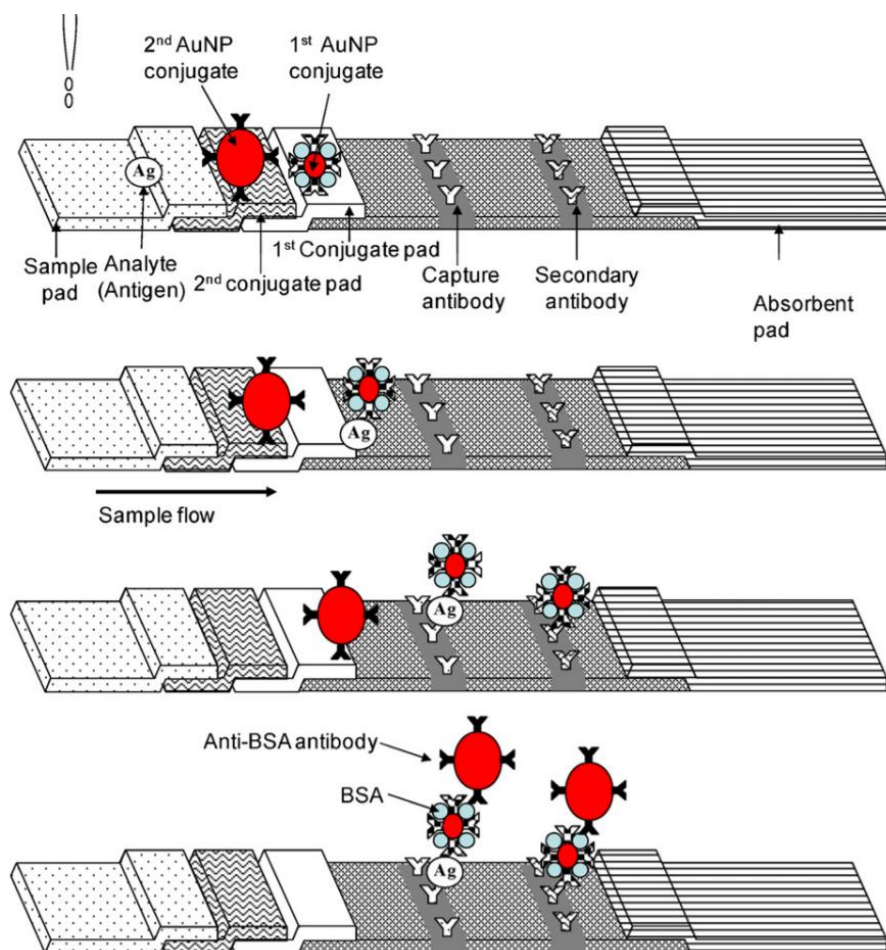
Figure 2.9: *Schematic illustration of a dual AuNP conjugate based LFA method developed in this study. AuNP and LFA are abbreviates of gold nanoparticle and lateral flow assay, respectively [71].*

As reported above, LFA Paper-based assays are made by different membranes, whose composition and pores dimension can be varied to play different roles and tune the assay's properties.

2.5 Biosensor/Detection

A biosensor is a sensor designed to selectively detect a molecule, or a class of molecules, by means of a biochemical/biological interaction. The working principle of a biosensor involves 3 main steps: recognition, transduction and signal processing/presentation (Figure 2.10). Ideally, a biosensor should be highly sensitive, highly specific and highly selective, as well as give a response in a short time and being easy to operate.
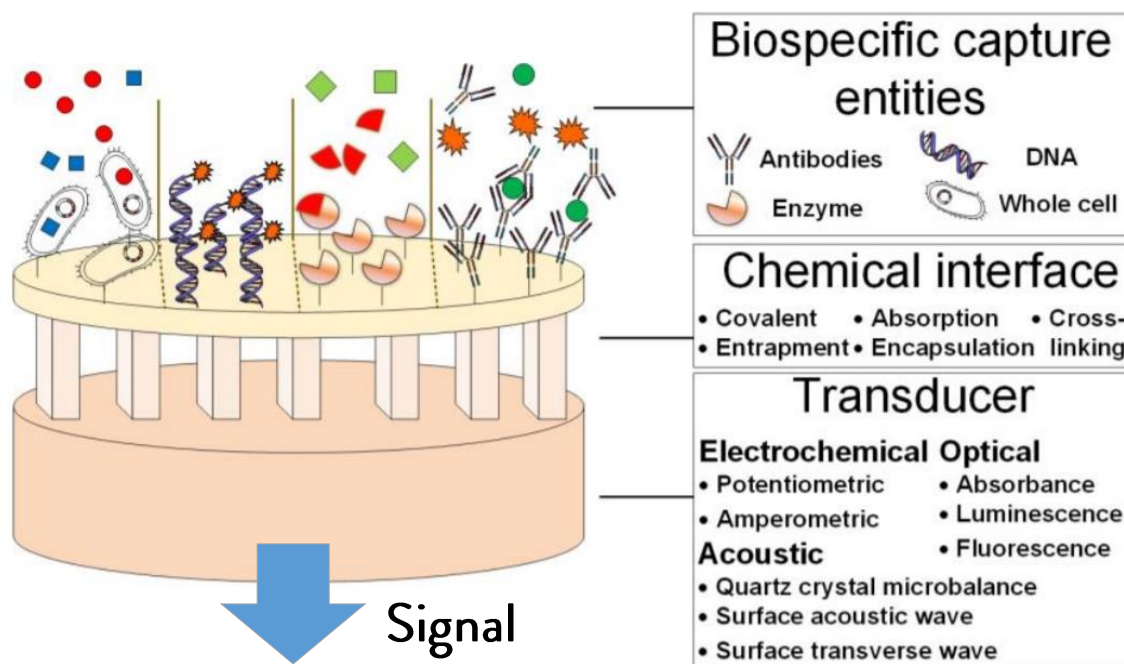
Figure 2.10: Schematic representation of a biosensor. *[72]* (modified)

Biosensors can be classified according to the transduction principle used: it can be acoustic, calorimetric, electrical or optical. Colorimetric biosensors have attracted significant attention for their ease of use and for their quick visual response, allowing signal detection without instrumentation (as suggested by "ASSURED", WHO).

2.5.1   Colorimetric Sensor

Colorimetric sensors are based on the change of colour due to the chemical or biochemical interactions between the target analyte and the colorimetric probes or reporter molecules. The concentration of the analyte molecule is determined with the aid of these probes [73]. Colorimetric sensors have proven particularly interesting for their cost effectiveness, ease of use and majorly because they usually do not require advanced instrumentation to operate. In fact, some colorimetric biosensors are designed to be visualised with naked eye. Many different colorimetric probes have been used as colorimetric reporters, such as conjugated polymers, enzymes, nanoparticles, fluorophores.

2.5.1.1   Polymer Based Detection

Conjugated polymers (CPs) are an interesting class of organic macromolecules: they are characterized by an alternation of single and double bonds, which grants them unique electrical and optical properties due to the delocalization of π electrons. According to their backbone structure, they can be classified in different categories (Figure 2.11).
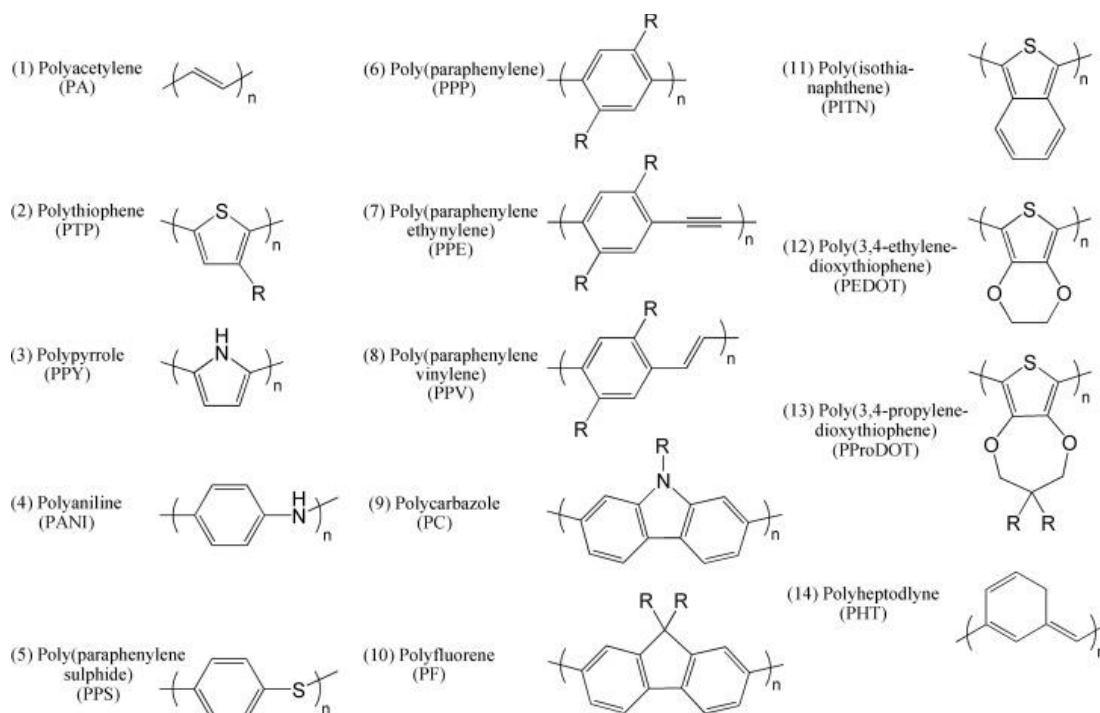
Figure 2.11: A selection of CPs that are frequently used for biosensor and bioassay applications. [74]

Because of their unique properties, CPs have many applications in electronics [75], energy conversion [76], sensing and biosensing [74]. The properties of conjugated polymers vary with temperature, pH, electric field and interaction with other molecules, forming supramolecular structures [74]. For biosensing, it is interesting to note that optical changes in CPs are driven by electrostatic and hydrophobic interactions with other molecules: these bindings affect the conformation and packing characteristics of the entire polymer backbone, resulting in an amplification or quenching of fluorescence [77].

The electrostatic interaction between polymers' side groups and other molecules allowed to detect stranded DNA [78], microbial particles [79], proteins [80] and many other types of biomarkers.

2.5.1.2   Enzyme Based Detection

Enzymes are highly selective proteins capable of accelerating chemical reactions with their catalytic functions. Enzyme-based biosensors are based on biological recognition: the enzyme must be available to catalyse a specific biochemical reaction and remain stable under the biosensors' operating conditions [81].

The most commonly enzyme-based biosensors are used for glucose detection, using glucose oxidase (GOx) as enzyme: glucose undergoes oxidation catalysed by glucose oxidase, producing hydrogen peroxide (H_2O_2) as by-product, through the following reaction (Figure 2.12).
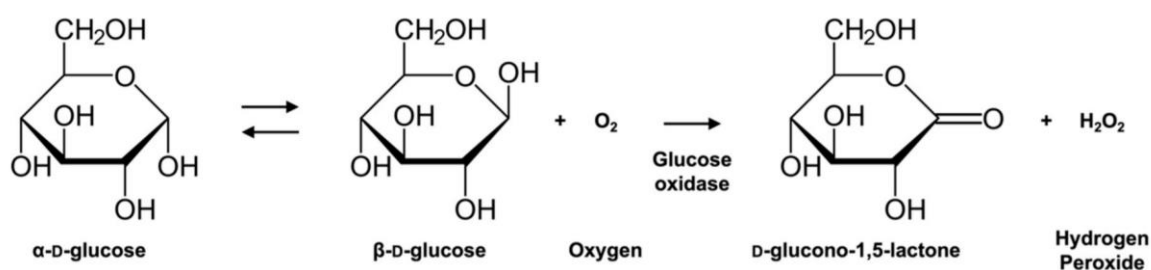
Figure 2.12: Reaction scheme of glucose oxidation catalysed by glucose oxidase. [82]

After this reaction, hydrogen peroxide then interacts with another compound, turning it into a differently coloured product. For example, titanium oxysulfate was used and turns yellow after being exposed to H_2O_2, highlighting the presence of glucose in the sample [83]. Various other assays have been developed, using oxidases and dehydrogenases as enzymes [81].

All these techniques have a major drawback: enzymes show a lower stability at room temperature, resulting in a reduction in their activity and therefore in the sensor's sensitivity.

2.5.1.3   Nanoparticle Based Detection

Metallic nanoparticles possess unique optical, electronic, chemical, and magnetic properties that largely differ from those of individual atoms or bulk material. In the biosensing field, gold, silver, and copper nanoparticles received considerable attention due to the characteristic colour that their colloidal solutions show. Spherical gold nanoparticles for example have an optical absorption at 520-560 nm

(varies with size) due to surface plasmon resonance [84]. The properties that metals show at wavelengths in the visible range are described by their complex, wavelength dependent dielectric constant [85]:

$$\varepsilon(\omega) = \varepsilon'(\omega) - i\varepsilon''(\omega)$$

Equation 2-1: Complex dielectric constant (permittivity), dependent on the wavelength of the incident light. ε': real part of the permittivity. ε": imaginary part of the permittivity.

Therefore, a complex refractive index can be defined, as a function of the refractive index (n) and of the absorption coefficient (κ):

$$\tilde{n} = \sqrt{\varepsilon} = n + i\kappa$$

Equation 2-2: Complex refractive index, calculated as square root of the dielectric constant. n: refractive index. κ: extinction coefficient.

This leads to different behaviours corresponding to different wavelengths, possibly leading to a negative dielectric constant: depending on the frequency of the incident light, the latter can be mainly transmitted, reflected, or absorbed. The variation of these two terms with respect to the light's frequency is represented in Figure 2.13.
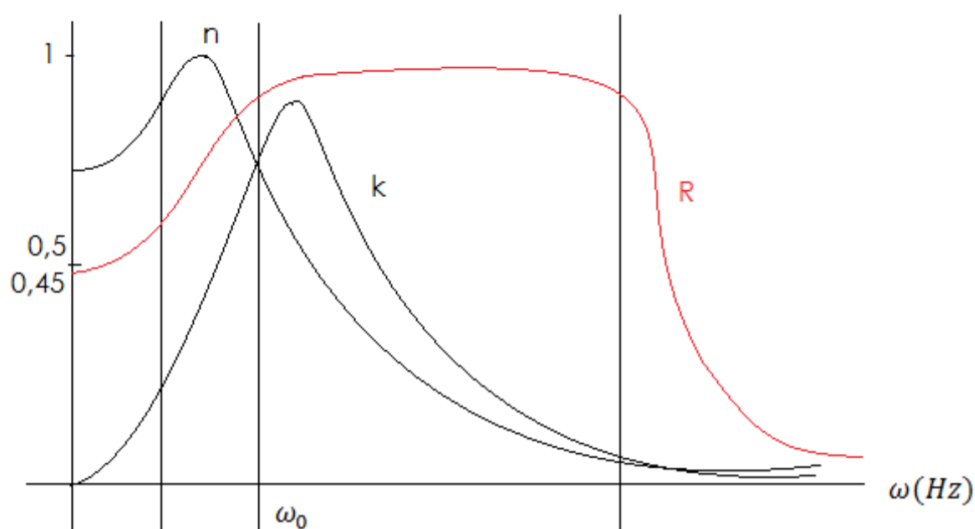
Figure 2.13: Complex refractive index components with respect to frequency of incident EM radiation. (From: Lecture Notes, Prof. Del Zoppo, Politecnico di Milano)

In the visible range, the refractive index of metals like gold is mainly composed by the absorption coefficient (κ) therefore, the permittivity results to be negative. When the incident photon frequency is resonant with the collective oscillation of the conduction electrons of the metal, it creates a surface plasmon: surface plasmon resonance (SPR) is the resonant oscillation of conduction electrons at the interface between negative and positive permittivity material stimulated by incident light [86]. A schematic representation of SPR is reported in Figure 2.14.
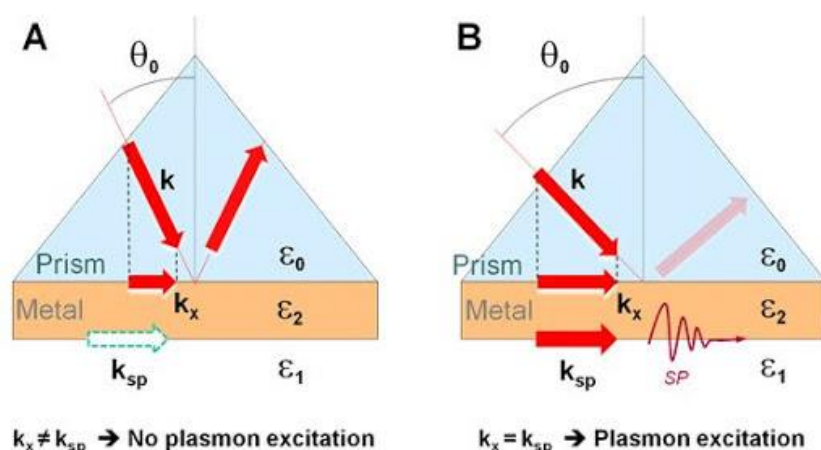
Figure 2.14: *Representation of surface plasmon resonance. (a) the incident wave is not in resonance with the plasma oscillation of electrons and is reflected. (b) the incident wave is in resonance with the plasma oscillation of electrons and generates an evanescent wave perpendicular to the surface, creating a surface plasmon on the opposite interface. [87]*

In the case of metallic films, the surface plasmon propagates up to hundreds of micrometres along the metal surface with an associated electric filed that decays exponentially [13]. In the case of small (negligible dimension with respect to the radiation wavelength) metal nanoparticles, the surface plasmon is confined in the nanoparticles: the conduction electrons inside the particle all move in phase upon plane-wave excitation, leading to the build-up of polarization charges on the particle surface that act as a restoring force, allowing a resonance to occur at a specific frequency [88]. A resonantly enhanced field builds up inside the NP, while a dipolar field is produced outside (Figure 2.15).
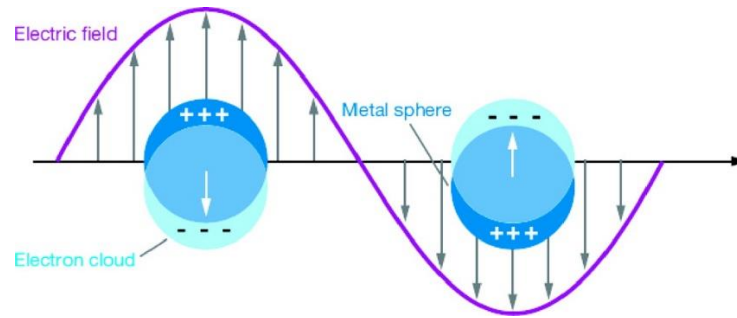
Figure 2.15: Schematic illustration of a localized surface plasmon of metal nanoparticles. [13]

This results in strong light scattering and intense surface plasmon absorption bands, which are defined by the Scattering Coefficient and Absorption Coefficient, reported below (Equations 2-3 and 2-4).

$$C_{abs} = 4\pi k a^3 \left\{ Im \left(\frac{\varepsilon - \varepsilon_d}{\varepsilon + 2\varepsilon_d} \right) \right\}$$

Equation 2-3: Absorption Coefficient of a metal nanoparticle in a dielectric medium. C_{abs}: scattering coefficient, k: wavevector of the EM radiation, a: size of the nanoparticle, ε: dielectric constant of the metal (dependent on ω), ε: dielectric constant of the medium. (From: Lecture Notes, Prof. Del Zoppo, Politecnico di Milano)

$$C_{scatt} = \frac{8\pi}{3} k a^6 \left| \frac{\varepsilon - \varepsilon_d}{\varepsilon + 2\varepsilon_d} \right|^2$$

Equation 2-4: Scattering Coefficient of a metal nanoparticle in a dielectric medium. C_{abs}: scattering coefficient, k: wavevector of the EM radiation, a: size of the nanoparticle, ε: dielectric constant of the metal (dependent on ω), ε: dielectric constant of the medium. (From: Lecture Notes, Prof. Del Zoppo, Politecnico di Milano)

The bandwidth, peak height, and position of the absorption and scattering depend on the particle material, size, geometry and on the dielectric constant of the surrounding environment [89]. The maximum of absorption and scattering is reached at resonance conditions, corresponding to $\varepsilon_{metal} = -2\varepsilon_{medium}$. Among all metal nanoparticles, gold nanoparticles are very interesting because of their LSPR in the visible region, showing an absorbance peak between 520 and 560 nm for small nanoparticles. As the size of the AuNPs increases, the EM radiation is no longer capable of polarizing the nanoparticles homogeneously, causing a red-shift and broadening of the surface plasmon band

[90]. Therefore, small AuNPs aggregates will make their surface plasmons combine and result in the colour change from red to blue [12].

These properties have been widely exploited in biosensors through various methods, such as aggregation/dispersion, etching or growth.

As described before, nanoparticle aggregation induces a colour change of the colloidal solution: this was exploited to detect various molecules, for example, DNA molecules were targeted functionalizing the AuNPs surface via thiol chemistry with complementary DNA. Once the functionalized nanoparticles encounter the target analyte, the complementary DNA molecules hybridize, causing aggregation of nanoparticles, ad reported in Figure 2.16, and a shift in the LSPR [91].
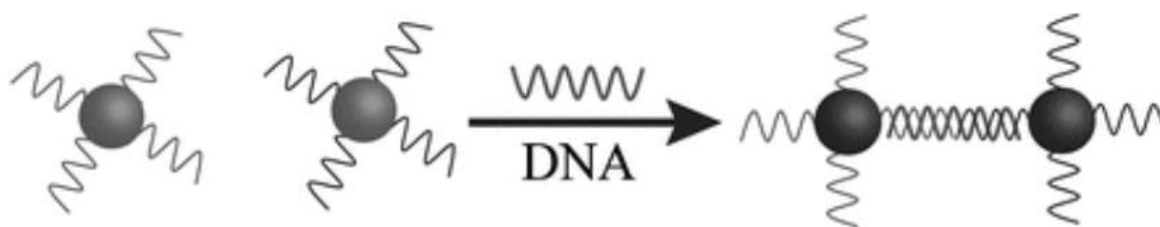
Figure 2.16: *Schematic representation of the interparticle crosslinking aggregation and colour change of AuNPs induced by target DNA. [16]*

Nanoparticle aggregation can also be induced without functionalization of AuNPs: citrate capped nanoparticles are characterized by an electrical repulsive double layer the renders them highly stable in solution under normal conditions [92], however, when exposed to high salt concentration, the force of this electrostatic repulsion diminishes significantly, allowing the aggregation of nanoparticles. This mechanism was used to measure the pH of solutions [93].

Non-functionalized nanoparticles have also been tested for food safety: a colorimetric assay for detection of melamine in milk was developed [94]. As in the previous experiments, AuNPs were stabilized by electrostatic repulsion due to the electrical double layer. Melamine molecules contain three amine groups ($-NH2$) and would easily bind onto the surface of AuNPs through the amine group [95]. Neighbour melamine coated gold nanoparticles were crosslinked by hydrogen bonds between melamine

molecules, as shown below in Figure 2.17, thereby inducing the aggregation of AuNPs and a colour change from red to blue.
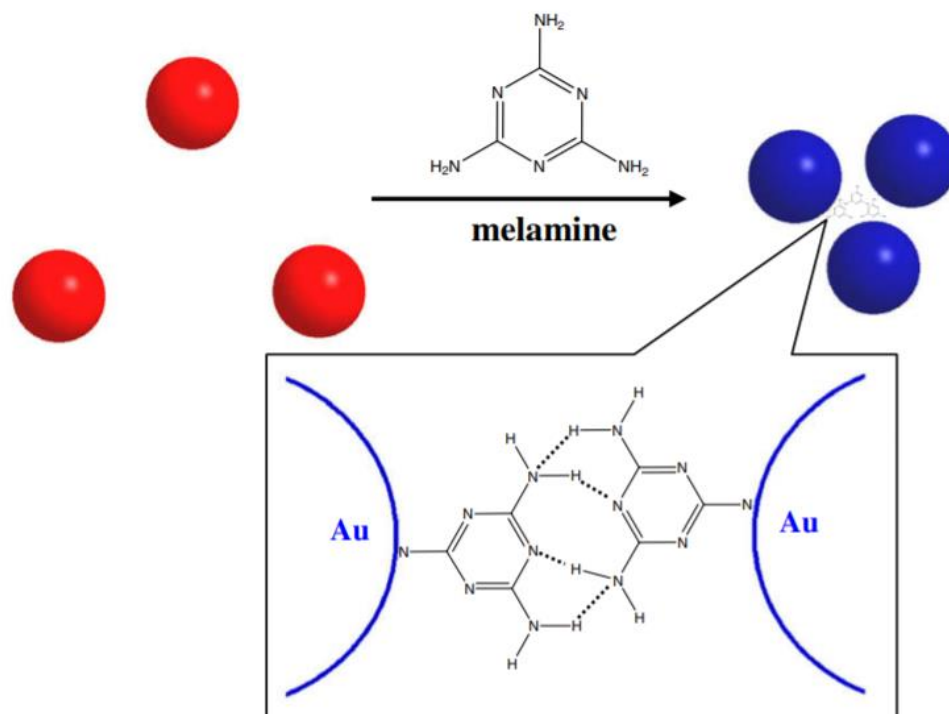
Figure 2.17: *Schematic representation of the AuNPs colorimetric mechanism for melamine detection. [94]*

Also the dispersion of gold nanoparticle has proven useful for biosensing: crosslinkers, as the ones represented in Figure 2.16, that keep the nanoparticles aggregated can be broken by target molecules, causing the opposite change in colour, from blue to red. This mechanism was used to detect enzyme capable of hydrolysing the DNA molecules that were keeping the AuNPs aggregated [96].

The etching of gold nanoparticles causes changes of shape or size, resulting in a shift of the LSPR. An example of biosensing with this method is a Co^{2+} sensor, using gold nanorods: Co^{2+} induced the decomposition of H_2O_2 to generate hydroxyl radicals, these radicals etched the AuNRs and underwent a shape conversion from rods to spheres with an obvious colour change from green to red [97].

Finally, AuNPs growth-based sensing is based on the growth of small gold nanoparticles using gold or silver ions by chemical or enzymatic transformation [23]. For example, a colorimetric assay for metal ion detection was developer exploiting the H_2O_2 ability as a reductant for AuNPs growth [98]: in absence

of Hg^{2+}, the gold nanoclusters catalysed the hydrogen peroxide decomposition, resulting in a slow growth of the nanoparticles, in presence of Hg^{2+}, the catalytic activity of gold nanoclusters was inhibited, enhancing the Au^{3+} reduction with H_2O_2. This resulted in a growth of AuNPs controlled by the amount of Hg^{2+}, which was clearly detectable by the different colours of the solution, as represented in Figure 2.18 [99, 100].
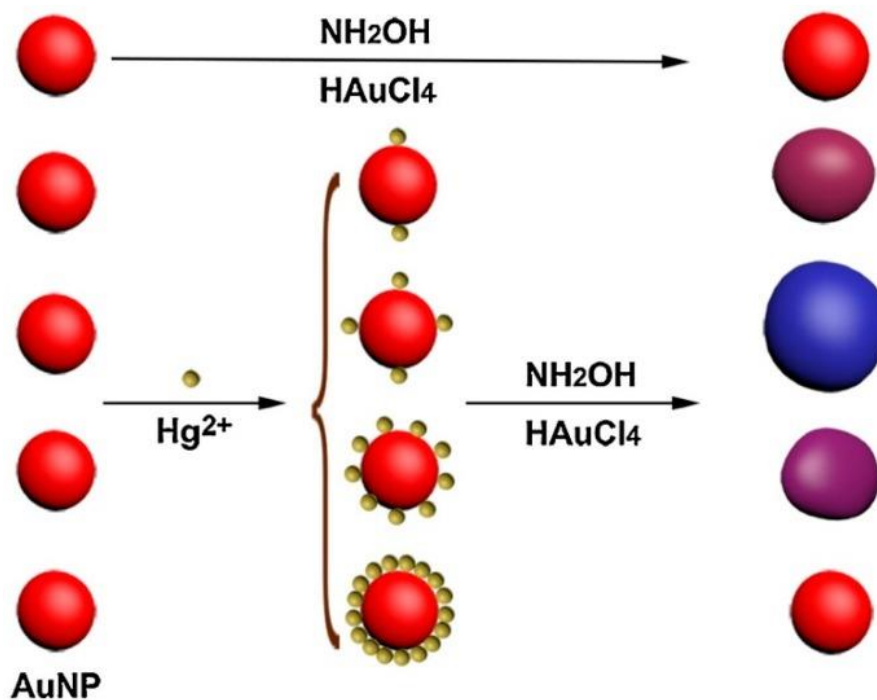
Figure 2.18: Schematic illustration of the amount of Hg on the surface of AuNP-controlled the growth of AuNPs. [100]

Gold nanoparticles have also been employed in non-optical biosensors, but this will not be discussed in this thesis.

Another class of nanoparticles frequently used in biosensing, as well as in other fields such as drug delivery, is magnetic nanoparticles (MNPs). Magnetic nanoparticles are usually chemically and biologically inert, therefore, they are often conjugated with enzymes, antibodies or nucleic acids to increase their functionality [101]. MNPs research has heavily focussed on in vivo magnetic resonance imaging (MRI): functionalizing the magnetic nanoparticles with receptors, they specifically bind to tumours and serve as contrast agents when hit by X-rays [102]. Magnetic nanoparticles are also used to

separate target molecules form the rest of the sample, creating a complex with the molecules functionalizing the particles and then separating them with an external magnet [103].

2.5.1.4   FRET Based Detection

Fluorescent technology has been extensively used in medical diagnosis, food safety, and environmental monitoring because of its inherent sensitivity and high selectivity [104]. An interesting class of fluorescence biosensors is ratiometric fluorescence biosensors, since they are capable of quantitively detect the target analyte [105].

FRET (Förster or Fluorescence Resonance Energy Transfer) is one of the approaches adopted to develop this type of sensors.
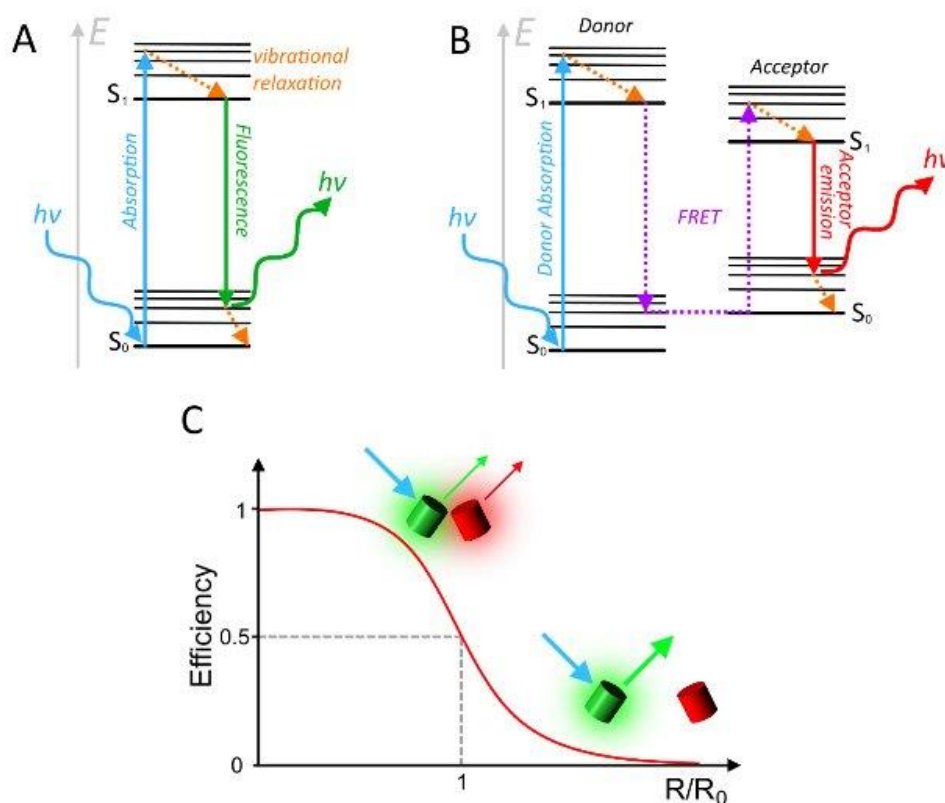
Figure 2.19: The basic principles of fluorescence and FRET. (A) Jablonski diagram, explaining the process of fluorescence. (B) Jablonski diagram, explaining the FRET process. (C) Correlation between the FRET efficiency and the distance between the fluorophores. [106]

A schematic representation of the FRET process is represented in Figure 2.19. It is a process involving a non-radiative transmission of energy from a donor molecule to an acceptor molecule: the donor molecule

initially absorbs the energy, which is then transferred to the acceptor. This resonance interaction occurs over greater than interatomic distances, without any molecular collision. The transfer of energy leads to a reduction in the donor's fluorescence intensity and excited state lifetime, and an increase in the acceptor's emission intensity, if this molecule is a fluorophore. These sensors thus rely on the distance-dependent transfer of energy from a donor molecule to an acceptor molecule. Due to its sensitivity to distance, FRET has been widely used to investigate molecular interactions [107].

A great amount of FRET based immunoassays has been developed due to their excellent stability, specificity and ratiometric measurements, without need of washing or separation steps [108]. For example, antigen (in this case troponin) were detected based on the conformational changes resulted from the binding of antigen and antibody: a donor labelled protein was bound to an acceptor labelled antibody, once the antigen is bound to the antibody, the distance between the donor and acceptor changes, influencing the fluorescence emission [109]. The FRET process was also exploited to produce an assay for detecting MMP-9 inhibition: a peptide labelled with a fluorophore (donor) and a quencher (acceptor) molecule was used to detect the protease activity. No fluorescence emission was detected when this setup was intact, upon exposure to the MMP, the peptide was cleaved, distancing the donor/acceptor pair, leading to fluorescence emission and therefore to the detection of the protease activity (Figure 2.20) [110].
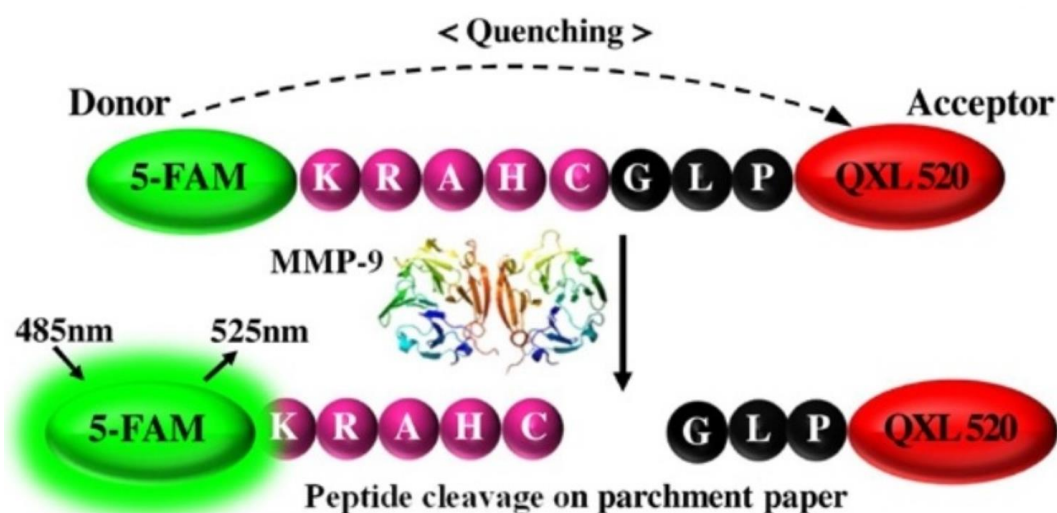
Figure 2.20: Schematic representation of a novel peptide-based fluorescent assay to determine the MMP-9 activities/inhibition. [110]

2.5.2 Peptides

Peptides are short chains of amino acids, linked by peptide bonds, formed by the condensation reaction between the carboxyl group and the amino group of two amino acids [111]. These molecules can be natural or synthetic, allowing to form peptide with the desired amino acid sequence [112]. For this reason, peptides are one of the most flexible devices in supramolecular chemistry and therefore in biosensing [113]. In fact, peptides have been employed as recognition elements in biosensing due to their stability, simple acquisition, specificity, cost effectiveness, standard synthetic protocol, accessibility, easy modification and versatility [114].

Peptides can also play a critical role in assays for enzymatic activity detection and screening of enzymatic inhibitors. This is of particular interests for this thesis: as described previously, MMPs are enzymes able to cleave proteins, catalysing their hydrolyzation. Similarly, these proteases cleave peptides in specific sites. The breakdown of proteins through hydrolysis is called proteolysis (Figure 2.21) and is usually characterized by a very slow kinetics. However, proteases have a strong catalytic effect on proteolysis, drastically accelerating it, resulting in a fast cleavage of the peptide [115].
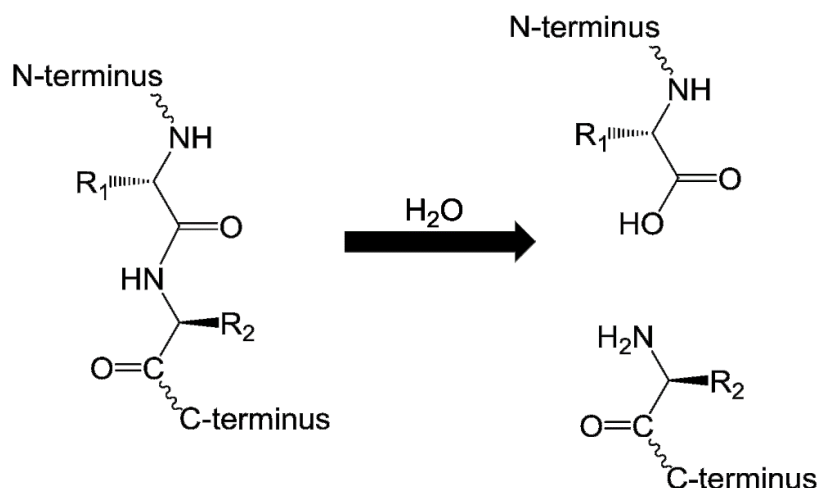
Figure 2.21: Schematic representation of proteolysis reaction

The catalytic activity that the protease has on the proteolysis reaction depends on the peptide sequence [116]. Peptide sequences can therefore be modified to show a recognition site for enzymes like matrix metalloproteinases, accelerating as much as possible the hydrolysis process [117, 118].

Chapter 3: Colorimetric Functional Assay

3.1   Introduction

As described in the previous chapters, matrix metalloproteinases have attracted considerable attention due to their potential use as cancer biomarkers. Our model protease, Matrilysin (MMP-7), is an indicator of salivary gland cancer and is believed to contribute to invasive growth and metastasis of colon carcinoma and numerous other human cancers. In this chapter, Matrilysin was detected using gold and alloy nanoparticles functionalized with a designed synthetic polypeptide (JR2EC): a peptide which contains two specific recognition and digestion sites for MMP-7.

Using gold–thiol chemistry, the surface of AuNPs can be tailored for specific molecular recognition and for tuning the stability of the particle suspension [119]. In particular, JR2EC bears 5 negative charges at pH 7 and renders the nanoparticles highly stable, even at a physiological salt concentration. Hydrolysis of the immobilized peptide by MMP-7 decreases its size and net charge, drastically reducing the colloidal stability of the suspension: the nanoparticles aggregate extensively upon exposure to MMP-7 resulting in a distinct concentration dependent localized surface plasmon resonance (LSPR) shift, sufficiently large to be detected by naked eye. This enables a quantitative monitoring of the presence and activity of the protease (Figure 3.1 [120]).

Figure 3.1: Peptide sequence and working principle of the colorimetric AuNP assay. [120]

3.2   Materials and Instruments

Absorbance scans and kinetic reading were taken using a Tecan Spark® plate reader.

Zeta potential and DLS measurement were done using Malvern Zetananosizer.

MMP-7 was synthesized in our laboratory (Centre for Biomimetic Sensor Science), with an estimated activity 10 times lower than the commercial Matrilysin.

JR2EC and JR2E'C were synthesized by GLBiochem , Shanghai (China).

All the other reagents and solvents were obtained from Sigma-Aldrich and used without further purification.

3.3   Gold Nanoparticles Synthesis and Characterization

Gold nanoparticles were synthesized using Turkevitch [121] method of citrate reduction of $HAuCl_4$: 1250 μL of 10 mM $HAuCl_4$ solution was added to 50 mL of Milli-Q water while being stirred and refluxed. The solution was kept under vigorous stirring and heating for 40 min. After that, 2.5mL of trisodium citrate solution (1% w/v) was quickly added to the solution with continuous vigorous stirring. The colour changed gradually to red suggesting the formation of gold nanoparticles, this mixture was stirred and refluxed for 60 min. Later, it was cooled down to room temperature. The synthesized nanoparticles were stored in 4 °C until further use. UV-Visible spectra were recorded for characteristic absorbance of gold nanoparticles. This protocol consistently resulted in the synthesis of AuNP with an absorbance maximum at 520 nm (±2 nm) with a narrow peak, suggesting a narrow size distribution. An example of the recorded spectra is shown in Figure 3.2.
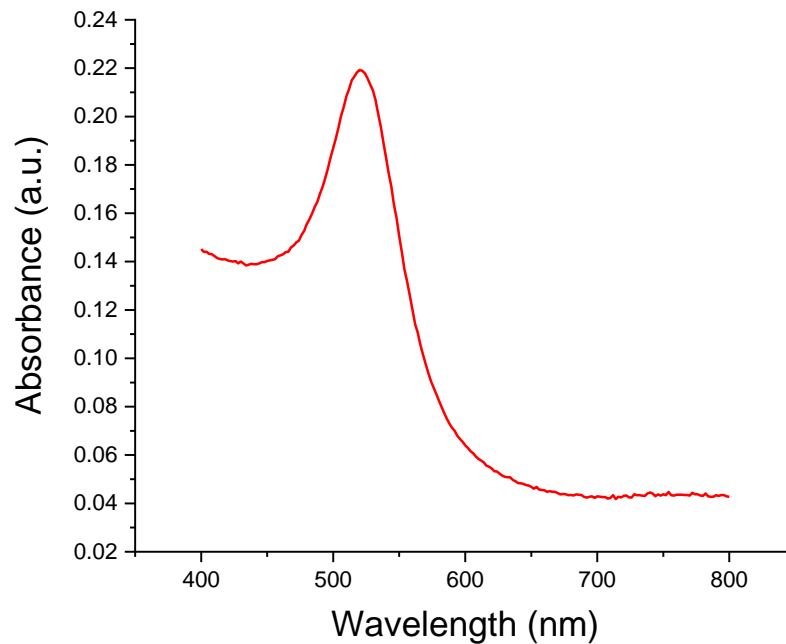
Figure 3.2: Absorbance spectrum for gold nanoparticles with maximum absorbance at 520 nm.

The nanoparticles were then analysed through DLS (Dynamic Light Scattering) and Zeta potential measurements, whose working principles are described below.

DLS is a characterization technique used to determine the size distribution of particles when suspended in solutions, exploiting their Brownian motions. During measurements, the sample solution is hit by a laser beam and the fluctuations of the scattered light, which depend on the particles speed in the solution, are detected at a precise scattering angle (θ). The relation between this speed and the particles dimension is given by the Stokes-Einstein equation (Equation 3-1):

$$D = \frac{k_B T}{6\pi\eta R_H}$$

Equation 3-1: Stokes-Einstein equation, defining the particles dimension from their fluctuation speed in solution. D: diffusion coefficient. k_B: Boltzmann constant. T: temperature. η: viscosity. R_H: hydrodynamic radius.

Determining the diffusion coefficient and knowing the solvent it is possible to obtain the hydrodynamic radius. Therefore, DLS allows to measure the average diameter of the nanoparticles, together with their distribution: a narrow peak means narrow distribution, while the presence of additional peak is indicative of presence of larger bodies, such as particle agglomerates or contaminations.

Zeta (ζ) potential is a technique used to evaluate the colloidal stability of the solution. When gold nanoparticles are dispersed into a solution, the negative charge on their surface attracts positive ions, arranging themselves and forming the electrical double layer. The Zeta potential is defined as the electric potential at the interface between electrical double layer and the rest of the dispersion medium. It is used as an indicator of stability for colloidal solutions: suspensions with Zeta potential lower than -30 mV (or higher than 30 mV) are considered stable. ζ potential was recorded by electrokynetic measurements: when an electric field is applied to the solution, the particles showing a Zeta potential move towards the electrode with opposite charge, with increasing velocity at increasing ζ potential.

The DLS (Dynamic Light Scattering) of the nanoparticles confirmed the narrow dimension distribution: an average diameter of ~26 nm with a single peak and a polydispersity index (PDI) of 0.045, as shown in Figure 3.3.
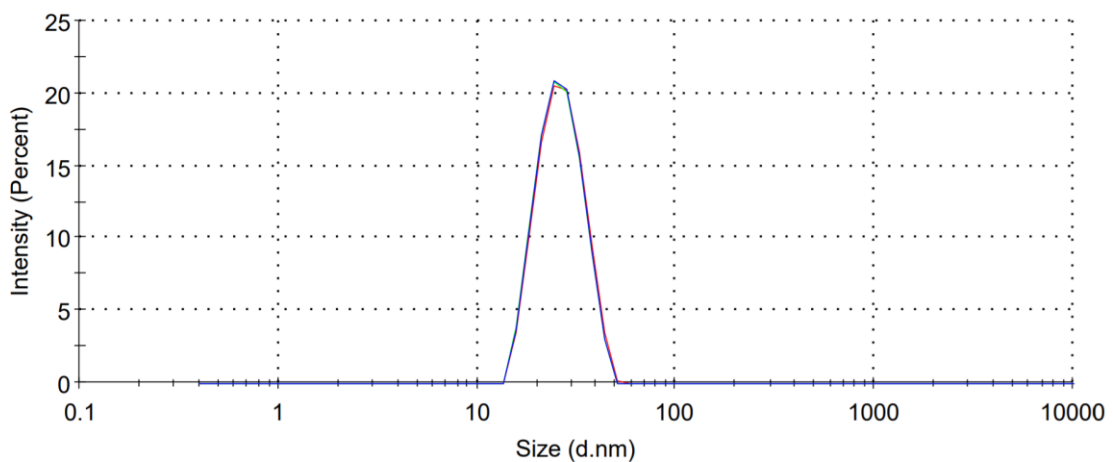
Figure 3.3: DLS measurements of AuNP, showing a single peak.

Finally, the measurement gave a Zeta potential of -41.3 mV, confirming the stability of the synthesized particles.

3.4   Alloy Nanoparticles Synthesis and Characterization

In a recent study carried out by Bo Liedberg's group [122], it was shown that the human eye's ability to detect the colour change derived by optical shifts depends on the starting wavelength of the shift: LSPR shifts of the same magnitude can be more or less perceptible by humans depending on the absorbance wavelength prior to enzyme exposure. In this case, this wavelength was found to be 500 nm, which was given by $Au_{0.8}Ag_{0.2}$ nanoparticles.

$Au_{0.8}Ag_{0.2}$ nanoparticles were synthesized by simultaneous citrate reduction of gold (III) chloride and silver nitrate solution [123]. Briefly, 960 µL of 10 mM $HAuCl_4$ solution and 240 µL of 10 mM $AgNO_3$ solution were added to 50 mL of Milli-Q water and was kept vigorous stirring and heating for 40 min. After that, 2.5 mL of trisodium citrate solution (1% w/v) was quickly added to the solution with continuous vigorous stirring. The colour changed gradually to orange red suggesting the formation of gold nanoparticles, this mixture was stirred and refluxed for 60 min. Later, it was cooled down to room temperature. Nanoparticles were stored in 4 °C until further use and UV-Visible spectra were recorded for characteristic absorbance of alloy nanoparticles.

The results obtained with this protocol were not repeatable enough: ideally, the absorbance should have a maximum at 500 nm (±2 nm), while in most cases, peaks are obtained at 508 nm or greater wavelengths. For this reason, a further optimization was needed for the alloy nanoparticles synthesis.

Silver nanoparticles of diameter 10-30nm usually show an absorption peak at around 400 nm [124], while gold nanoparticles previously synthesized showed it at 520 nm. This suggests that increasing the ratio between silver ions and gold ions dispersed in the solution, this peak should shift to lower wavelengths [125]. By decreasing gold chloride concentration (from 10 to 8.5 and then 8mM) it was possible to reach a repeatable synthesis of alloy nanoparticles with an absorbance maximum at the desired wavelength: as reported in Figure 3.4, the absorption peak shifts from 512 nm, for 10 mM $HAuCl_4$, to 500 nm, for 8 mM $HAuCl_4$.
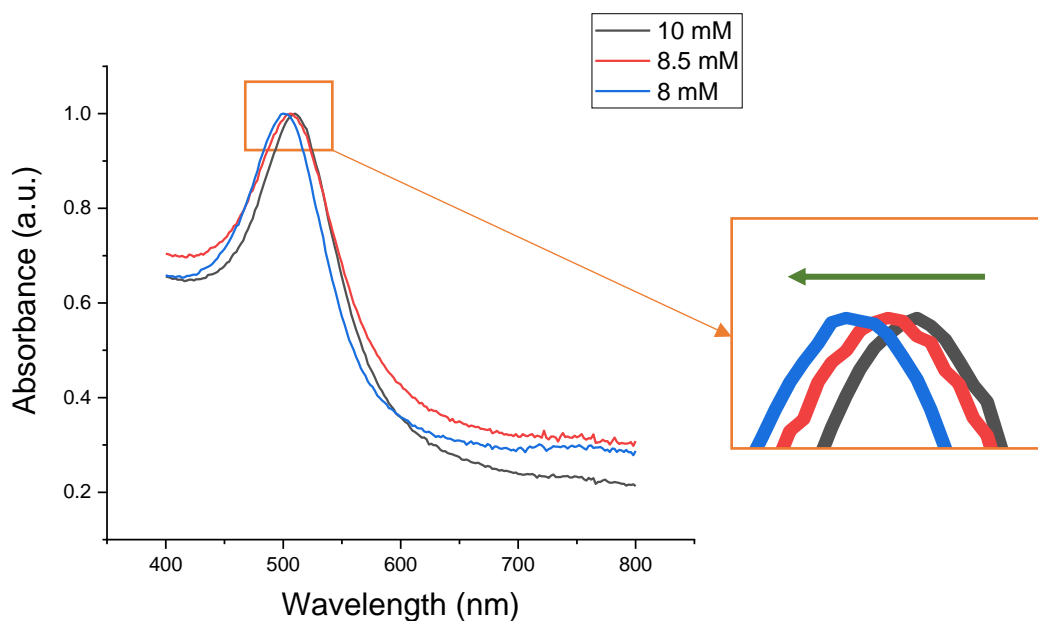
Figure 3.4: *Normalized absorbance spectra for AuAg nanoparticles, absorbance peak shifts to lower wavelengths (from 512 nm to 500 nm) with decreasing concentration of HAuCl$_4$, highlighted in the zoom-in on the right.*

Despite the satisfying absorption spectra, the nanoparticles turned out to be less stable than the ones synthesized with the previous protocol, probably due to the higher silver fraction: in fact, silver nanoparticles are much less stable than gold nanoparticles and tend to aggregate more [126]. Therefore, the chemicals and their molarity were kept as in the protocol, while other parameters were optimized.

The protocol was repeated at different temperatures: 960 μL of 10 mM HAuCl$_4$ solution and 240 μL of 10 mM AgNO$_3$ solution were added to 50 mL of Milli-Q water and was kept vigorous stirring and heating until the desired temperature was reached, then, 2.5 mL of trisodium citrate solution (1% w/v) was quickly added to the solution with continuous vigorous stirring.

The analysed temperatures were: 90, 100, 110, 120, 130 °C. As shown below (Figure 3.5), 90 °C have a very different result from the other experiments, with a very broad absorbance peak at 526 nm, suggesting a broad dimension distribution, meaning that it was not a sufficient temperature to induce enough atom cluster growth to obtain nanoparticles with acceptable characteristics, even after 3 hours or reaction time. Considering the other temperatures: the nanoparticles' absorption peak shifts towards

lower wavelengths with increasing temperature until 120°C, once this limit has been reached, the peak shifts towards higher wavelengths again.
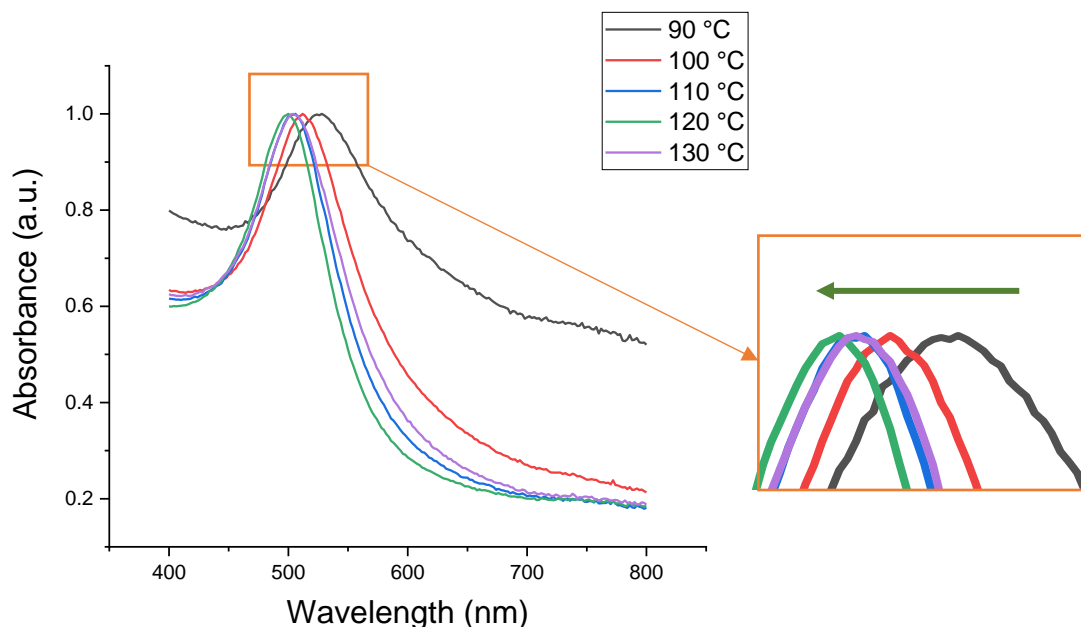
Figure 3.5: *Normalized absorbance spectra of AuAg nanoparticles, synthesized at different temperatures. On the right, zoom-in of the maxima, highlighting the peak shift (from 526 nm to 500 nm).*

These results show that 120 °C is the right temperature to consistently obtain AuAgNPs with absorbance maxima at 500 nm. The continuous shift obtained for temperatures between 90 and 120 °C can be explained by the fact that nucleation is more favoured at high temperatures, forming more nucleation sites and therefore particles, which results in smaller particles. The opposite trend observed at 130 °C can be attributed to a re-crystallization of the particles and to Ostwald ripening, resulting in the excessive particle's growth at the expense of smaller nanoparticles at high temperatures [127, 128].

120 °C is therefore the temperature at which particle nucleation and growth are at the perfect equilibrium to obtain the desired nanoparticle dimension.

Also in this case, DLS and Zeta Potential measurements were recorded. The Dynamic Light Scattering data is reported in Figure 3.6: larger nanoparticles were obtained with respect to the AuNPs, with an average diameter of ~42 nm and a PDI of 0.237.
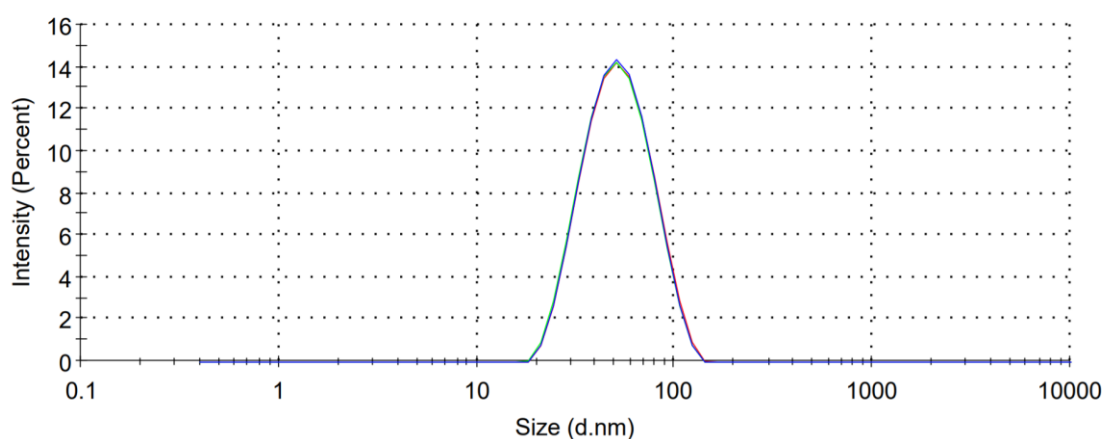
Figure 3.6: DLS measurements of AuAgNP, showing a single peak.

Also for AuAg nanoparticles, Zeta potential measurements confirmed the stability of the nanoparticles, resulting in the measurements of -46.8 mV at the electrical double layer interface.

3.5   Functionalization of Nanoparticles

Nanoparticles were incubated overnight with 10 μM peptide solution (final concentration) at pH 6 (10 mM sodium citrate). Four repeated centrifugations for 15 min at 10000*g* were done to remove the unbound peptide with 10 mM phosphate saline buffer with 0.01% Tween 20 at pH= 7.2: after centrifugation, the functionalized nanoparticles remain on the bottom of the tube, with the unbound peptides dispersed in the solution above them, this solution was removed and substituted, moreover, the final volume of the solution was finally decreased by 4 times, resulting in the concentration of nanoparticle by the same amount. After that, the functionalized particles were stored at 4°C until further use.

3.6   Colorimetric Activity Assay

Protease activity of MMP-7 on JR2EC functionalized nanoparticles assay was carried out at 25 °C, adding 5 μL of enzyme solution to 25 μL of nanoparticle solution. The UV-Visible spectra were recorded over time for different concentrations of MMP-7 (0 - 25 μg/mL).

During the enzyme exposure, the peptides get cleaved, and their negative charge is reduced from -5 to -1 per chain, which leads to aggregation of nanoparticles. The aggregation of nanoparticles causes a change in colour, from red to blue, which is represented in the spectra by a shift of the peak (Figure 3.7),

together with a broadening of the latter, suggesting aggregation with a broader size distribution of the aggregates.
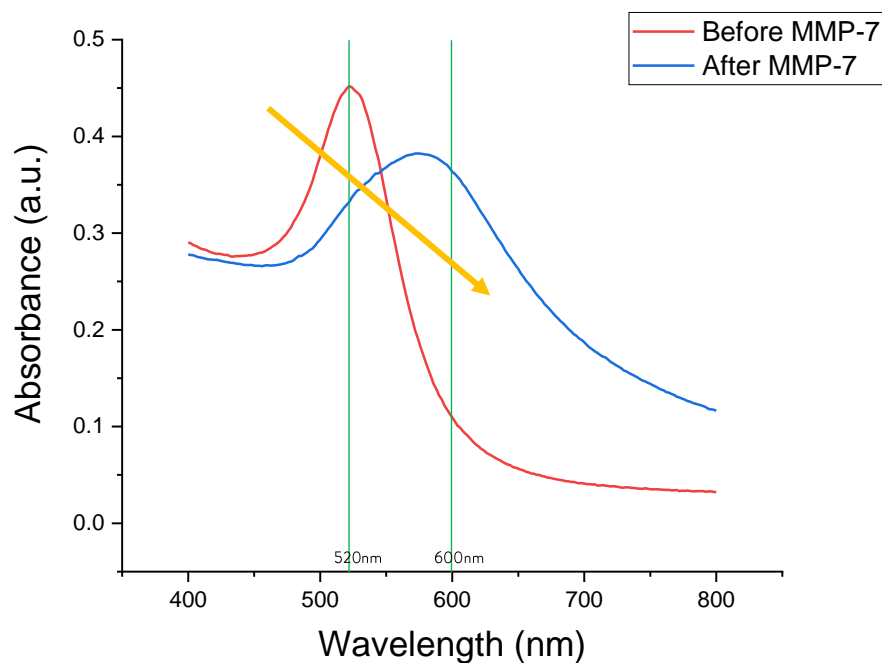
Figure 3.7: *Optical shift of functionalized AuNPs spectra prior exposure to MMP-7 and after, caused by the aggregation of the nanoparticles.*

To numerically evaluate the change in colour, the ratio between absorption at 600 nm and 520 nm (500 nm for AuAgNP) was calculated and plotted over time, as reported in Figure 3.8. This allows to quantify the change in colour and to understand how much time is needed to reach its saturation, permitting to compare assays carried out with different parameters and therefore optimizing the colorimetric assay.
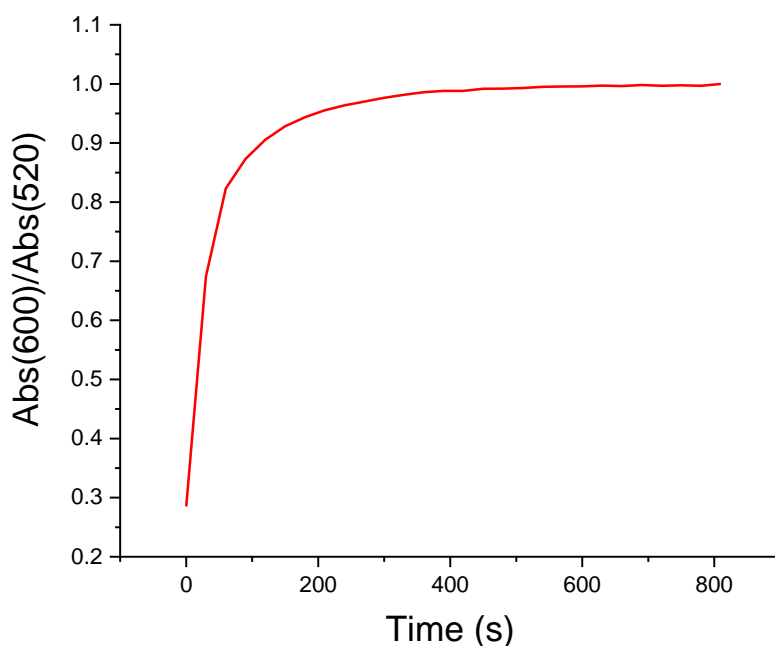
Figure 3.8: Ratio between absorbance at 600 nm and at 520 nm over time of AuNPs exposed to MMP-7.

3.6.1   Optimization of Colorimetric Activity Assay

3.6.1.1   Nanoparticle Concentration

Nanoparticle concentration was the first parameter optimized: a too high concentration can cause steric hindrance, preventing the enzyme from reaching the cleavage site and slowing down the process. Moreover, even if some peptides get cleaved, causing aggregation of NP, there would still be a large fraction of stable nanoparticles since the number of peptides to be cleaved is too large, which results in a less evident change of colour. At the same time, a too low concentration of particles would result in a low intensity colouring, which renders the colour less detectable in both prior and after enzyme detection.

In the following experiments, three MMP-7 assays were carried out, each with a different concentration of AuNPs: starting from the concentration resulted from the functionalization process (Chapter 3.5), 10 times diluted, and 2.5 times concentrated solutions were prepared and exposed to the same concentration of enzyme (20 µg/mL). The results of the three assays are reported below (Figure 3.9).
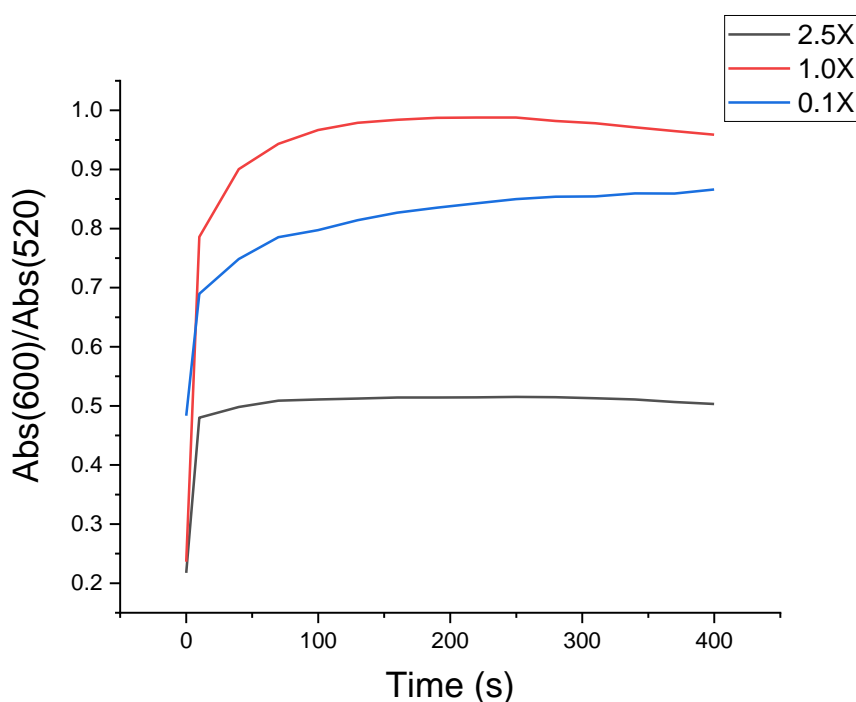
Figure 3.9: Comparison of Abs(600)/Abs(520) over time for different concentrations of functionalized AuNP when exposed to MMP-7.

For the highest concentration of AuNPs, the colour change was barely visible: the MMP-7 could not cleave enough peptides due to the high number of nanoparticles, therefore even if some of them aggregated, the majority remained separated with enough intact peptides on the surface, keeping the colour very similar to the starting one.

The other two cases reached similar values of Abs(600)/Abs(520), but the lower concentration assay showed a less intense coloration, which is confirmed by a very high starting value of the ratio, meaning that the absorption peak of the starting solution reaches lower absorbance values.

In this case, the optimized concentration is evident without other analyses: the 1X concentration is a good compromise between sensitivity and colour intensity, allowing an easy detection of MMP-7 by naked eye.

3.6.1.2   Peptide Number on Gold Nanoparticles

The number of peptides immobilized on the AuNP surface drastically changes the performance of the colorimetric assay: if this quantity is very low, the peptides are not able to render the colloidal solution stable enough to prevent aggregation, even without peptide cleavage. On the other hand, a too high concentration would lead to an inefficient immobilization of molecules and a consequent waste of peptides once they are washed away in the following steps.

Gold nanoparticles were functionalized with varying number of peptides: they were incubated overnight with 1, 10, 100 mM JR2EC. After the unbound peptides were removed, 20 µg/mL MMP-7 was added to the functionalized nanoparticles solution and the UV-Visible spectra were recorded over time, the results are reported below (Figure 3.10)
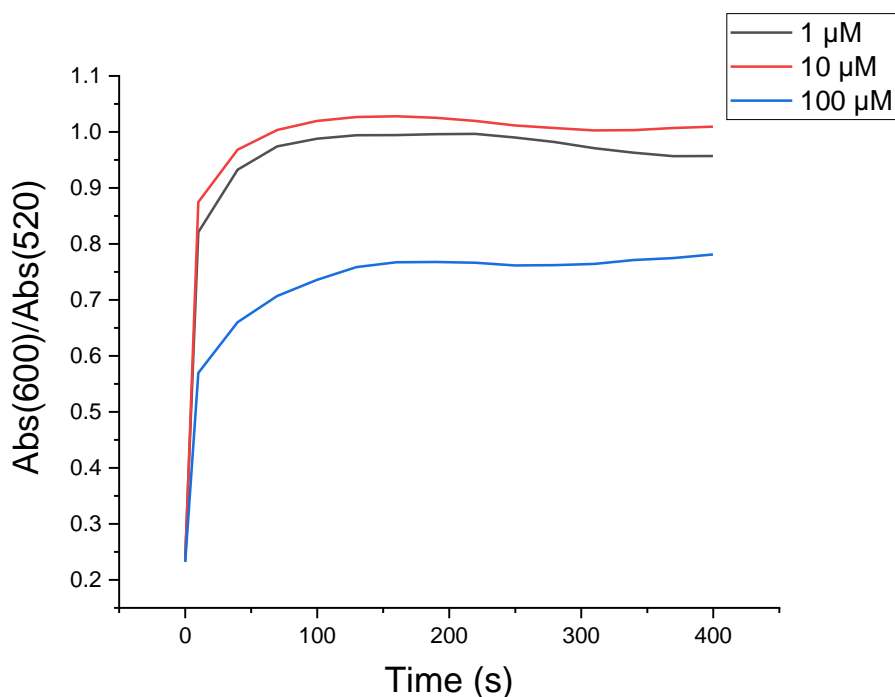
Figure 3.10: *Comparison of Abs(600)/Abs(520) over time of AuNP functionalized with varying concentrations of peptides when exposed to MMP-7.*

The nanoparticles functionalized using 100 mM peptide solution showed an inferior behaviour with respect to the others: the number of peptides immobilized on the particles' surface is too high, in fact,

even if at high concentration, MMP-7 is not able to cleave enough peptides and cause a complete aggregation of nanoparticles. Both 1 and 10 mM performed similarly, reaching a similar value of colour change. However, at 1 mM the amount of peptide on the particles' surface is not enough to effectively stabilize them and therefore, aggregation may result in buffers with different pH or composition, resulting in false positives.

In conclusion, 10 mM is the ideal concentration for functionalization of AuNP since it renders the nanoparticles stable enough when the peptides are intact but allows aggregation effectively when exposed to the enzyme

3.6.1.3   Peptide Sequence

The catalytic effect that MMP-7 has on the proteolysis of the chain depends on the peptides sequence itself. Optimizing this sequence results in the improvement of the reaction kinetics for the reaction and therefore faster nanoparticles aggregation and colour change.

A comparison between two synthetic polypeptides was carried out: JR2EC and JR2(ELKIA)C, two molecules bearing the same amount of charges when intact and rendering the colloidal solution very stable.

The peptides were immobilized on the gold nanoparticles following the same protocol. The solutions were then exposed to 20 μg/mL of MMP-7 and the UV-Vis spectra were taken over time. This experiment was repeated 3 times in order to verify the repeatability and reliability of the results.
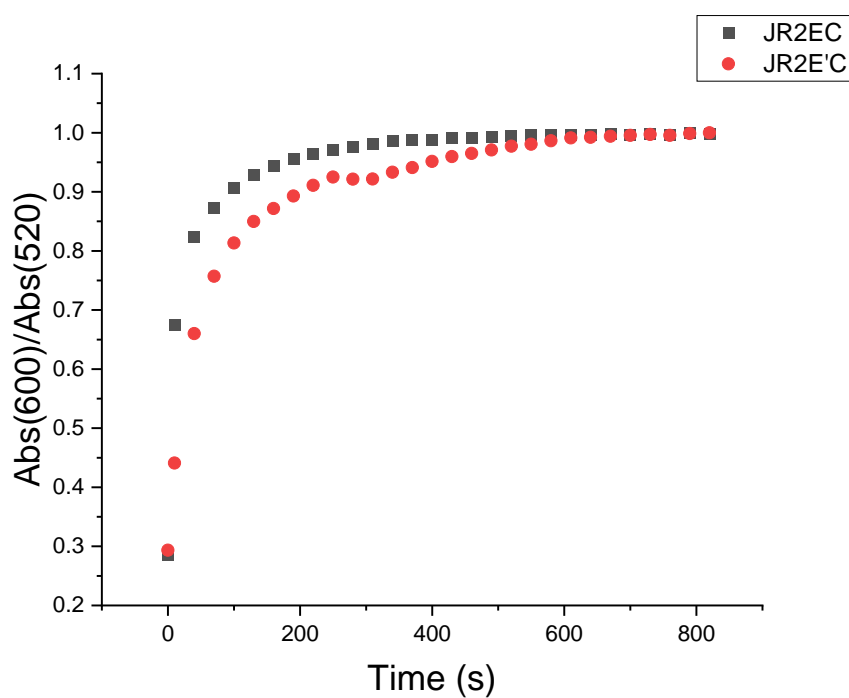
Figure 3.11: Comparison of Abs(600)/Abs(520) over time of AuNP functionalized with two different peptide sequences when exposed to MMP-7.

To compare the two molecules, the ratios between absorption at 600 nm and 520 nm were normalized with respect to their respective maximum and plotted over time (Figure 3.11). Then, the linear fit of the datapoints in the plot's linear part were compared (Figure 3.12). A steeper slope means that the cleavage reaction has a faster kinetics, since the saturation of the colour change is reached in a shorter time.
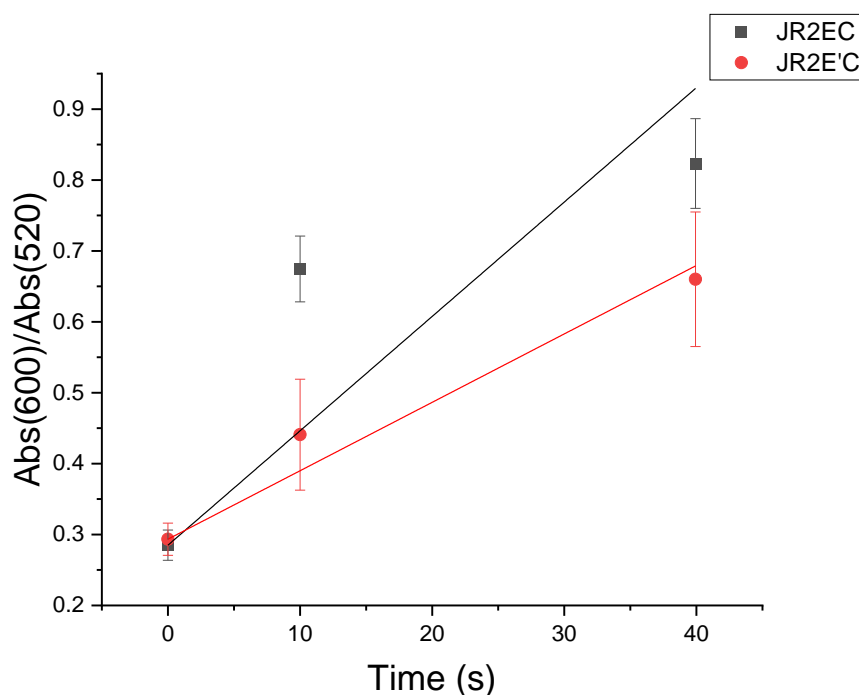
Figure 3.12: *Linear fit of Abs(600)/Abs(520) over time in the first 40 seconds. The slopes obtained were: 0.01613 for JR2EC and 0.00965 for JR2E'C.*

Both molecules reach similar value of optical shift, but JR2EC shows a 67% greater slope than that of JR2(ELKIA)C, therefore it is the best peptides for this assay setup, allowing a faster detection. Since the reaction with 20 µg/mL MMP-7 is very fast, a lower concentration of enzyme should be used and the spectra readings should be taken more frequently, in this way it would be possible to obtain more points regarding the linear part of the graphs, allowing a more precise analysis. However, the difference between the two peptide sequences observed in this experiment was very clear, therefore it was not repeated.

3.6.2   Stability Studies

One of the major drawbacks usually experienced with biosensors concerns their robustness: these setups usually show great behaviour in laboratory experiments but cannot be used in real applications because of their short shelf life [129]. It is therefore important to determine the stability of this setup during time, carrying a colorimetric assay comparing the behaviour of freshly functionalized AuNPs and particles functionalized and then stored for a considerable amount of time before use.

Both citrate capped AuNPs and functionalized gold nanoparticles are extremely stable when in solution: they remain suspended in a colloidal solution for over one year when stored at 4°C [130]. Similarly, no change in peptide activity is detected when JR2EC or JR2E'C are stored at -20°C, with possible degradation caused by repeated freeze and thaw cycles. The remaining variable which can influence the assay's robustness is the activity showed by the peptide when immobilized on the nanoparticles and exposed to MMP-7, after being stored at 4 °C for long times. In the following experiment, the colorimetric assay was carried out using particles functionalized 3 months earlier and comparing their behaviour to AuNPs functionalized the previous day to the experiment.
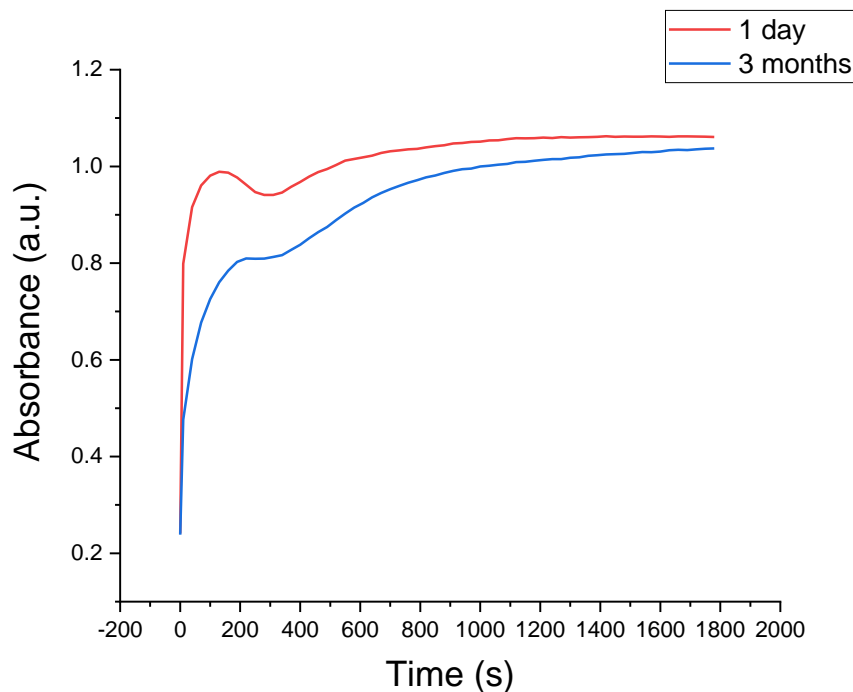
Figure 3.13: *Comparison of Abs(600)/Abs(520) over time of functionalized AuNP, stored for varying periods before assay, when exposed to MMP-7.*

Figure 3.13 shows the comparison between the two assays: the freshly functionalized nanoparticles reached a higher saturation level compared to that reached by the others in the. However, the initial slope is similar, and these saturations are obtained at the same time. A colour change could be detected in less than 2 minutes, and the two assays reached similar values of optical shift after enough time, making the assay usable even after long storage periods.

This colorimetric assay is capable of quantifying the amount of MMP-7 based on the extent and kinetics of the optical shift, with faster reaction and more intense colour change corresponding to a higher concentration of enzyme. Based on the results obtained with this experiment, it was observed that the relation between reaction kinetics and enzyme concentration detected should be normalized with respect to the storage time of the functionalized nanoparticles.

3.6.3   Assay in Human Plasma

The colorimetric assay was then carried out in Milli-Q and in 10% plasma, with the addition of the same amount of MMP-7 (20 μg/mL). The results show a very different behaviour between the two experiments: Figure 3.14 represent the absorbance spectra of the AuNPs in Milli-Q and in 10% plasma after being exposed to MMP-7.
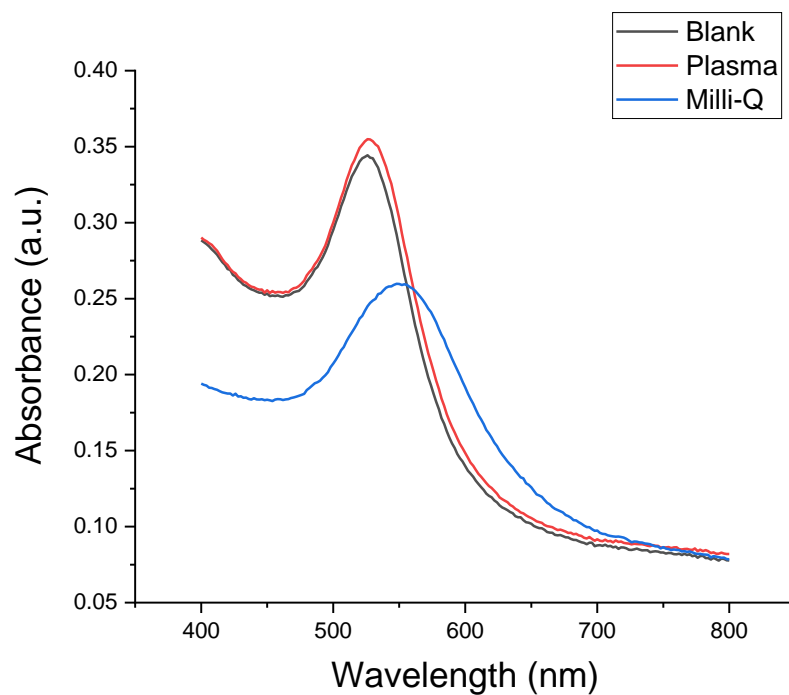
Figure 3.14: Absorbance spectra of functionalized AuNP (blank), functionalized AuNP exposed to MMP-7 in 10% plasma and functionalized AuNP exposed to MMP-7 in Milli-Q.

The exposure to MMP-7 in Milli-Q showed a clear colour change, represented by the peak shift with respect to the blank reading, while it had no effect in 10% plasma: no peak shift is observed, while the

slight increase of absorbance intensity is due to the different matrix rather than MMP-7. This is due to two main reasons:

- The enzyme in these complex matrices is not able to reach the cleavage site of the peptide due to the presence of large molecules (such as albumin) that envelop the nanoparticles denying access to the peptides. These molecules can also surround the enzyme, preventing it from diffusing freely in the solution and finally reaching the nanoparticles.
- Even if the enzyme reaches the peptide and cleave it, the macromolecules present in the solution and surrounding the nanoparticles would prevent aggregation and therefore a change in colour.

This behaviour does not change changing the assay parameters or using alloy nanoparticles instead of AuNP, since this would just help to detect the colour change by naked eye, without influencing the cleavage or aggregation mechanism. This demonstrates the inherent issue with plasmonic assays.

3.7   Conclusions

The setup described in this chapter allowed colorimetric naked-eye detection of MMP-7 in a relatively short time: even if the measurements were taken for 30 minutes, the colour change is evident after less than 2 minutes, with varying kinetics for different MMP-7 concentrations. The in-solution assay is even characterized by a good robustness when stored at the right conditions, showing a LSPR shift upon enzyme exposure even after 3 months of storage at 4°C. However, the limit of detection established for these experiments is 12.5 μg/mL and is therefore far over clinically relevant concentrations, which are in the order of 10 ng/mL [131], making the assay's sensitivity insufficient. This low sensitivity is due to two main reasons:

- JR2EC and JR2E'C did not show enough activity when exposed to MMP-7.
- To have aggregation of nanoparticles, a high number of peptides must be cleaved. This means that if the peptides cleavage does not reach a certain threshold, no change in colour can be detected, even if some peptides are getting cleaved, the remaining peptides would still be enough to cause enough aggregation. This threshold value can, in theory, be lowered functionalizing the

NPs with less peptides, however, this would render the colloidal solution less stable and could cause aggregation in buffers with different pH, resulting in false positives.

Moreover, this behaviour could not be detected in diluted plasma or other human serums, requiring further sample treatment before assaying.

Chapter 4: Fluorometric Functional Assay

4.1 Introduction

In this chapter, a functional assay for MMP-7 activity detection in plasma is proposed. The assay is designed to be carried out using a syringe, minimizing sample handling while at the same improving the enzyme activity forcing the sample through a series of membranes. Simulating this setup, it was possible to detect significantly lower concentrations than those detected in the previous chapter, with relatively short incubation times (30 minutes). The ideal assay setup is depicted in Figure 4.1.
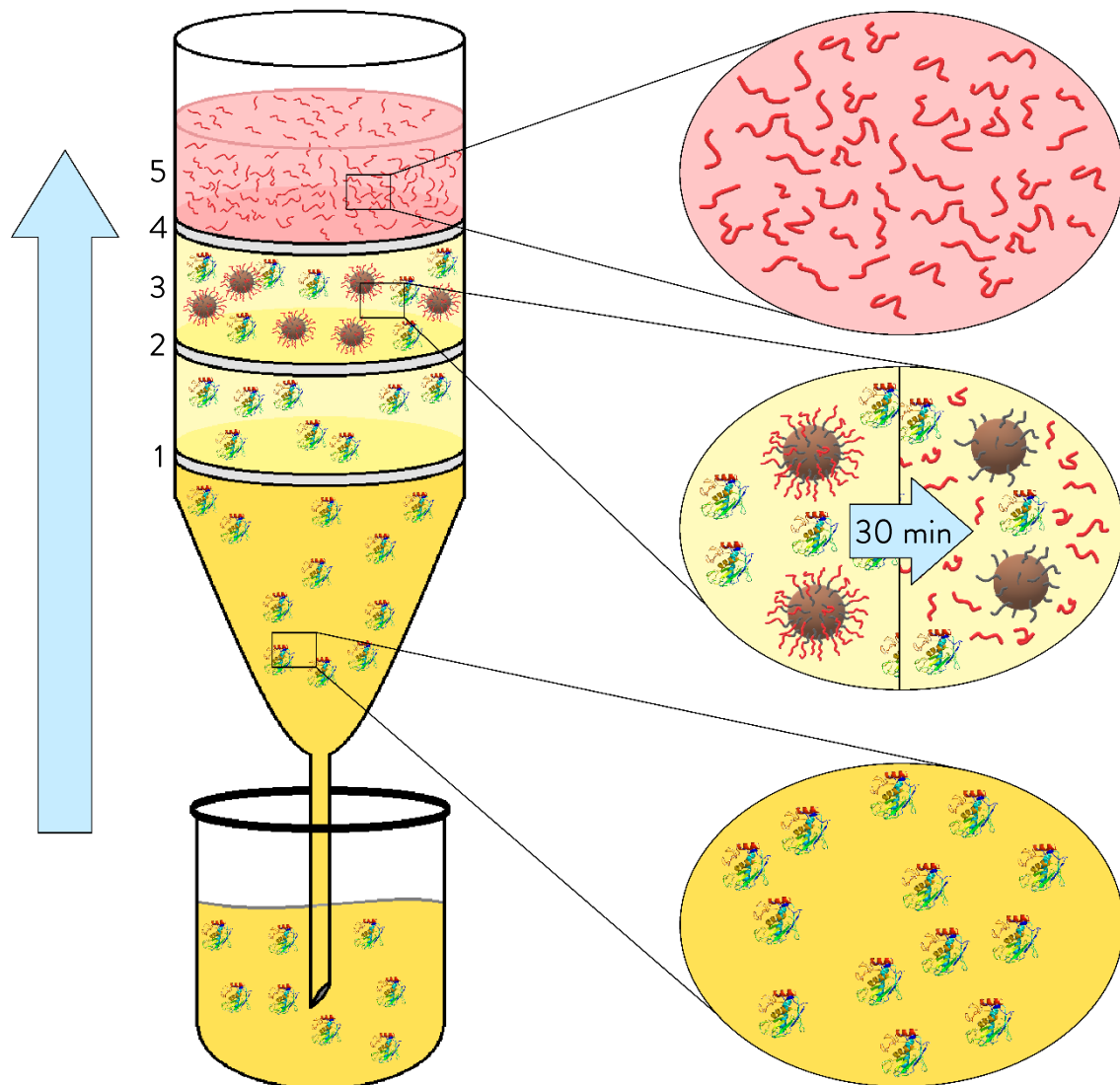
Figure 4.1: *Representation of the syringe functional assay: (1) Filtration membrane for plasma, (2) Particle support membrane, (3) Reaction zone, (4) Particle separation membrane, (5) Reporter zone.*

The enzyme detection is based on FRET peptides immobilized on beads: since nanoparticle aggregation was hindered in complex matrices, a commercial peptide labelled with a fluorophore and a quencher was used. This peptide shows a higher sensitivity to MMP-7 and does not require further physical phenomena after cleavage to give a response: as explained previously, after cleavage, the fluorophore emits light since it is distanced from the quencher [110], without being directly influenced by the state of the nanoparticles or their stability.

The functional assay was designed and optimized to detect MMP-7 in human plasma. This matrix is particularly complex for two main reason: plasma drastically reduces the activity of MMP-7 and has significant optical properties, like its own fluorescence emission at low wavelengths or low transparency in the visible range.

As depicted in Figure 4.1, the ideal syringe setup includes 3 membranes, each with a specific role and therefore with different requirements.

- The first membrane encountered by the sample improves the enzyme activity, filtering out the plasma molecules affecting it and letting MMP-7 flow through with minimized losses.
- The second membrane has the only role of supporting the functionalized beads and release them into the solution once it passes through the membrane. This step has no effect on plasma activity or on its fluorescence properties and must let MMP-7 pass through without losses.
- Finally, the last membrane separates the cleaved peptides fragments, labelled with the reporter molecule, from the beads. Additionally, it filters out large molecules contained in plasma which cause disturbances to the fluorescence signal.

These membranes divide the syringe into two main zones: the reaction zone, where the enzyme reacts for 30 minutes with the peptides, and the reporter zone, where the fluorescence signal is observed.

However, the ideal setup described was not applied in this thesis: experiments were carried out in three different steps: sample pre-treatment, simulating the plasma filtration membrane; release of particles in the solution and reaction, involving the particle support membrane and reaction zone; readout of the signal, simulating particle separation membrane and reporter zone.

4.2   Materials and Instruments

Fluorescence scans and kinetic reading were taken using a Tecan Spark® plate reader.

Portable UV lamp (265 nm, 8W) was used in a dark room to observe the fluorescence emission of samples.

Sony ILCE-7R camera was used to take pictures reported in this chapter.

ThermoFisher Scientific DynaMag™-2 Magnet was used for magnetic separation of magnetic beads.

Fisherbrand™ Sterile Syringes for Single Use were used for experiments with syringes.

Single use syringe filters, reusable cartridges and membranes and centrifuge tubes from Merck.

FRET peptide, referred to as pep0 with sequence: Mca-KPLG~L-Dpa-ARGK$^{(Me3)}$C-NH$_2$.

MMP-7 was synthesized in our laboratory (Centre for Biomimetic Sensor Science), with an estimated activity ten times lower than the commercial Matrilysin.

Fret peptide used for Trypsin detection in FAM experiments: Ac-GLLGDFARRAKEKIGC.

Trypsin from Sigma-Aldrich was used for selectivity studies.

Ocean NanoTech Maleimide Super Mag Magnetic Beads, 0.05 μm and 3 μm.

All the other reagents and solvents were obtained from Sigma-Aldrich and used without further purification.

4.3   FRET Peptide

One of the major issues showed in Chapter 3 was sensitivity: even when diluted in Milli-Q, the limit of detection was found to be too high with respect to clinically relevant concentrations.

The first step required to improve the LOD is changing the peptide sequence: it was decided to use a commercially available peptide (named pep0), which is depicted in Figure 4.2.
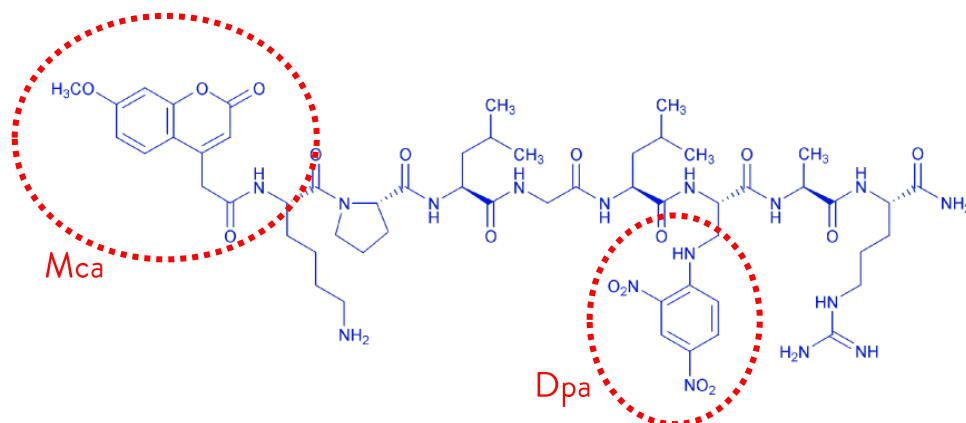
Figure 4.2: Molecular structure of pep0, highlighting the presence of Mca (fluorophore) and Dpa (quencher).

This peptide is labelled with a fluorophore, Methoxycoumarin-4 acetic acid (Mca), at the end of the chain and a quencher, Dicyclomine anion (Dpa), exploiting the FRET phenomenon (Förster, or Fluorescence, Resonance Energy Transfer): when a molecule is excited, the excited state energy can be dissipated to the environment in several ways: as light, heat or transferring this energy directly to another molecule. FRET is the non-radiative transfer of the excited state energy from the initially excited donor to an acceptor by long-range dipole-dipole interaction between the two molecules, which is distance dependent. The donor molecule is a fluorophore that typically emits at wavelengths that overlap with the absorption of the acceptor [132].

This is exactly what happens when pep0 is hit by light: with an intact peptide, when the fluorophore is excited by light (maximum absorbance: 320 nm), its excited state is transferred to Dpa, which is a non-fluorescent quencher and dissipates this energy through heat. Once the peptide gets cleaved by MMP-7, the cleaved peptide fragments are distanced from each other, allowing Mca to emit radiation by fluorescence (maximum emission at 405nm).

4.3.1   FRET Peptide Sensitivity

The effect on the MMP-7 catalytic efficiency of this peptide was tested exposing the peptides to varying concentrations of MMP-7, following this protocol:

- 10 µL of 50 µM peptide solution was prepared.

- 80 µL of Buffer (same buffer used for peptide and enzyme dilution) was added to the 10 µL peptide solution and mixed.

- 10 µL of MMP-7 at several concentrations (10 times higher concentration than desired) was added to the previously prepared solution.

- Immediately after the addition of the enzyme, fluorescence intensity (emission at 405 nm and excitation at 320 nm) was measured over time, with readings every 20 seconds, resulting in a kinetics measurement quantifying the amount of cleaved peptide.

It was observed that the reaction followed two very different trends depending on the buffer in which it was carried out: an example of the different behaviours of peptide cleavage in Milli-Q and Assay Buffer (20 mM Tris, 10 mM $CaCl_2$, 20 mM $ZnCl_2$, 0.05% Brij) is shown below (Figure 4.3):
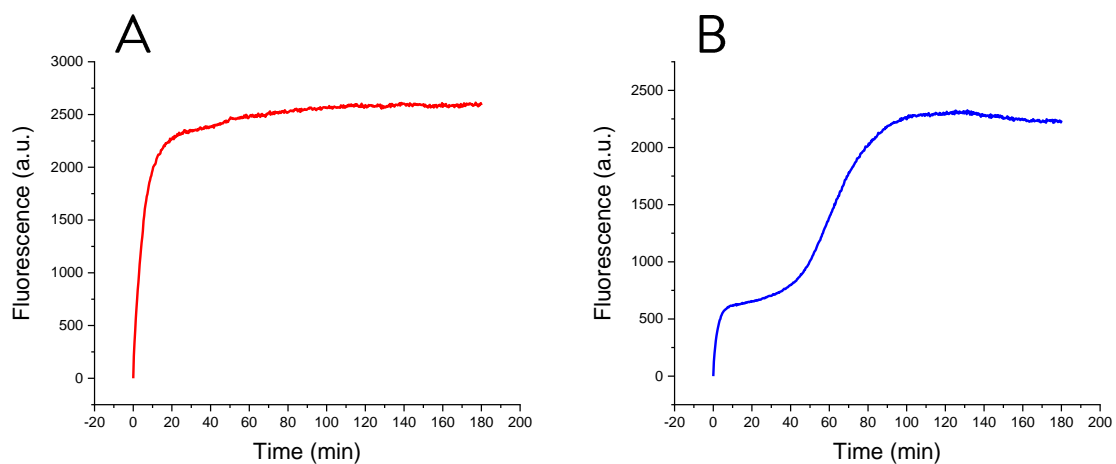
Figure 4.3: *Fluorescence intensity at 405 nm over time of pep0 during MMP-7 exposure. The kinetics measurements show a different behaviour (A) in Assay Buffer and (B) in Milli-Q.*

The two readings reach a similar fluorescence intensity, suggesting that in both cases nearly all the peptides were cleaved, however the reaction kinetics appeared to be very different: when using Milli-Q, substrate inhibition has an important role in the kinetic behaviour [133], while, when using Assay Buffer, this aspect did not seem to influence the peptide cleavage.

This may be due to an aggregation of molecules in water that causes steric hindrance and prevents the enzyme from reaching the rest of the substrate, after the enzyme had enough time to reach the rest of

the peptides, the reaction starts again, reaching similar values of fluorescence to the ones obtained in Assay Buffer. Since this does not happen in Assay Buffer, it was hypothesized that the detergent molecules present in it prevent the peptide aggregation [134], allowing the enzyme to easily reach the cleavage site of the molecules.

Thus, thee experiments were carried out in Assay Buffer, at 0.5, 1, 2 and 5 µg/mL of MMP-7. Most of these concentrations were easily detectable, with the higher ones resulting in a faster kinetics and more intense fluorescence signal. 0.5 µg/mL could not be detected effectively: even after 2 hours the difference between the fluorescence intensity of the blank reading and of 0.5 µg/mL was negligible.

An example of the results obtained is reported in Figure 4.4.
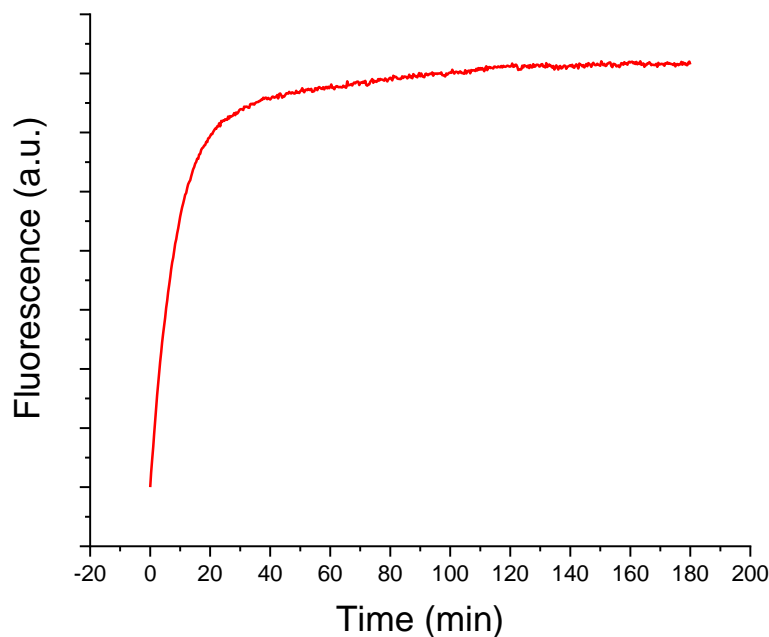
Figure 4.4: Kinetics measurements of fluorescence intensity (at 405 nm) during MMP-7 (at 1 µg/mL) exposure in solution, representing the number of peptides cleaved over time.

For 1 µg/mL of MMP-7, the fluorescence saturation value was reached after 20 minutes, showing an improvement in sensitivity by 12.5 times with respect to the ones obtained with the setup described in Chapter 3, and slower kinetics, probably due to the lower concentration of enzyme.

4.4   Functionalization of Magnetic Beads

The FRET peptides were then immobilized on magnetic beads with maleimide activated surface: maleimide allows to create a chemical bond with thiol groups (Figure 4.5), which was included at the opposite end of the peptide sequence with respect to Mca.

Figure 4.5: Schematic representation of maleimide activated magnetic beads functionalization with peptides.

This process results in a monolayer of peptides bound to the surface, with no fluorescence emission prior to MMP-7 exposure. When exposed to the enzyme, the peptides get cleaved: the fragment labelled with Dpa (quencher) remains immobilized on the surface, while the one containing the fluorophore (Mca) is released into the solution and distanced from the quencher, emitting light by fluorescence when excited.

Peptide functionalized maleimide activated beads were prepared through the following protocol:

- The lyophilized MBs powder (20mg for 50 nm beads and 80 mg for 3 μm beads) was weighted and diluted in 400 μL of Coupling Buffer (10 mM PBS 0.01% Tween 20). The solution was then vortexed until the beads were completely resuspended in the solution.

- The solution containing pep0 was added to the MBs and let react for 2 hours at room temperature with continuous mixing.

- The solution was then transferred in a magnetic separator, once the supernatant was clear, the supernatant was removed and stored. 400 μL of PBS 0.01% Tween 20 was added before resuspending the beads with vortex. This step was repeated four times.

- The final product was stored at 4°C until further use.

- The stored supernatants and functionalized MBs were diluted 20 times and exposed to a high concentration of MMP-7 (5 μg/mL) for 30 minutes. After that, their fluorescence spectra were

recorded, verifying the presence of peptides on the beads and their absence in the last supernatant removed.

4.4.1   Advantages of Immobilizing Peptides on Magnetic Beads

There are three possible ways in which peptides can be arranged for a functional assay: directly diluted in the sample, immobilized on a surface or immobilized on beads which are dispersed in the sample. Immobilization on beads was preferred for several reasons.

Beads can easily be deposited on membranes, allowing to easily release them into the sample solution once the latter passes through the membranes. Due to their much smaller dimension, depositing peptides molecules on a membrane can be much more challenging since they would easily go through it or get stuck in its pores, negating their release into the solution. To avoid this, the membrane's pores should be very small, making it more difficult for samples, especially more complex ones like plasma, to flow through them.

Functionalized beads even showed a better behaviour when exposed to a high concentration of MMP-7 (5 μg/mL) in 10% plasma: Figure 4.6 shows that the signal given by peptides immobilized on MBs is much less disturbed.
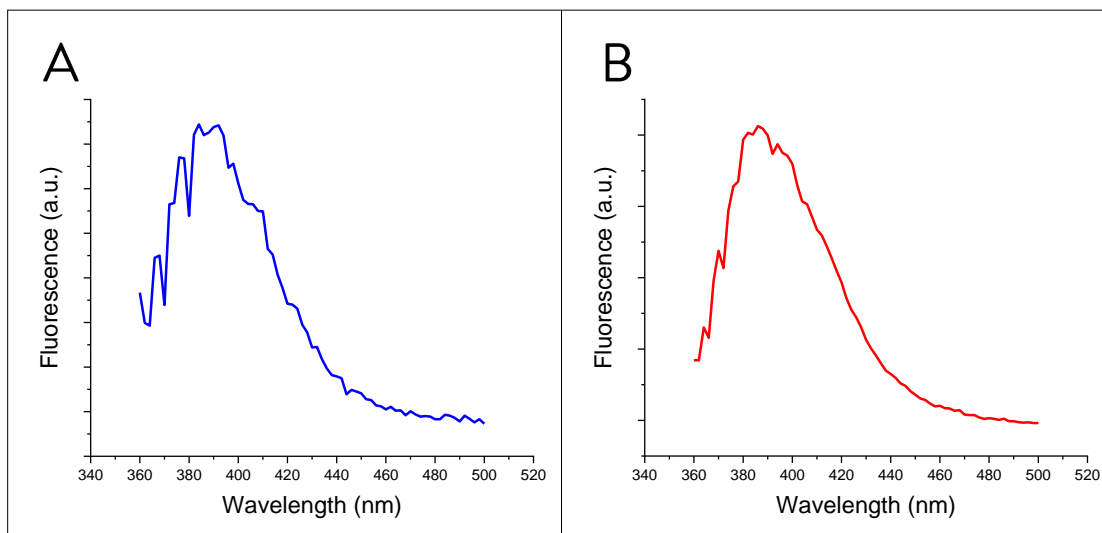
Figure 4.6: *Fluorescence spectra of pep0 after exposure to MMP-7, (A) directly diluted in 10% plasma and (B) immobilized on MBs and then diluted in 10% plasma. Fluorescence intensity in this case does not suggest higher activity since the exact number of peptides used in the two experiments could not be compared since immobilizing the peptides on MBs leads to the loss of some molecules. For this reason, this parameter is not included in the comparison.*

Beads were preferred to surfaces like syringe walls or membranes since they offer greater surface/volume ratio, in the cylindric volume of a syringe, thus allowing to immobilize a greater number of peptides, that, once cleaved, give a stronger fluorescence signal, contributing to an easier naked eye detection.

Finally, magnetic beads were chosen because of their magnetic properties, which permit to easily separate them from the rest of the solution. This allows to take fluorescence readings of the solution containing the cleaved peptides fragments without time consuming processes or disturbances on the signal. MBs can also be coated with maleimide, which permits the chemical binding with peptides, and are readily available in the market.

4.4.2   Limit of Detection of FRET Peptide Immobilized on Beads

Two set of experiments were carried out to establish the LOD for functionalized beads in Milli-Q and in 10% plasma: several dilutions of MMP-7 in both matrices were prepared and added to the MBs solution, adding 99 µL of MMP-7 solution to 11 µL of MBs. After 30 minutes the magnetic beads were separated, and the fluorescence spectra of the remaining solution were recorded.
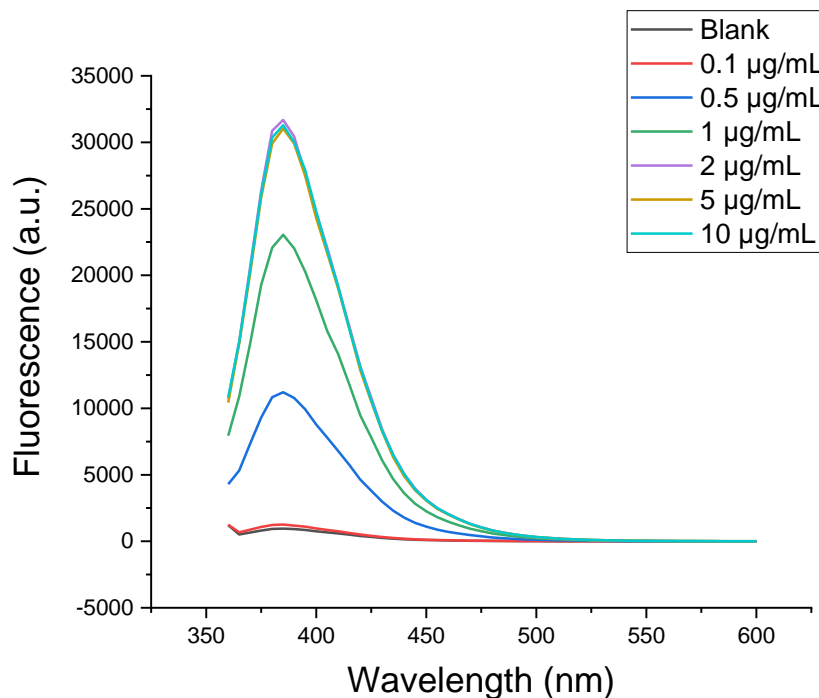
Figure 4.7: *Fluorescence spectra of cleaved fragments of pep0 after exposure to varying concentrations of MMP-7 and separation of MBs, in Milli-Q.*

Figure 4.7 represents the obtained results in Milli-Q: the lowest concentration of MMP-7 clearly detected is 0.5 µg/mL, with 0.1 µg/mL being at approximately the same intensity as the blank reading. These values are already remarkably improved with respect to those obtained with the setup described in Chapter 3, which had a limit of detection of 12.5 µg/mL.

As depicted in Figure 4.8, also the behaviour in plasma was greatly improved, obtaining a LOD in 10% plasma of 10 µg/mL, while the colorimetric functional assay using functionalized gold nanoparticles was ineffective at all concentrations of MMP-7.
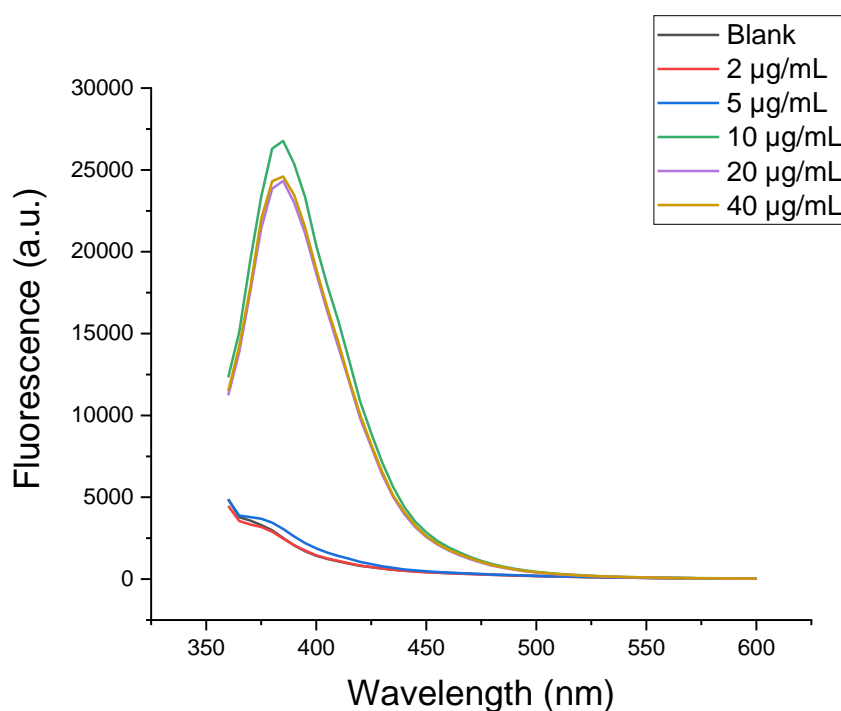
Figure 4.8: Fluorescence spectra of cleaved fragments of pep0 after exposure to varying concentrations of MMP-7 and separation of MBs, in 10% plasma.

The final setup of the functional assay should further decrease the limit of detection in plasma, approaching as much as possible clinically relevant concentrations.

4.5   Optimization of Membranes

As reported at the beginning of this chapter, each membrane included in this functional assay has a specific role. A comparison between several materials and pores dimensions was carried out, establishing the most efficient material and pores dimension for each step.

4.5.1   Plasma Filtration Membrane

The first membrane encountered by the sample has the role to filter out plasma molecules which decrease MMP-7 activity, without preventing MMP-7 from passing through. For this purpose, a set of membranes with different composition and pore size was tested.

As a first step, the efficiency of the exclusion of molecules hindering the activity of MMP-7 was tested, taking out of the equation the possible losses of enzyme when passing through the membrane. These experiments were carried out filtering plasma with the membranes and spiking the enzyme into the filtered solution, then, this solution was added to the functionalized beads, allowing a high concentration of MMP-7 to interact with the peptides. Finally, the fluorescence spectra were recorded after 30 minutes. In this way it was possible to study the effectiveness of the filtration using the exact same amount of enzyme in every experiment.

Both filtration through centrifugation and using a syringe were tested, using both centrifuge tube filters and syringe filters. A large set of membranes was tested in three experiments and are the following:

- CA 0.1 µm, PA 0.1 µm membranes in centrifuge tubes and PES 0.22 µm, PVDF 0.22 µm membranes in syringe filters.
- PCTE 0.01 µm, PCTE 0.03 µm, PEEK 0.03 µm, PES 0.1 µm membranes in reusable cartridges.
- Al_2O_3 porous membranes in reusable cartridges

The alumina membranes were readily excluded because of their brittleness, which made their handling challenging and would significantly reduce the assays robustness.

The membranes tested in the first experiment did not show any beneficial effect for MMP-7 (Figure 4.9): after filtration, the fluorescence signal and therefore the activity of the enzyme did not improve

with respect to that shown in unfiltered plasma. In this case, the reported results show the difference between the fluorescence spectra obtained exposing the MBs to 10 µg/mL and the ones obtained in the respective blank measurement, highlighting the difference in fluorescence intensity caused by the peptide cleavage.
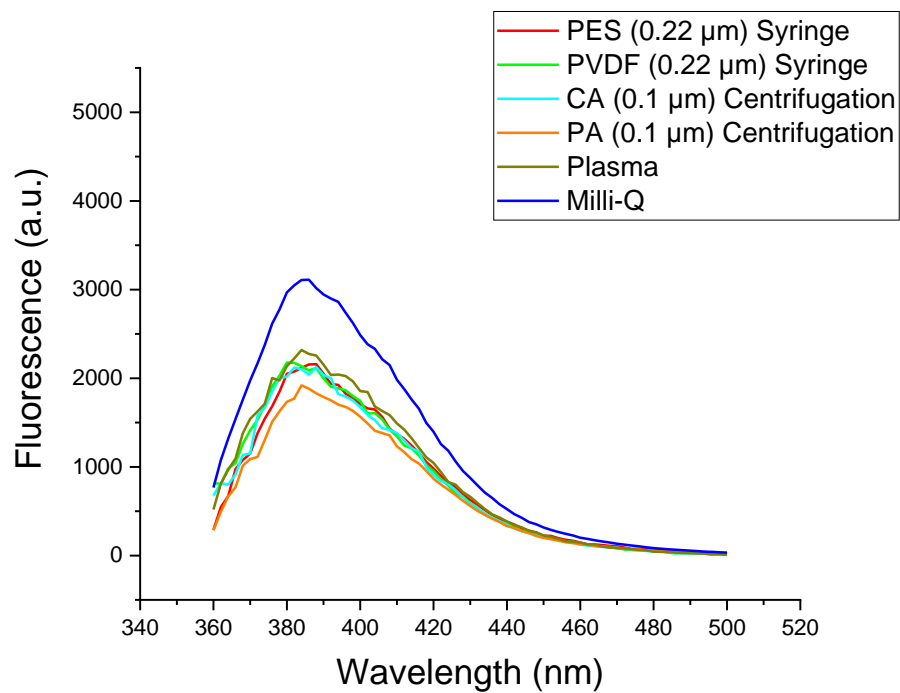
Figure 4.9: *Fluorescence spectra of pep0 after MMP-7 exposure, comparing plasma filtration efficiency of several membranes. The respective blank readings were subtracted to all readings to obtain a clearer representation.*

Experiments using membranes in reusable cartridges showed more interesting results, however filters characterized by very smaller pores (PCTE or PEEK) permitted to hardly push through them the solution, resulting in the in the breakage of the membrane.

However, it was still possible to filter enough volume of 10% plasma solution through the membranes with 0.03 µm pores before breakage, but this was not possible with the 0.01 µm PCTE membrane. As reported below (Figure 4.10) the PES membrane did not show any filtration effect, while both 0.03 µm membranes resulted in an increase of enzyme activity, with PEEK 0.03 µm having the most significant and visible effect on plasma: the solution that passed through it was more transparent and clearer

compared to the starting plasma dilution and, more importantly, the activity of MMP-7 in this solution resulted to be greater compared to that showed in diluted plasma, approaching the fluorescence signal obtained in water.
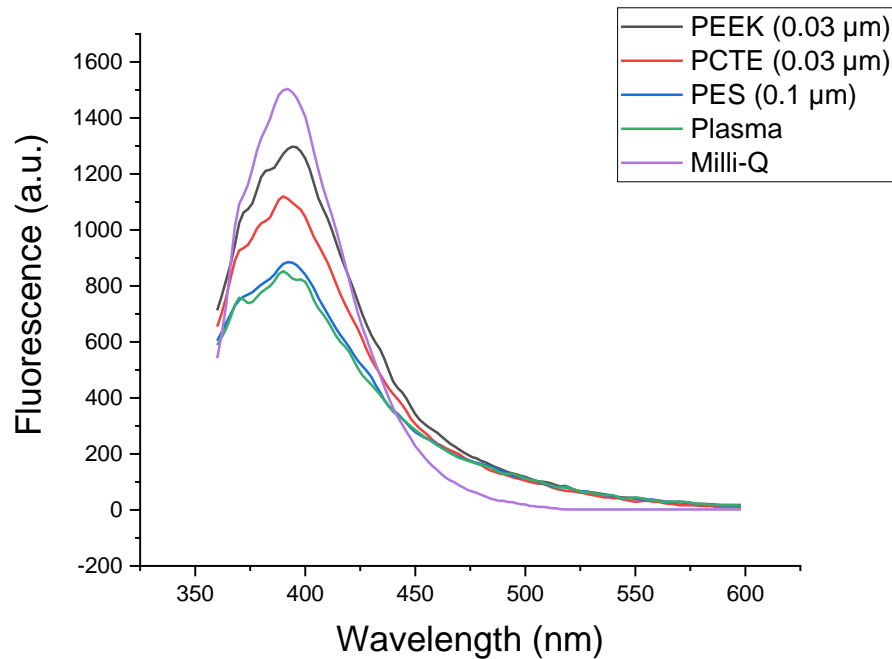
Figure 4.10: Fluorescence spectra of pep0 after MMP-7 exposure, comparing plasma filtration efficiency of several membranes. The respective blank readings were subtracted to all readings to obtain a clearer representation.

Since the solution was not easily flowing through the 0.03 µm pores, PEEK 0.1µm was tested.

The enzyme activity for the two membranes was very similar (Figure 4.11): the signal given by spiking MMP-7 (2 µg/mL) in the filtered plasma was even higher PEEK 0.1 µm, probably due to the contamination caused by the breakage of the filter in the case of the 0.03 µm pores membrane. Moreover, as expected, the solution was easier to push through the filter with larger pores. Finally, a larger pore dimension should allow the enzyme to pass through the membrane more easily, minimizing the losses when the latter is spiked in plasma before filtration.
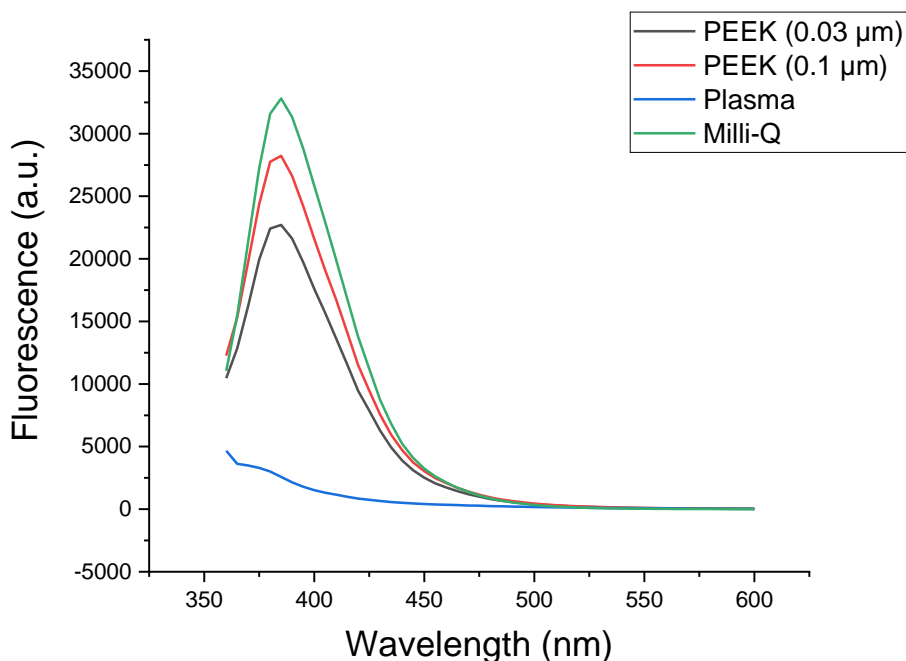
Figure 4.11: *Fluorescence spectra of pep0 after MMP-7 exposure in Milli-Q, diluted plasma and diluted plasma filtered through PEEK membranes with varying pores dimension.*

These results suggest that the filtration efficiency is due to the chemical composition of the membrane and not just to the pores' dimensions, since no large difference between the two PEEK membranes was detected and other membranes with the 0.1 μm pores showed little to no effect. It would be interesting to characterize the membranes and plasma after filtration to understand which molecules are getting stuck on the filter and their interaction with PEEK.

Improving the activity of MMP-7 spiked in the filtered plasma dilution is not enough: in real samples the enzyme is already dispersed in the solution and therefore, when using the functional assay, it passes through the membranes together with the whole sample. Therefore, MMP-7 must pass through the filters to reach the magnetic beads and interact with the peptides. To properly simulate this scenario, the enzyme was spiked into plasma, diluted 10 times and then filtered through the PEEK membrane. After that, the filtered solution was added to the functionalized MBs and, after 30 minutes, the fluorescence spectra were recorded.
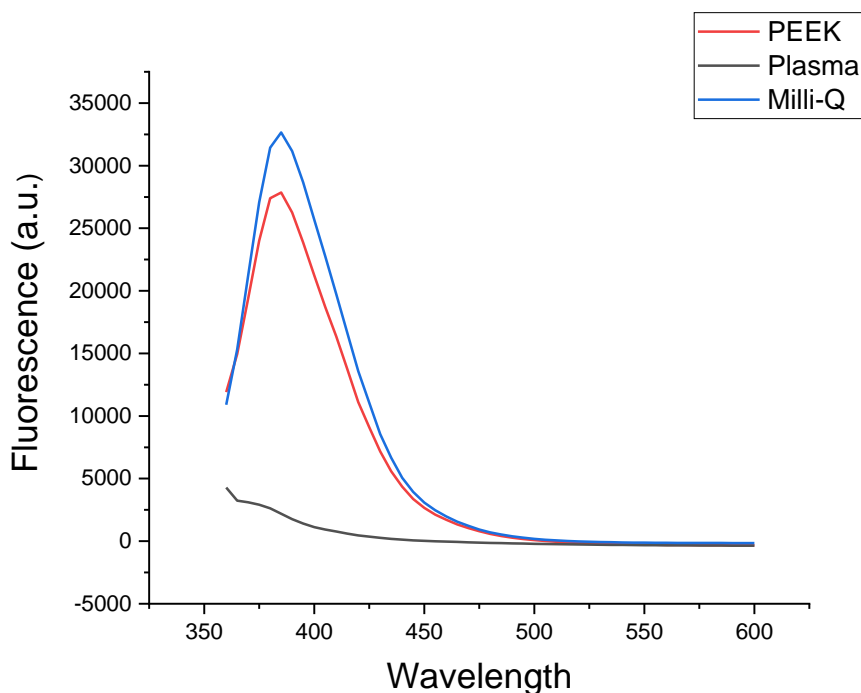
Figure 4.12: *Fluorescence spectra after spiking MMP-7 in diluted plasma, filtering it with PEEK 0.1 µm membrane and adding it to the MBs solution. Compared to the results obtained exposing MBs to MMP-7 in unfiltered plasma and Milli-Q.*

Figure 4.12 shows the spectra recorded for plasma filtered with PEEK (0.1 µm), unfiltered plasma and Milli-Q: It was possible to detect 2 µg/mL of MMP-7 (final concentration after dilution), with minimum losses after passing through the membrane. This was not possible in unfiltered plasma, where the limit of detection was established at 10 µg/mL.

PEEK (Polyether ether ketone) with 0.1 µm pores was therefore chosen as the plasma filtration membrane of the functional assay.

4.5.2 Particle Support Membrane

The role of the second membrane is to support MBs on its surface and release them when the liquid flows through it. For this purpose, this membrane should:

- Allow to deposit the magnetic beads on it.

- Allow solution to flow though it fast enough to release the functionalized MBs.

- Allow the enzyme to flow through without losses.

Since PES membranes are commonly used for immunoassays and show very low binding with biomolecules [135], both 0.22 μm and 0.45 μm PES membranes were tested. Similarly to previous experiments: MMP-7 was spiked in Milli-Q and 10% plasma an was filtered through these filters. The filtered solutions were then added to the functionalized MBs and compared with unfiltered ones.

No significant difference was reported for enzyme activity, meaning that no losses were present due to MMP-7 interaction with PES and therefore both PES (polyethersulfone) membranes are perfect candidates for this role.

4.5.3   Particle Separation Membrane

The final membrane has the role of eliminating the interferences on the fluorescence signal emitted by the cleaved peptide fragments. These interferences include magnetic particles, which give a brownish colour to the solution, interfering with both colour and fluorescence emission, and large plasma molecules that disturb the fluorescence signal. In this case, MMP-7 has already reacted with the peptides and it is not important whether it passes through the membrane or not, since it has no effect on fluorescence or colour.

As reported in Chapter 4.5.1, membranes with 0.1 μm pores or larger did not have effects on the fluorescence signal (with the exception of PEEK which was already used and would not be useful in this case), while the filters with pores 0.01 μm or could not let the solution flow through them and resulted in the breakage of the membrane. Therefore, a membrane with dimension in-between 0.01 μm and 0.1 μm is needed for this role. Moreover, since the cleaved peptide fragments are very small, there should be no significant losses of them when flowing through the membranes with pores larger than 0.01 μm.

It was decided to use the membrane with the smallest possible pores that at the same time allowed the liquid to easily flow through it. Since PES showed no interaction with the cleaved peptide fragments and was the material that let the liquid pass more easily, PES (polyethersulfone) 0.03 μm membrane was chosen for this role.

4.6   Optimization of Fluorescence Signal

In this functional assay, the signal is given by the cleaved peptide fragments and should be visible to the naked eye (by fluorescence emission under UV light). For this reason, this signal must be strong enough to be detected. The next optimizations focus on this aspect, analysing:

- Beads dimensions to have an efficient release of particles in the sample solution

- Optimal concentration of magnetic beads released in the sample solution

- Number of peptides immobilized on the particles

- Properties of the reporter molecule conjugated to the peptide

4.6.1   Magnetic Beads Dimension

The role of the membrane on which the magnetic beads are deposited is not only to support them but to release them when the sample flows through it. Up to this point, the MBs used had a diameter of 50 nm.

When the particles were immobilized on the PES membrane (both 0.22 μm and 0.45 μm), pulling up the solution through these membranes using a syringe resulted in a transparent and clear solution, leading to the conclusion that the particles were not released from the membrane in a sufficient quantity. Different kind of solutions were pulled up, using larger syringes in order to apply more pressure on the solution, and therefore more force on the beads, but no satisfactory results were obtained.

Since chemical or physical interactions between the functionalized particles and the membrane were excluded, it was hypothesized that the reason for this behaviour is that the magnetic beads were not just deposited on the membrane surface but were stuck inside of the pores, making it more difficult to release them when pulling up liquids. For this reason, it was hypothesized that larger particles would be released more easily, as they would not fit inside the pores.

This was confirmed by experimental evidence: when depositing particles with a diameter of 3 μm, they were released easily when pulling up the solution.

Finally, no significant difference in MMP-7 activity was detected between peptides immobilized on 50 nm beads or 3 μm ones. Therefore, 3 μm maleimide activated magnetic beads were used for the next experiments and for the functional assay.

4.6.2   Magnetic Beads Concentration

The fluorescence signal obtained after MMP-7 exposure increases with increasing number of peptides, therefore it increases with higher concentration of functionalized beads. At the same time, if this concentration is too high, the particles are too close to each other, hindering the enzyme diffusion and its interaction with the peptides, reducing the fluorescence signal after exposure. Therefore, the maximum fluorescence is obtained with the highest possible concentration of MBs that does not reduce MMP-7 activity because of steric hindrance.

The initial solution of MBs (10 mg/mL) was diluted 10, 20, 40, 80, 160 and 320 times, then, a high concentration (5 µg/mL) of MMP-7 was added to them. After 30 minutes, the beads were separated with a magnetic separator and the remaining solution containing the cleaved fragments was analysed recording their fluorescence spectra.
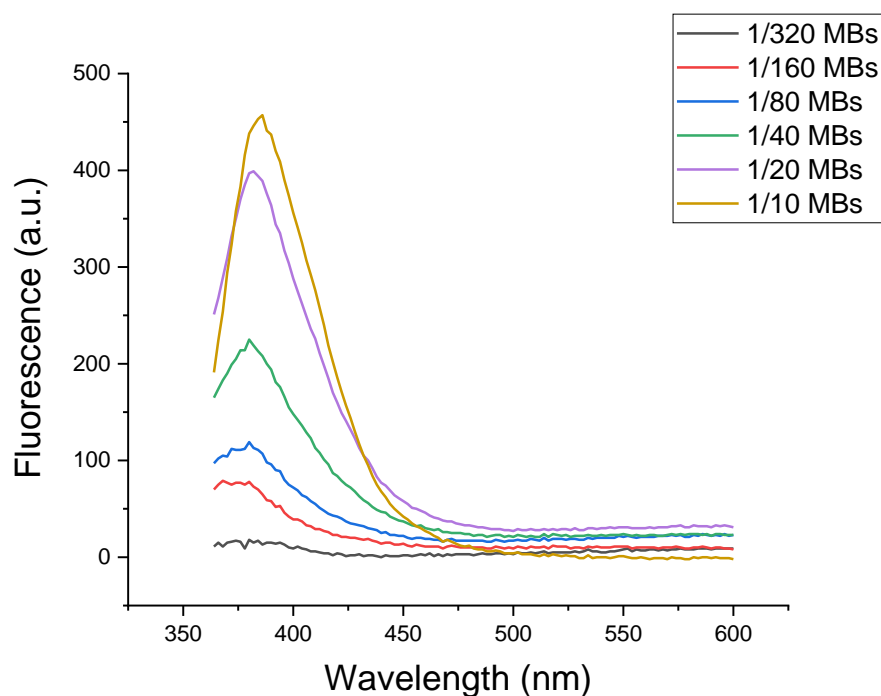
Figure 4.13: Fluorescence spectra resulting from different concentrations of functionalized beads after MMP-7 exposure.

As reported in the graph above (Figure 4.13), the fluorescence intensity maxima increase linearly with increasing MBs concentration up to a certain dilution level, meaning that every peptide present in the solution is getting cleaved, since increasing the quantity of beads means increasing the peptide number and therefore the fluorescence intensity once all get cleaved. This happens until the 20 times dilution is reached: when analysing the 10 times dilution, the fluorescence intensity is not doubling up, this is due to the fact that the particles are too concentrated and close to each other, causing steric hindrance and preventing the enzyme to reach the peptides easily.

The optimal concentration for functionalized beads to properly interact with the enzyme and to give the strongest possible signal is 0.5 mg/mL, or 1/20 MBs.

4.6.3   Number of Peptides Immobilized on Magnetic Beads

The next step to intensify the fluorescence signal is to increase the number of peptides immobilized on the magnetic beads' surface.

The protocol for beads functionalization was repeated, adding 5, 10 and 20 µL of 2 mM peptide to the 400 µL solution in which 80mg of MBs powder (corresponding to 4mg of magnetic beads) was added. A high concentration of MMP-7 was then added to the 20 times diluted MBs and washes' leftovers, once all the available peptides were cleaved, the MBs were separated with the Dynamag-2 magnet and the fluorescence reading of the solution was taken.

Ideally a saturation point would be reached when the maximum amount of peptide immobilized is reached: fluorescence intensity maximum is reached once the concentration of peptide molecules added to the solution is high enough to saturate all the maleimide immobilization sites available on the particle surface. Further increasing the number of peptides in the solution would have no effect on the quantity of immobilized peptides, and therefore on fluorescence signal, since the excess peptides would just be washed away during the following steps.

The results are represented in Figure 4.14: the number of peptides immobilized on the MBs kept increasing, without reaching saturation. However, the readings of the washes showed rapidly increasing

levels of fluorescence intensity, meaning that most of molecules did not bind to the surfaces and got wasted in the process.
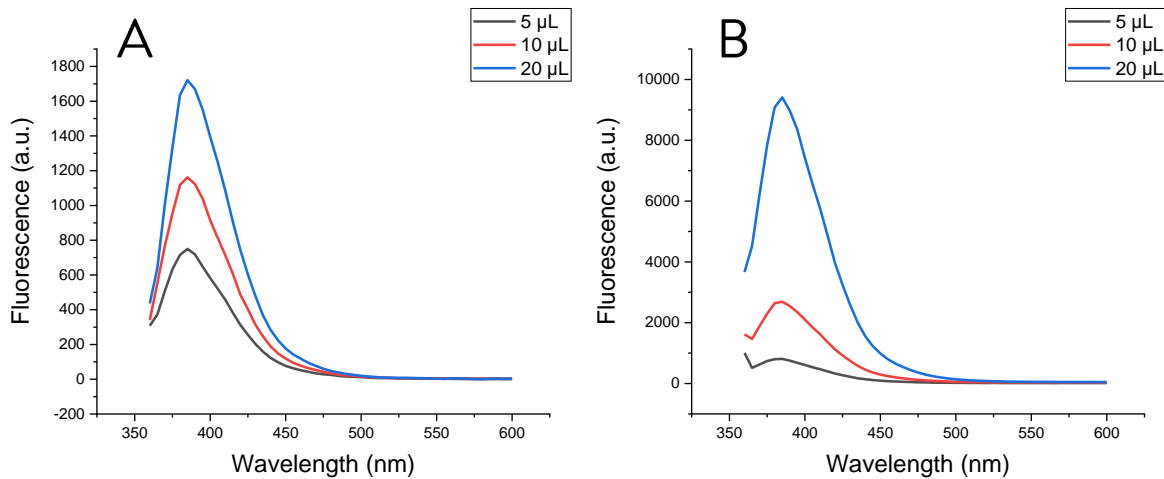
Figure 4.14: *Fluorescence spectra of (A) beads functionalized with varying concentrations of peptide and (B) the respective leftover solution after separation of MBs during washing, after exposure to MMP-7.*

The explanation to the fact that some peptides do not bind to the particles is found in the Brownian motion of molecules: the molecules move randomly in solutions, leading to a certain number of particles never meeting the immobilization sites and remaining dispersed into the solution, independently on their concentration. Moreover, steric hindrance plays an important role also in this case: as more peptides get immobilized on maleimide sites, it will be less probable for other molecules to fit in-between them and reach the binding site.

For this reason, it was decided to not further increase the peptide quantity since this would lead to very high losses of molecules during the washing steps. Since the particles functionalized with 20 μm peptide solution showed a significantly higher fluorescence value with respect to the others, it was decided to use these functionalized beads for the functional assay.

4.6.4   Reporter Molecule

The reporter molecule is the last important factor for the visual detection to be successful, since it gives the final optical feedback for what happens to the peptide when exposed to MMP-7. For an optical biosensor, this molecule can be a chromophore or a fluorophore.

The reporter molecule for these experiments was Mca (Methoxycoumarin-4 acetic acid), a fluorophore absorbing at 320 nm and emitting blue light (405 nm). The intensity of this emission under UV light is difficult to detect by naked eye: it is not very intense, with the additional factor that the blue emission is easily confused with the scattering of transparent objects (as syringes or Eppendorf tubes) which appears blue (Figure 4.15).

Figure 4.15: Cleaved peptide fragments in Eppendorf tubes obtained exposing MBs to different concentrations of MMP-7 in Milli-Q, under UV light (265 nm).

Therefore, the reporter molecule should be optimized, aiming at a more intense signal emitted at more detectable wavelength for the human eye. This molecule must be conjugated with the peptide without losing its properties and, moreover, its dimension should not cause steric hindrance for the enzyme while reaching the cleavage site. To be effective, a chromophore should have a high extinction coefficient (which determines how much a molecule attenuates light at a certain wavelength, absorbing it) leading to a more intense colouring, while a fluorophore should have both high extinction coefficient and a good quantum yield (which determines the number of times a specific event, in this case photon emission by fluorescence, occurs per absorbed photon), converting the absorbed radiation into emitted light efficiently. It is uncommon to see dyes conjugated to peptides without losing their properties, while peptides conjugated with fluorophores are commonly used and readily available, for this reason it was decided to use one of the commonly peptide conjugated fluorophores as reporter molecule.

Among these, the one with best quantum yield and extinction coefficient combination, together with a reasonable dimension, is Carboxyfluorescein (FAM), which, in addition to be the best option as a

fluorophore is characterized by visible a yellow colour, due to its high extinction coefficient. In fact, FAM has an extinction coefficient (ε) of 75,000 cm^{-1}/M at 490 nm and a quantum yield (ϕ) of 0.95 [136], while Mca shows ε= 11,820 cm^{-1}/M at 320 nm and ϕ= 0.18 [137].

The fluorescence emission of the two fluorophores is shown below: when irradiated with UV light, FAM emits a very intense yellow/green light, while the same amount of Mca is barely visible (Figure 4.16), however, this pictures were taken under a 265 nm UV light, which does not correspond to the maximum absorption wavelength for these fluorophores and may alter the results.
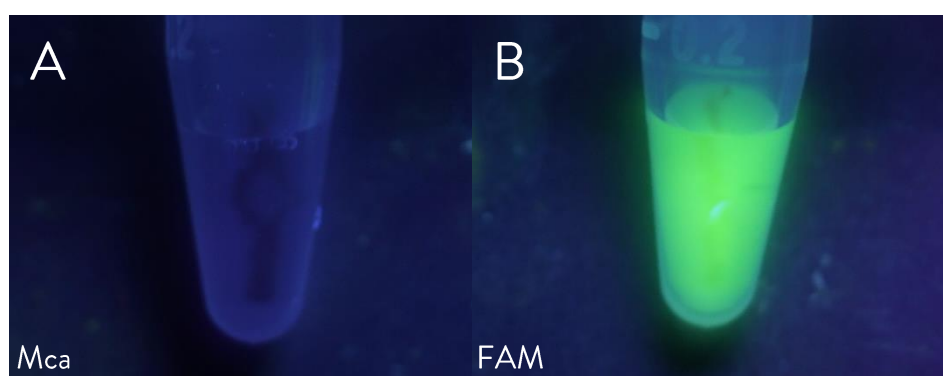
Figure 4.16: (A) Mca and (B) FAM at the same concentration under UV light (265 nm).

Further evidence of this difference is given by the fluorescence spectra of the two solutions, recorded exciting each molecule at the ideal wavelength and with the same reading parameters. As reported in Figure 4.17, the fluorescence emission of Carboxyfluorescein is approximately 3 times more intense than that of Mca: the maximum fluorescence intensities were recorded at ~8000 for Mca and at ~25000 for FAM (emission peak is at ~520 nm, the lower wavelength spectra is due to the excitation wavelength being very close to the emission one).
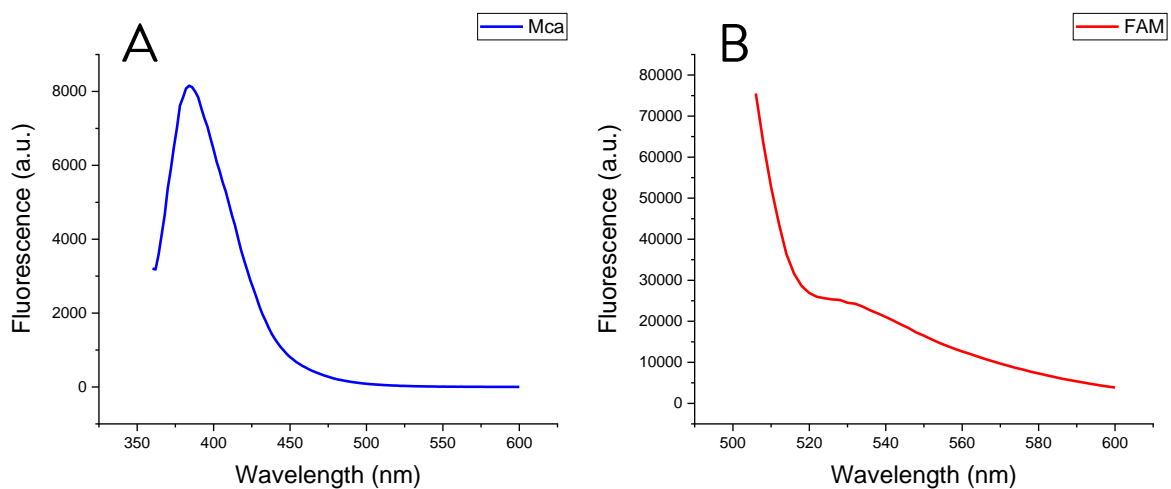
Figure 4.17: *Fluorescence spectra of (A) Mca excited at 320 nm, (B) FAM excited at 490 nm.*

Finally, the peptide sequence used until now shows both a fluorophore (Mca) and a quencher (Dpa). Since in the final setup of the functional assay, the peptides are immobilized on the particles and the fluorescence signal is observed in the reporter zone, where just the cleaved peptide fragments have passed through, the quencher molecule that previously remained on the MBs is not necessary anymore. However, adding a quencher molecule to the peptide chain offers the possibility to distinguish between cleaved peptide fragments and peptides that were physically stuck in-between bound peptide chains or beads instead of being chemically bound and that can be released without peptide cleavage, reducing the possibility of false positives. For this reason, it would be appropriate to couple FAM with an appropriate quencher molecule.

Since the final optimized peptide will be used in the functional assay, it is important to verify if this fluorophore is able to pass through this last filter. This was done functionalizing magnetic beads with another peptide sequence, named FAM-ARRA, which is labelled with FAM and gets cleaved by trypsin.

A simple assay experiment was carried out in Eppendorf tubes: 0; 1 and 10 µg/mL (final concentration) Trypsin were added to the 20 times diluted solution of functionalized magnetic beads in PBS 0.05% Tween 20. After 10 minutes, the solutions were pushed through 0.03 µm PES membranes placed in reusable cartridges and the filtered solutions were analysed.

Two pictures of the solutions are reported below. Figure 4.18 (A) is under daylight, in these conditions, it is already possible to see the yellow colour given by FAM, due to its high extinction coefficient, suggesting that the peptide has been cleaved and passed through the membrane. Figure 4.18 (B) shows the fluorescence under UV lamp: in both cases the fluorophore gives very high intensity, confirming that FAM, conjugated to the cleaved peptide fragment, is able to pass through the membrane.
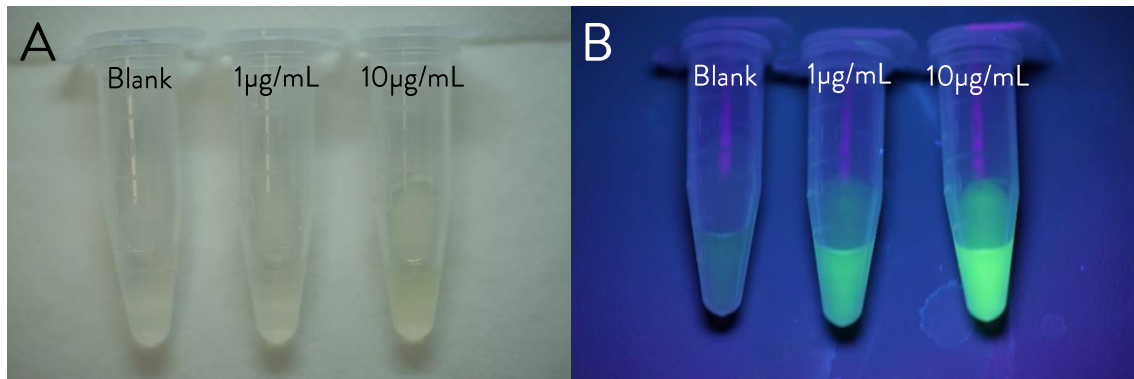
Figure 4.18: *Cleaved FAM-ARRA fragments after functionalized beads exposure to 0.1 μg/mL and 10 μg/mL of MMP-7, (A) under daylight and (B) under UV light (265 nm) and filtration through 0.03 μm PES membranes.*

As shown in Figure 4.18 (B), it is still possible to see a slight fluorescence in the blank sample, this is due to the absence of quencher molecule in the peptide sequence and, as explained before, some of these peptides can be released and then pass through the particle separation membrane. The fluorescence spectra of the solutions, with excitation wavelength at 490 nm, are reported in Figure 4.19, confirming the increasing fluorescence intensity with increasing enzyme concentration, after an incubation time of 10 minutes.
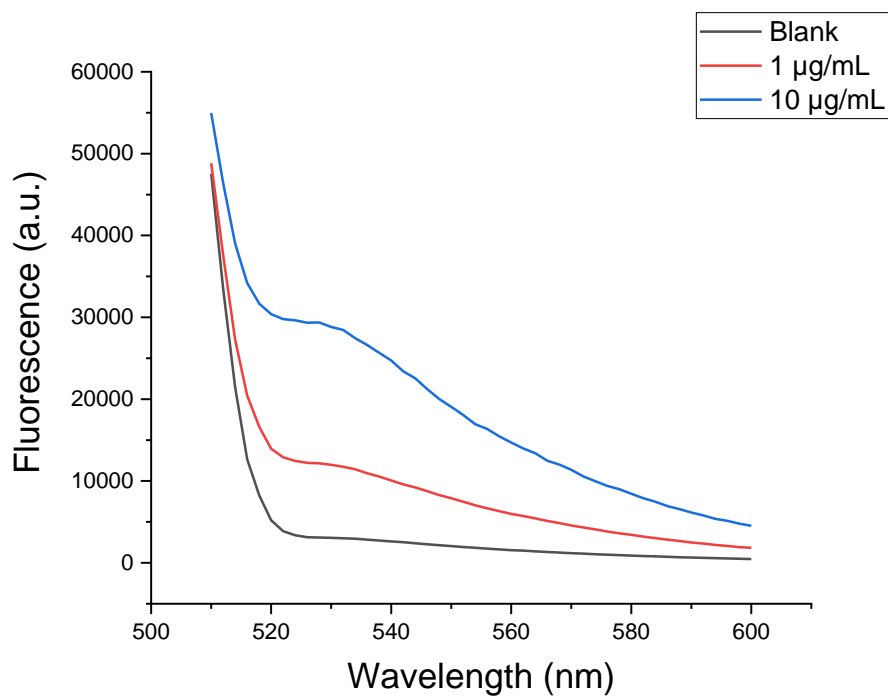
Figure 4.19: Fluorescence spectra (excitation wavelength: 490 nm) of cleaved peptide fragments solution obtained after FAM-ARRA functionalized beads exposure to 0.1 μg/mL and 10 μg/mL of Trypsin and filtration through 0.03 μm PES membranes.

The 0.03 μm PES membranes after filtration of the beads solutions are show below (Figure 4.20), showing the beads remained on the membrane.
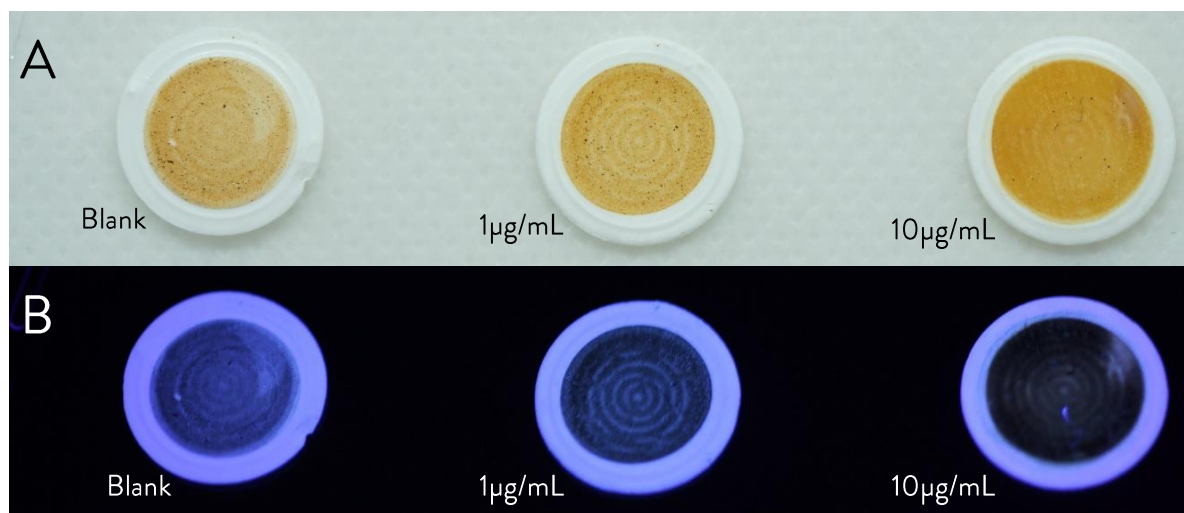
Figure 4.20: 0.03 μm PES membranes after filtering FAM-ARRA functionalized MBs after exposure to varying concentrations of Trypsin, (A) under daylight and (B) under UV light (265 nm).

It is interesting to observe them under UV light, in fact, since no quencher is present in this peptides, the membranes containing MBs with intact peptides (blank experiment) look more luminous than the one with all the peptides cleaved (higher concentration of trypsin) with the one in the middle showing a colour in-between the two since it still contains some fluorophores bonded due to the low concentration of enzyme and limited incubation time.

The results obtained with this optimization were not used for the next experiments: in this project, the usual pep0 sequence labelled with Mca and Dpa was used. In this way, it was possible to further optimize the functional assay parameters without adding other variables.

4.6.5   Buffer

The MMP-7 digestion experiments on MBs were carried out both in 10 mM PBS and Assay buffer (20 mM Tris, 10 mM $CaCl_2$, 20 mM $ZnCl_2$, 0.05% Brij). As reported below (Figure 4.21), no substantial difference is detected between the two cases: the slight difference in fluorescence intensity is due to the fact that the buffer enhances the fluorescence emission, not the enzyme activity.
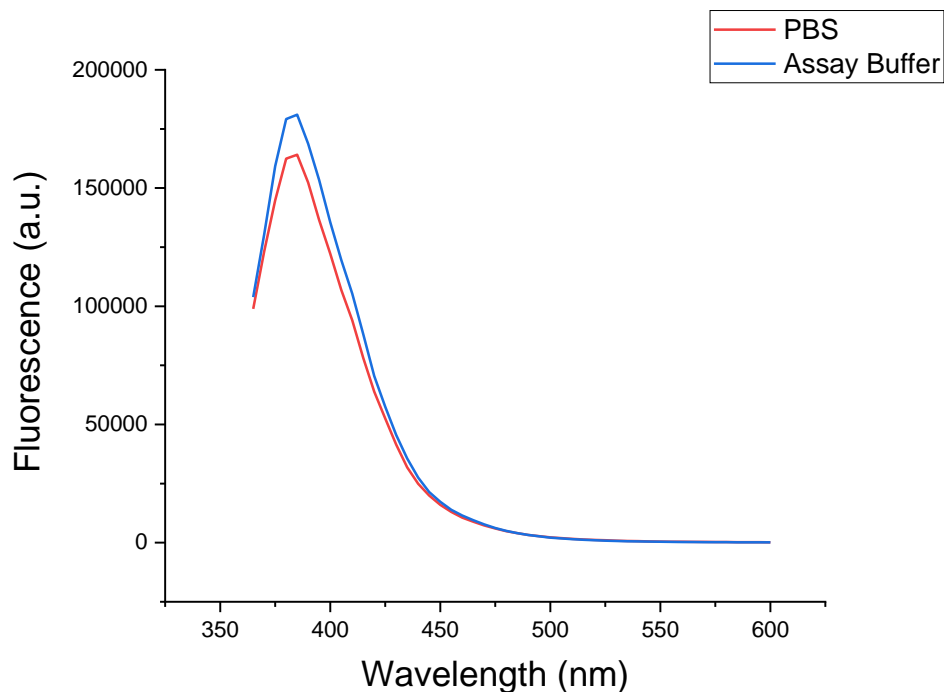
Figure 4.21: Fluorescence spectra after pep0 functionalized beads to MMP-7 in different buffers.

Since PBS is closest buffer that resembles human serum and is commonly used in biosensing experiments, it was decided to use this buffer for the functional assay, both for detection in buffer and for plasma dilutions.

4.7   Optimization of Particle Release

The following optimizations concern the second membrane (PES), the MBs deposited on it and their release.

Since particle deposition and release in solution occurred equally for both functionalized and blank magnetic beads, suggesting that no interaction was present with PES in both cases, all the of the optimization experiments were carried out with blank 3 μm maleimide activated magnetic beads, assuming that the results are equivalent for functionalized beads.

4.7.1   Beads Deposition on Membranes

The first optimization concerns the technique used to deposit the beads on the membrane: this technique must be able to control the number of deposited beads, allowing to compare the effects when varying this parameter and to obtain repeatable results, and must permit a homogeneous distribution of particles over the whole membrane, improving the release of beads even with liquid flowing through the membrane through specific areas instead of the whole filter.

The functionalized beads were deposited in 3 different ways, on 0.22 μm PES membranes:

- Lyophilizing the MBs and depositing them manually on the membranes
- Drop casting the MBs solution on the membrane and letting it dry
- Pushing through the membrane the solution containing the MBs

The first two method were not effective for different reasons, while the third one turned out to be the best alternative:

- Lyophilized magnetic powder is difficult to handle and therefore obtaining a homogeneously coated membrane is challenging and involves possible losses of particles. Moreover, due to the losses and the impossibility to weight this powder, it is not possible to properly control the

number of particles deposited on the membranes resulting in low repeatability and difficulties in optimizing this step.

- Drop casting allowed to control the amount of MBs, knowing the concentration of their solution and the volume casted on the membrane. However, this technique required long times to dry at room temperature, and a higher temperature for prolonged times may degrade the peptides. In addition to this, during the time required for the drop to dry, the MBs were able to move in the solution and aggregate, resulting in a poor homogeneity after drying.

- Pushing through the solution allows to easily control how many particles are deposited on the membrane: the beads remain on the top of the membrane while the rest of the solution passes through. The number of particles can be controlled varying the concentration of the initial solution or its volume. Moreover, increasing the volume of the solution pushed through allowed to obtain more a homogeneous coverage, since it allows to reach and wet the whole area of the membrane.

Therefore, the MBs were deposited on the membranes pushing them though the filter cartridges. This technique was briefly optimized, improving the ability to control the number of deposited particles, their distribution and the time needed to dry the membrane, obtaining the following protocol:

The functionalized beads were immobilized slowly pushing the diluted beads solution through the membrane with a 3mL syringe. 500 µL of Milli-Q were pushed through the membrane twice to make sure that every bead reached the membrane. The membrane was then dried pushing through air (3mL per 3 times) and waiting at least 30min before use.

4.7.2 Pores Dimension of Particle Support Membrane

It was previously established that both 0.22 µm and 0.45 µm PES membranes did not cause losses from the enzyme point of view. After the dimension of beads was determined, a study on the homogeneity of MBs deposition and their release when the sample flows through the membrane was carried out, comparing the two membranes.

The deposition of MBs was carried out following the established protocol: 600 µL of particles solution, which was 20 times diluted with respect to the initial concentration, was pushed through the membrane. After this, 500 µL of PBS was pulled up to observe the release of beads into the solution.

The following pictures show the comparison between the two sets of membranes.
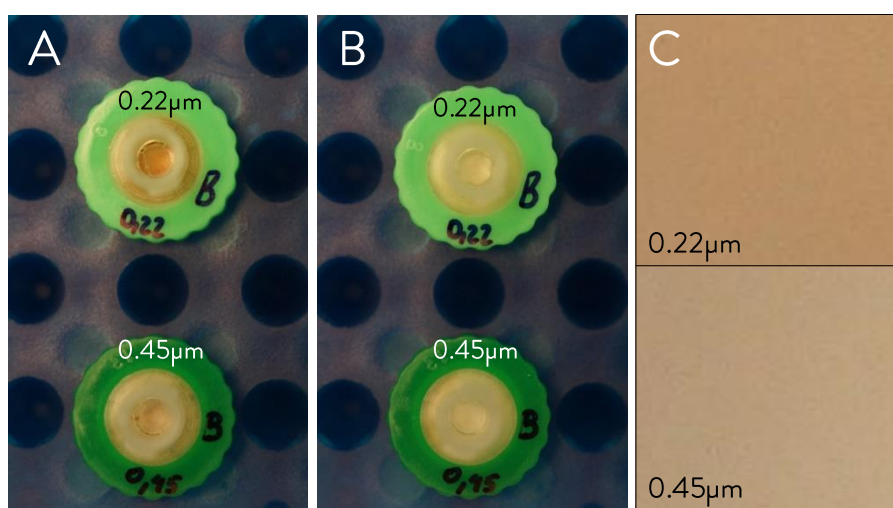
Figure 4.22: *0.22 µm and 0.45 µm membranes (A) after MBs deposition and (B) after pulling up solution and release of MBs. (C) Comparison of pulled up solutions, pixels taken from Eppendorf tubes pictures for colour comparison.*

As reported in Figure 4.22 (A), 0.22 µm PES allows a more uniform coverage of particles, this may be due to the rugosity influence on the particles movement: rugosity caused by small pores can barely influence the movement of large particles, as the pores get bigger, they start to influence the particles movement more, leading to a reduced mobility once they touch the surface. Therefore, the particles are not able to distribute homogeneously on the membrane. In fact, the particles seem to remain on the edges of the filter, which is the first area reached by the solution when pushing it through.

Figure 4.22 (B) shows the remaining particles on the membranes after pulling up the solution. This is useful to predict how many particles have been released but also to know if the particles are released evenly from the whole membrane. The white colour of 0.22 µm PES suggests that approximately all the beads have been released in the solution, with few particles remaining on the edge of the filter, while this does not happen with 0.45 µm PES, where a much higher number of particles is shown near the edges.

Finally, the colour intensity of the solution pulled up from the 0.22 µm membrane shows a much darker colour, as reported in Figure 4.22 (C), suggesting a higher concentration, and therefore a greater release of particles. This was confirmed by the absorbance spectra of the two pulled up solutions (Figure 4.23).
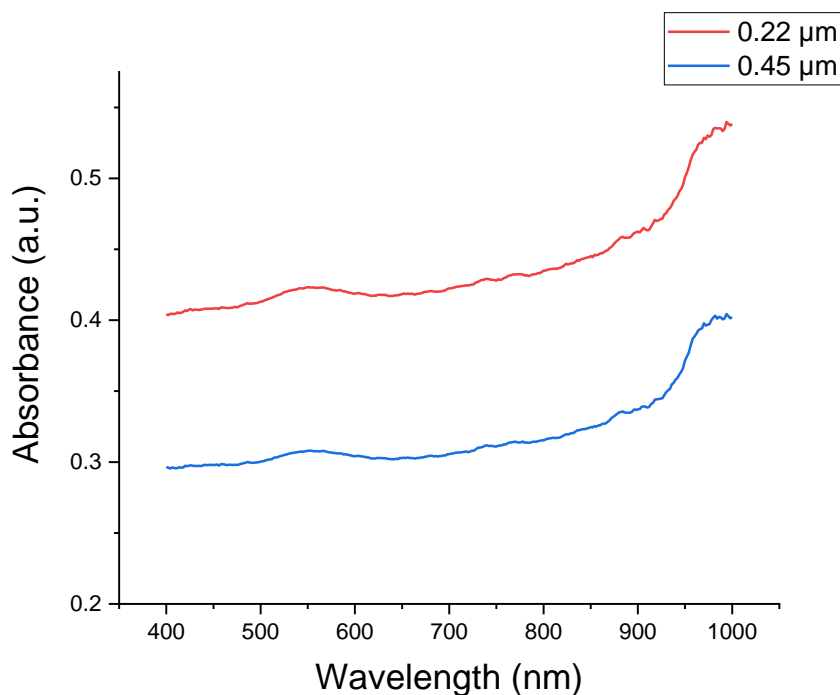
Figure 4.23: Absorbance spectra of pulled up solution through 0.22 µm and 0.45 µm PES membranes.

Since these solutions contain the same type of beads diluted in 10 mM PBS, the difference in absorbance and scattering intensity is accountable to the difference in concentration. The Beer-Lambert law (Equation 4-1) in fact, states that the absorbance, or extinction in this case since scattering is involved, at a determined wavelength of a solution linearly increases with the concentration of the solute:

$$A = \varepsilon \, l \, c$$

Equation 4-1: Beer-Lambert law. A: absorbance, ε: molar attenuation (absorption and scattering) coefficient, l: optical path length, c: concentration of the attenuating species.

The difference between the release of beads from the two sets of membranes was hypothesized to be due to the different speed at which the solution passes through the membranes' pores: as stated by the

Darcy's Law (Equation 4-2), a solution subject to a constant force (in our case applied by the syringe) flows at a higher speed with decreasing pore dimension.

$$Q = \frac{-k\,A}{\mu}\,\frac{dp}{dx}$$

Equation 4-2: Darcy's law. Q: volumetric flow rate, k: permeability, μ: viscosity, A: cross-section area, p: pressure, x: length.

When passing through the membrane, the solution with a determined speed hits the beads, which are then pushed towards the flow direction and released into the solution. A higher speed results in a greater force with which the MBs are pushed into the solution and therefore more beads released.

In conclusion, the most efficient membrane to deposit and release the MBs on is 0.22 μm PES.

4.7.3   Tween 20 Concentration in PBS

The release of magnetic beads was further optimized with the addition of detergent molecules (Tween 20) to the PBS solution, the release of particles was improved since detergent generally contribute to separate the various elements present in a solution.

A similar experiment to the previous one was carried out: with the pulled-up solution being 10 mM PBS with the addition of 0.01%, 0.025% and 0.05% Tween 20.

Figure 4.24 confirmed the hypothesis: with increasing concentration of detergent molecules, the concentration of particles released in the pulled-up solution increased. In addition, the presence of Tween 20 did not influence the enzyme activity and could be used with no drawbacks.
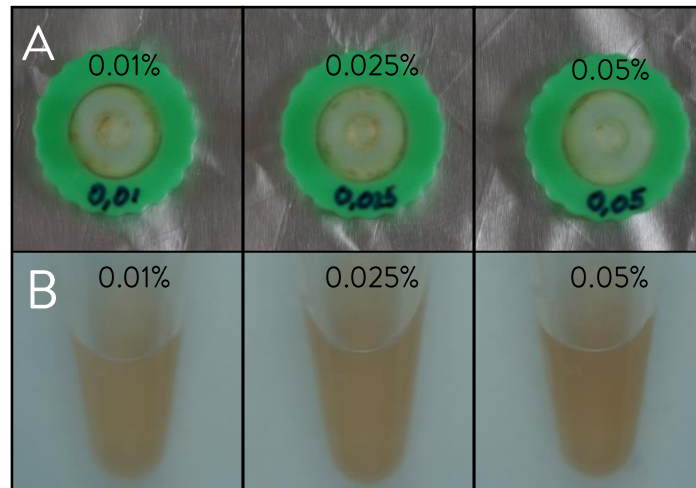
Figure 4.24: (A) Membranes after pulling up 10mM PBS with varying concentration of Tween 20 and releasing the MBs. (B) Pulled up solution from each membrane.

Further evidence of this is provided by the absorbance spectra of these solutions: the absorbance increased with increasing Tween 20 concentrations (Figure 4.25)
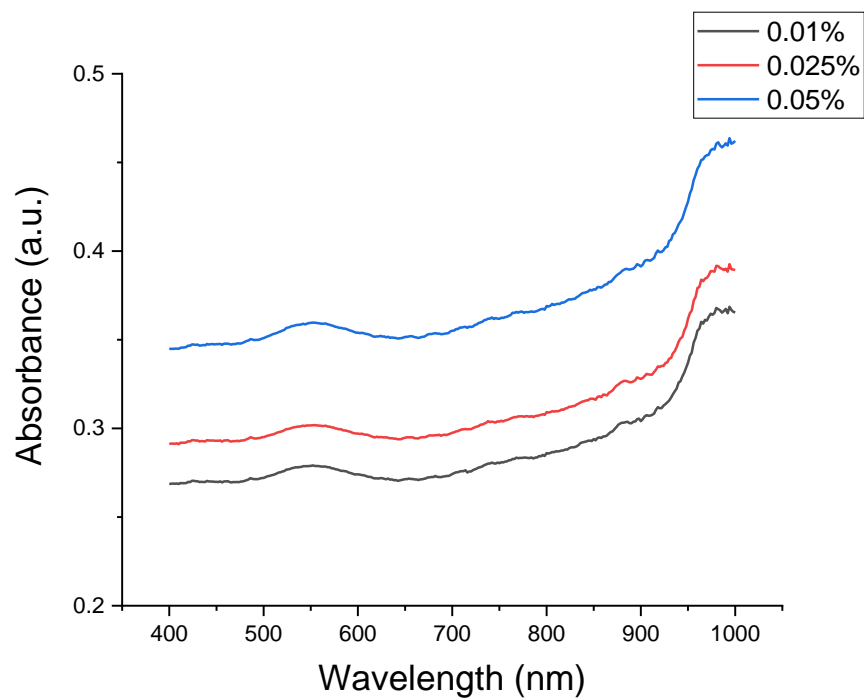
Figure 4.25: Absorbance spectra of the pulled op solutions with varying concentration of Tween-2.

Thus, the optimized buffer used for the following experiments was: 10 mM PBS 0.05% Tween 20.

4.7.4 Number of Beads Deposited on Membrane

In a previous experiment (Chapter 4.6.2), the optimal concentration of functionalized MBs was found to be 0.5mg/mL, which corresponds to a 20 times dilution of the initial concentration of beads. The next step in this optimization process is to make sure that the pulled-up solution shows the same beads concentration as the optimized one.

Since the pulled-up volume was fixed at 500 µL, together with its composition and volume, the only variable left was the amount of MBs deposited on the membrane.

For this purpose, MBs were immobilized on a set of 5 membranes (0.22 µm PES), pushing through them different volumes of 20 times diluted MBs solution: 100, 200, 400, 600, 800 µL. Each of these membranes was then used to pull up 500 µL of PBS 0.05% Tween 20. The membranes in Figure 4.26 (A) show an increasing amount of MBs deposited on the filters, corresponding to a darkening in their colour, which remained uniform enough though the membranes for all volumes pushed through.
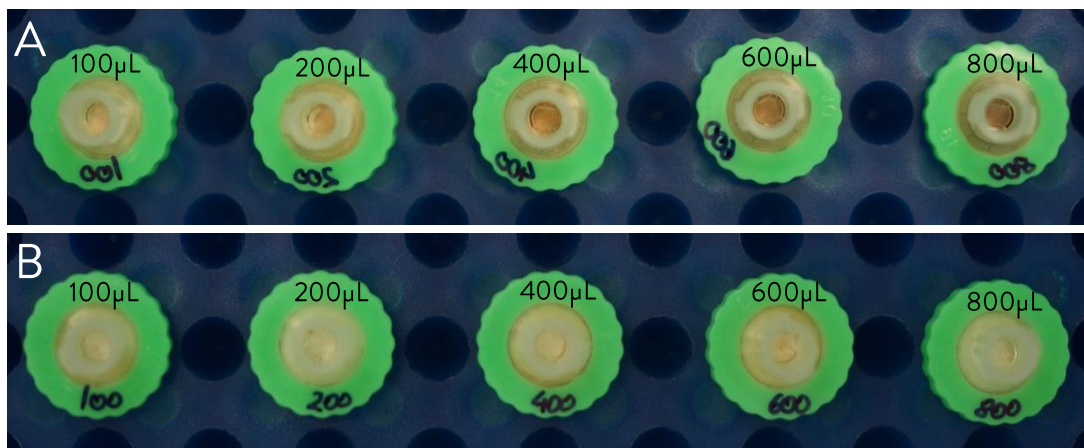
Figure 4.26: (A) Membranes with varying amount of deposited MBs. (B) Membranes, previously supporting varying number of MBs, after pulling up solution through them, releasing the MBs.

After pulling up the volume, the 5 membranes looked clearer, with some still showing a relatively high amount of MBs left, as shown in Figure 4.26 (B). The random way in which beads remain stuck on membranes, leads to the fact that the efficiency of particles release does not strictly depend on the number of the MBs deposited on the surface: in fact, the membrane where 600 µL or even 100 µL were deposited show a darker colour with respect to the 800 µL one after pulling up the solution. From this,

we can conclude that there will always be a varying number of beads stuck on the membrane and therefore lost, but this is acceptable up to the degree showed in this experiment.
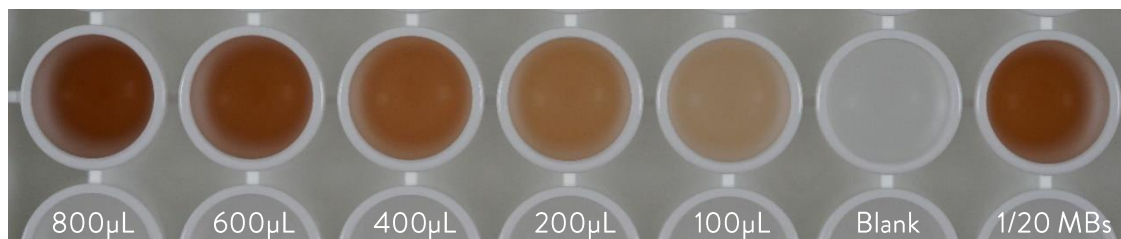
Figure 4.27: *Pulled up solution through the membranes represented in Figure 4.25, Blank and 1/20 MBs solutions were added for comparison.*

As reported in Figure 4.27, higher amounts of MBs deposited on the membrane resulted in a higher a concentration in the pulled-up solution. For comparison, the solution of 20 times diluted MBs was added. Since the 600 μL solution has approximately the same colour, and therefore same concentration, of the optimal concentration required for the assay.
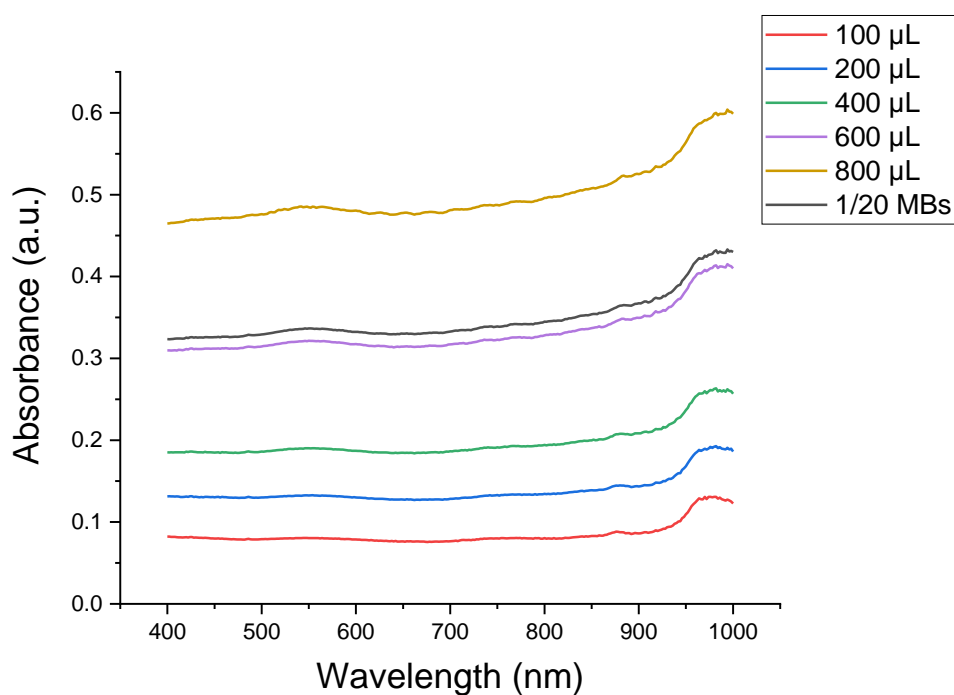
Figure 4.28: *Absorbance of the pulled up reported in Figure 4.26.*

84

This result was confirmed by the absorption spectra of these solutions (Figure 4.28): the concentration of 1/20 MBs solution and of the pulled-up solution through the 600 μL membrane were approximately the same, leading to the conclusion that the optimal amount of MBs solution to use for beads deposition, when pulling up 500 μL of sample, is 600 μL.

4.7.5   Sample Volume

Until now, the pulled-up volume was fixed at 500 μL. This last optimization experiment was carried out to check the release of MBs with different pulled-up volumes: 250, 500, 1000 μL were tested using membranes with the previously optimized number of particles deposited. The membranes after this procedure are shown below (Figure 4.29).

Figure 4.29: PES membranes after pulling up varying volumes of solution and releasing MBs.

There is no significant difference between 500 and 1000, suggesting that 500 μL is already enough volume to release most of the particles, even if there is a very small difference when comparing edges of the membrane. The first membrane instead, shows a darker colour, suggesting that pulling up 250 μL is not enough to release this amount of MBs.
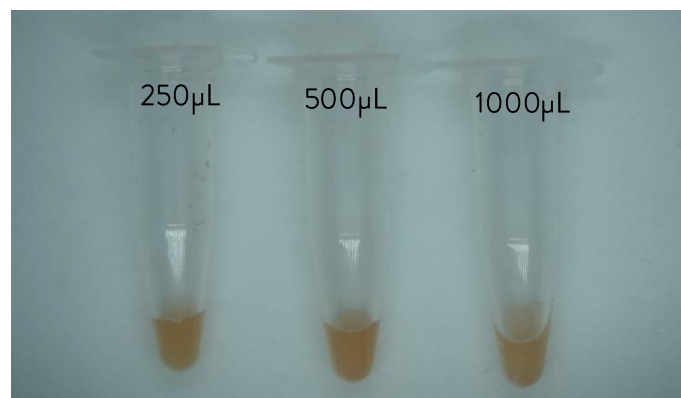
Figure 4.30: Solutions pulled up through the membrane in Figure 4.28, reduced to the same volume for comparison.

This result is confirmed by the pulled-up solutions, which were reduced to the same volume keeping their concentration constant (Figure 4.30). The higher concentration was detected in the middle tube, corresponding to 500 µL, while the others look slightly clearer. This confirms that this volume is enough to release approximately all the nanoparticles. In fact, pulling up 1000 µL may have taken up more beads but these were diluted in a larger volume, resulting in a lower concentration. The result for 250 µL were unexpected: some particles left on the membranes were predictable but also the concentration of the solution is lower with respect to the 500 µL. The reason for this was hypothesized to be that a low volume of pulled-up solution was not enough to wet the whole membrane, leaving some areas of the filter and thus some MBs unaffected by the liquid flow.

4.8   Assays for MMP-7 Activity Detection

Once the parameters were optimized, assays in solution and simulating the proposed setup were carried out, establishing the limit of detection both in buffer and plasma.

4.8.1   In Solution Assays

The in-solution assays were carried out in a total volume of 250 µL. The MMP-7 dilutions were prepared and then added to the MBs solution, diluting it 20 times. After 30 minutes, the magnetic beads were separated, and the fluorescence scans of the solution were taken. In order to not consider the fluorescence due to plasma or other factors, the results shown represent the reading for each well after subtracting the data recorded for the blank reading (0 µg/mL MMP-7).

The MMP-7 concentrations reported below are calculated over the final volume of the assay volume of (MBs, plasma, buffer and enzyme together), while the functionalized beads concentration in the same solution is fixed at 0.5 mg/mL (1/20 MBs).

4.8.1.1   Buffer

The first experiments were carried out in PBS 0.05%Tween 20 at 0, 0.125, 0.25, 0.5, 11 2.5, 5, 10, 15, 20 µg/mL of MMP-7.
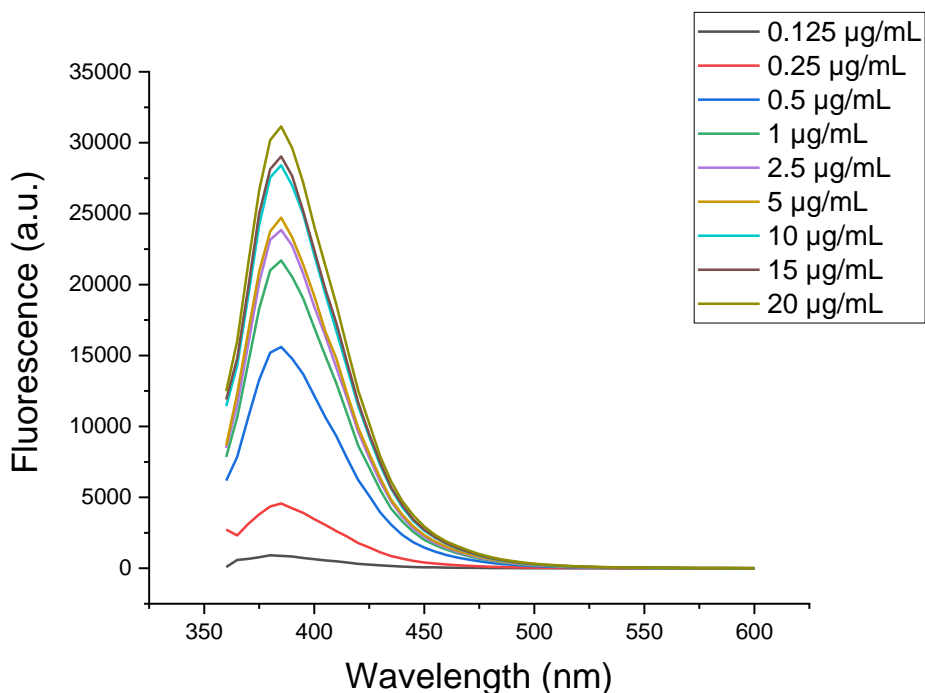
Figure 4.31: *Fluorescence spectra after exposing functionalized MBs to varying concentrations of MMP-7 in 10 mM PBS 0.05% Tween 20. Blank reading was subtracted to each reading for a clearer representation.*

As reported in Figure 4.31. when diluted in PBS 0.05% Tween 20, MMP-7 was detectable down to 0.25 µg/mL. Moreover, it is interesting to see how low concentrations like 1 µg/mL give a signal comparable to the highest concentration, suggesting that a relatively low concentration is already enough to cleave the majority of the peptides in 30 minutes, supposedly with a slower kinetics.

In comparison, the limit of detection in buffer with the previous setup (gold nanoparticles functionalized with JR2EC peptide) was 12.5 µg/mL. This means that pep0 immobilized on 3 µm beads has a sensitivity 50 times greater than the AuNP setup.

4.8.1.2   Plasma

The same experiment was carried in 10 times diluted plasma, the concentrations in the total final volume were:

- 1/10 human plasma (containing MMP-7)
- 17/20 PBS 0.05% Tween 20
- 1/20 MBs from the stock solution

In these experiments, MMP-7 was first spiked in plasma, then diluted and finally added to the MBs solution.

Varying concentrations of MMP-7 were analysed: 0, 0.125, 0.25, 0.5, 11 2.5, 5, 10, 15, 20 µg/mL (concentrations calculated over the final volume).
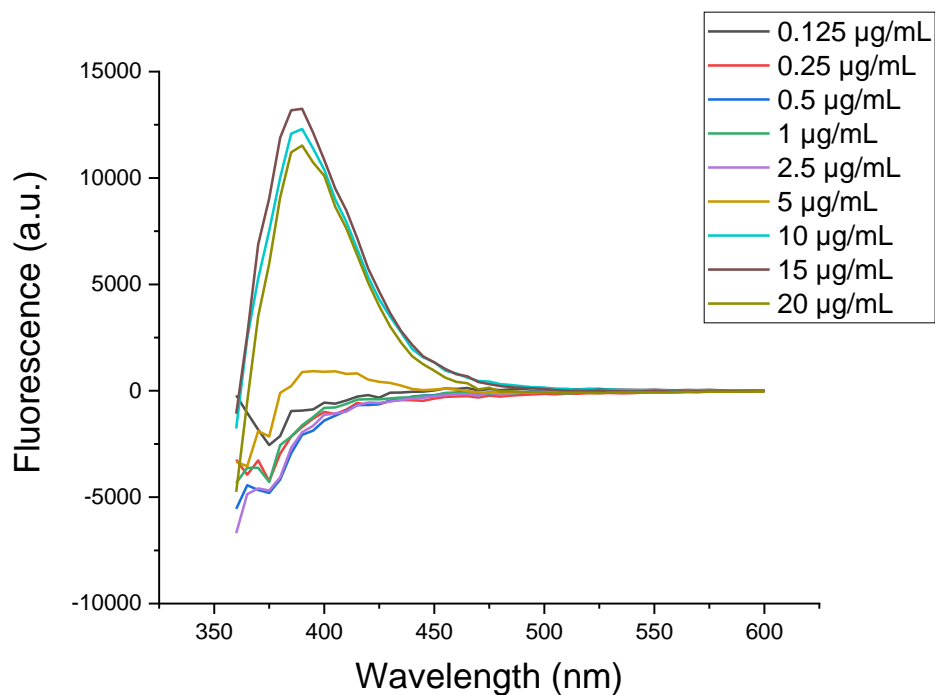
Figure 4.32: Fluorescence spectra after exposing functionalized MBs to varying concentrations of MMP-7 in 10% plasma (diluted in 10 mM PBS 0.05% Tween 20). Blank reading was subtracted to each reading for a clearer representation.

In this case the results showed a lower sensitivity with respect to the experiments in buffer (Figure 4.32), with the limit of detection established at 5 µg/mL. Also in this case, higher concentrations had similar outcome, suggesting a complete cleavage of peptides in 30 minutes. This result already improved the LOD found in the plasma assays carried out before optimizations, for which the signal at 5 µg/mL of MMP-7 was negligible, meaning that the optimizations carried out improved the enzyme detection in solution, even without plasma filtration involved.

4.8.2   Assays Using a Syringe

The following assays were carried out with a syringe setup: similarly to what would happen with real samples, the sample containing MMP-7 was prepared and then pulled up through the 0.22 µm PES membrane covered with the functionalized beads. In this case the concentrations of MMP-7 and other components are calculated on the volume of 500 µL, prior to pulling up and without considering the MBs, which were released in the sample once the solution passes through the membrane.

After pulling up the sample through the PES membrane, the solution was left in the syringe for 30 minutes, then, it was transferred the Eppendorf tube for magnetic separation of the particles.

4.8.2.1   Buffer

The samples analysed were prepared in PBS 0.05% Tween 20 at different concentrations of MMP-7: 0, 0.25, 0.5, 1, 5, 10, 20 µg/mL.

The following pictures show that even after the optimization steps, the membranes did not release particles uniformly. The membranes were coated uniformly and with the same number of beads (Figure 4.33 (A)), but once the solution was pulled up, a varying amount of beads remained stuck in the cartridge (Figure 4.33 (B)), resulting in very different concentrations when comparing the pulled up solution (Figure 4.33 (C)), in which the enzyme detection took place.
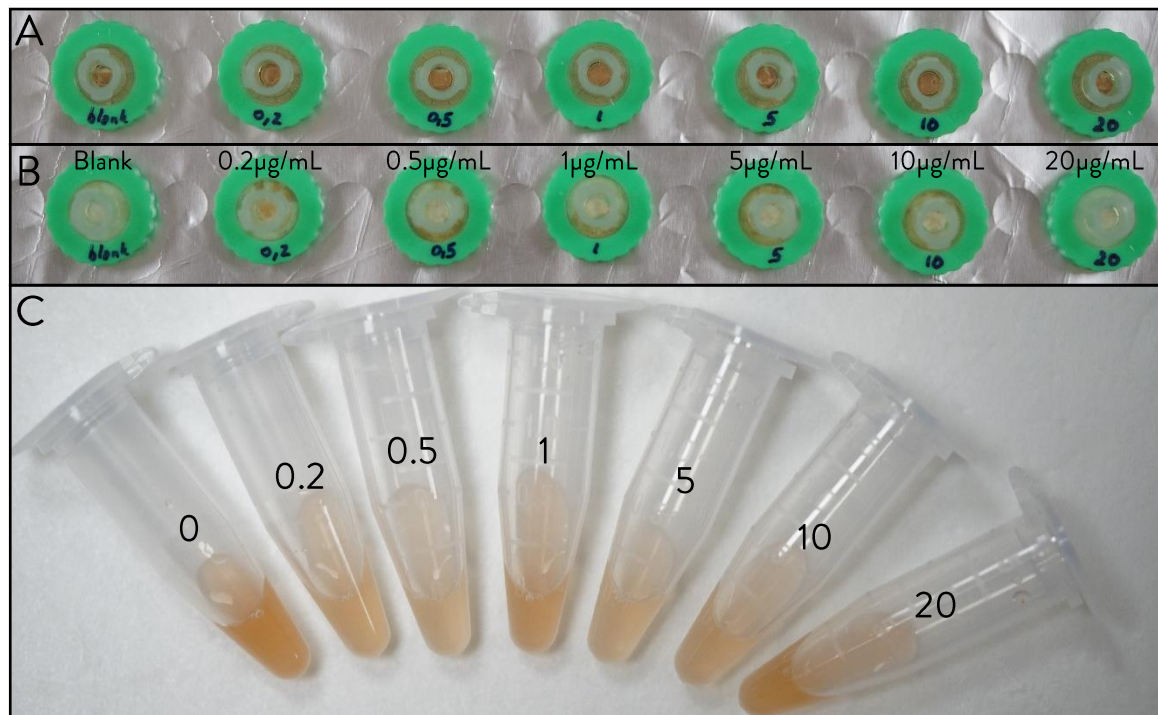
Figure 4.33: (a) Membranes supporting MBs. (b) Membranes after pulling up solutions of varying concentration of MMP-7 in 10 mM PBS 0.05% Tween 20 and releasing the MBs. (c) Concentrations obtained after pulling up the solutions through the membranes.

This issue is represented also in the data below (Figure 4.34): the fluorescence intensity detected does not always increase with increasing enzyme concentrations, for example, 10 μg/mL has comparable intensity with 5 and 1 μg/mL, but not with 20 μg/mL. Since the fluorescence intensity is given by the number of cleaved peptides, the intensity of the readings recorded are dictated by the limited quantity of available peptides to be cleaved rather than the concentration of enzyme, due to the low concentrations of functionalized beads released in most of the solutions.
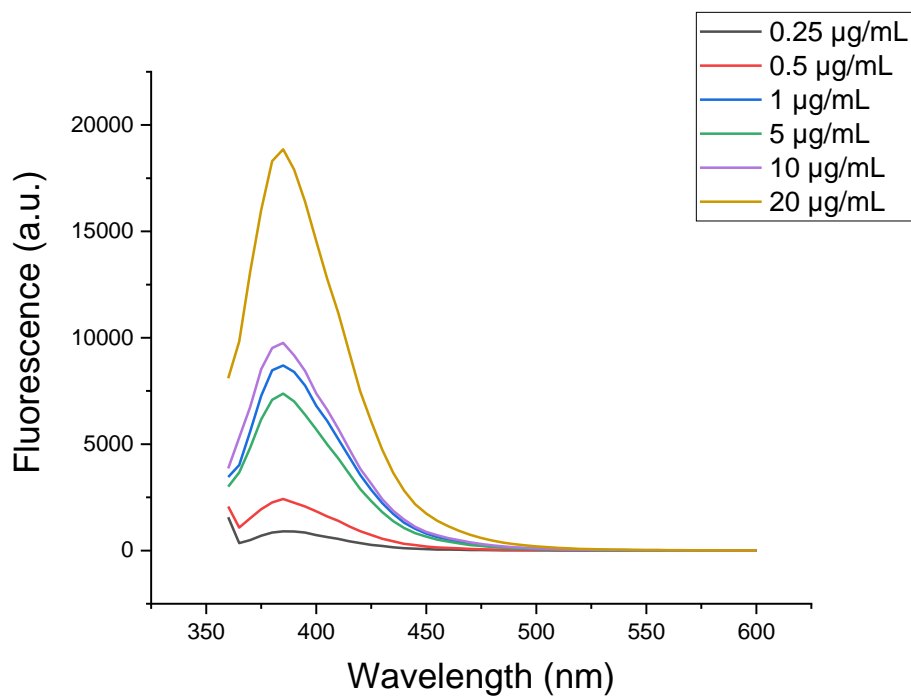
Figure 4.34: *Fluorescence spectra after pulling up varying concentrations of MMP-7 in 10 mM PBS 0.05% Tween 20 through the membranes showed in Figure 4.33 and letting the solution react for 30 minutes. Blank reading was subtracted to each reading for a clearer representation.*

This inhomogeneous release of particles may be due to the fact that the solution wets a limited area of the membrane first and then preferentially passes through that area, instead of flowing through the whole membrane. This may happen because the membrane shows more wettability in one area due to a filter not completely dry or just because the water reaches one spot first and start wetting it there.

Despite this issue, it was still possible to collect useful data: the LOD remained at 0.25 µg/mL, even if detected at a lower intensity, which may be due to the low amount of MBs released or to some losses caused by flowing through the membrane.

4.8.2.2   Plasma

The same experiment was repeated in 10% plasma, diluted in PBS 0.05% Tween 20, with 0, 5, 10 and 20 µg/mL of MMP-7. The experiment had similar issues, with the 5 µg/mL membrane showing a high number of particles still stuck on the membrane and a less concentrated pulled up solution (Figure 4.35).
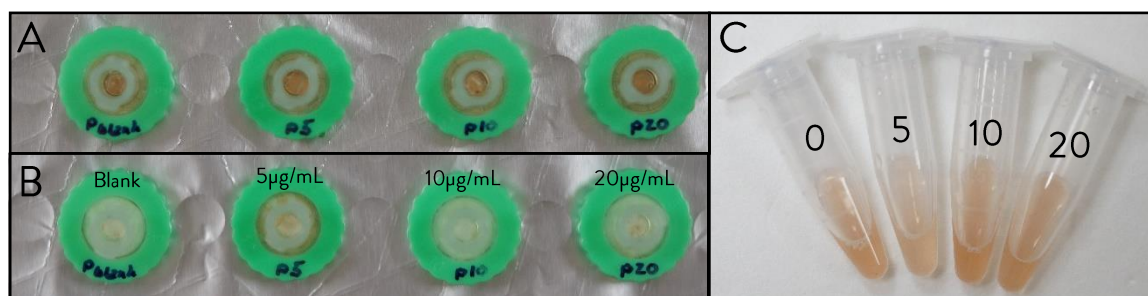
Figure 4.35: (A) Membranes supporting MBs. (B) Membranes after pulling up solutions of 10% plasma and releasing the MBs. (C) Concentrations obtained after pulling up the solutions through the membranes.
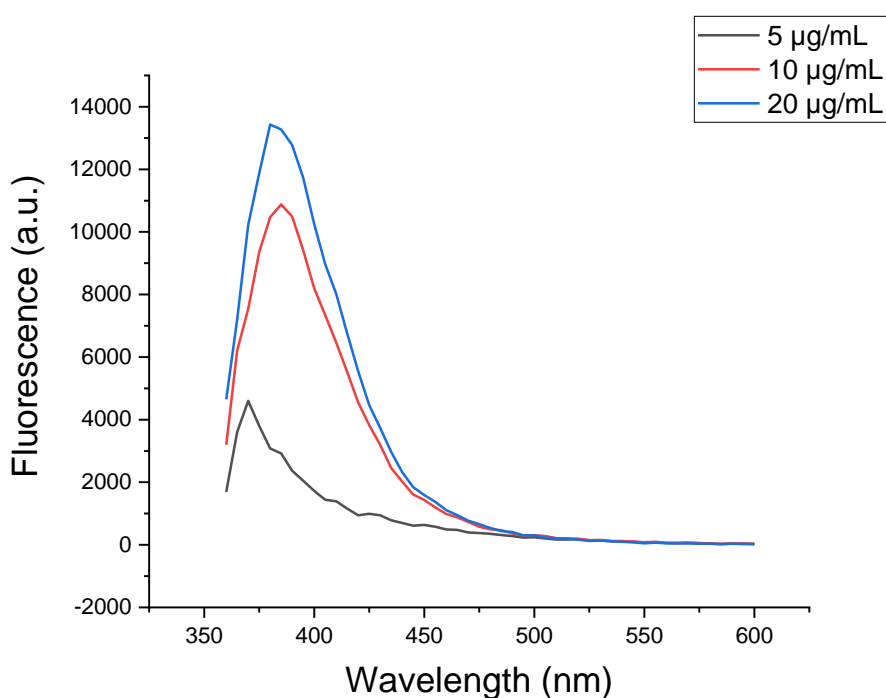
Figure 4.36: Fluorescence spectra after pulling up varying concentrations of MMP-7 in 10% plasma through the membranes showed in Figure 4.34 and letting the solution react for 30 minutes. Blank reading was subtracted to each reading for a clearer representation.

The results (Figure 4.36) show that the limit of detection in 10% plasma has increased to 10 µg/mL with the syringe setup: the peak shown on the graph does not represent the detection of MMP-7 since it is shifted with respect to the emission wavelength of Mca and is not present in the rest of the experiments. In fact, this peak is probably due to other molecules of plasma or to instrumental errors. As for the

previous experiment, this decrease in sensitivity is probably be due to the losses of MMP-7 within the membrane together with a decrease of MBs present in the solution.

4.8.3 Functional Assay Using a Syringe

The proposed setup for the functional assay includes a series of 3 membranes, through which the sample passes by pulling it up with a syringe. Repeating this exact setup was not possible using filter cartridges and reusable cartridge because of the high volume losses that would occur, not properly replicating what would happen in the final assay. For this reason, a simulation of this assay was carried out carrying out each step separately:

- MMP-7 was spiked buffer or diluted plasma (as in Chapter 4.8.2)

- The solution was filtered through a 0.1 μm PEEK membrane (as in Chapter 4.5.1)

- The filtered solution was pulled up through a 0.22 μm PES membrane on which functionalized beads were deposited.

- The solution was passed through a 0.03 μm PES membrane (as established in Chapter 4.5.3) to exclude MBs and other large molecules interfering with the fluorescence emission (this step was carried out just for diluted plasma).

The previous experiments with syringe setup highlighted the need for a further optimization in order to guarantee a constant beads concentration in the pulled-up solution. This issue should be solved once the membranes are put into the final configuration of our assay, where the membranes are contained in a cylindrical shape, different from the filter cartridges, and the solution will remain in contact with the fraction of MBs that is not yet released into the solution, allowing to detach the functionalized beads from the surface just by shaking the syringe. Thus, this scenario was simulated in the next experiments: after pulling up the sample, the syringe was shaken while the solution was still in contact with the membrane, consistently releasing most of the MBs, after that, the solution was pulled more into the syringe and let react for the usual 30 minutes, as in Figure 4.37.
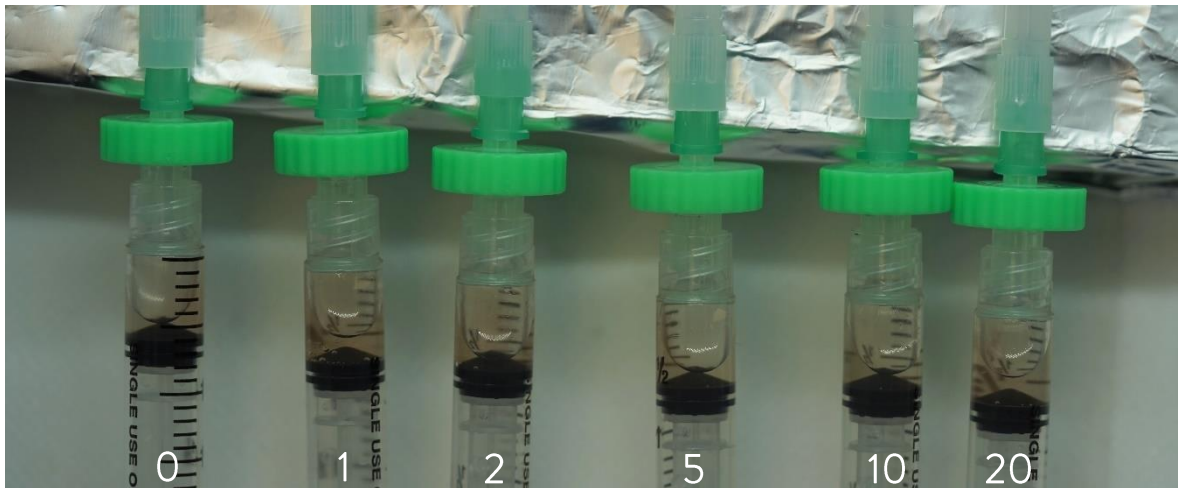
Figure 4.37: MMP-7 pulled up solutions reacting with the released nanoparticles, after shaking the syringe.

This method does not require a high volume to release all nanoparticles, therefore it can be varied. In the next experiments it was reduced to 250 µL, which is the same volume used for the assays in solution and is preferable since it requires less human serum to be carried out. Consequently, after a brief optimization, the number of magnetic beads deposited on the membrane was reduced by pushing through 600 µL of 0.25 mg/mL (1/40) of MBs solution instead of 0.5 mg/mL (1/20).
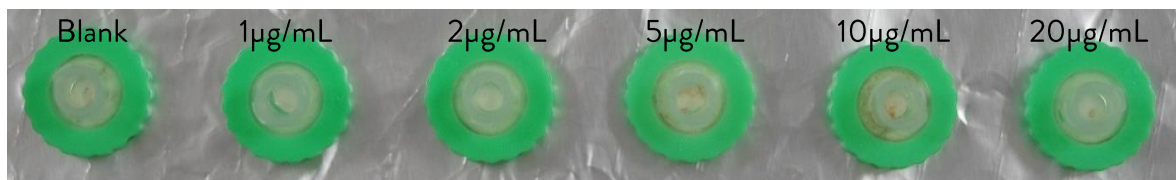
Figure 4.38: PES membranes through which the solutions represented in Figure 4.36 were pulled up.

Figure 4.38 shows that after this process, the membranes look clearer than in the previous experiments, suggesting an improved release of beads, which provides a constant and optimal MBs concentration during the MMP-7 exposure.

Despite the shaking, some particles remain attached to the membrane, especially on its edges. Therefore, the beads concentration obtained after pulling up 250 µL of solution and shaking it was approximately the same of 1/20 MBs, guaranteeing the perfect condition for the enzyme detection.

4.8.3.1 Buffer Sample after 0.1 µm PEEK Filtration

The experiments in buffer showed a lower sensitivity with respect to the ones carried out without PEEK filtration, as reported in Figure 4.39. The assay sensitivity significantly decreased: 1 µg/mL MMP-7 was still detectable but all the fluorescence scans showed a much lower intensity compared to the previous ones, suggesting a higher limit of detection. Moreover, disturbances are present in the readings with lower enzyme concentrations.
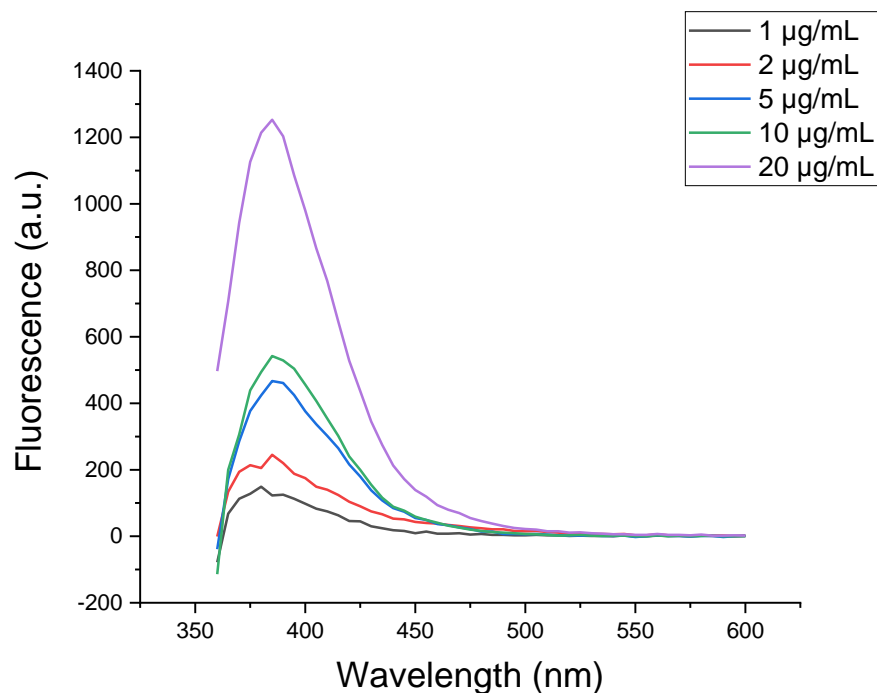
Figure 4.39: *Fluorescence spectra after pulling up the previously filtered solutions of MMP-7 in 10 mM PBS 0.05% Tween 20 through the membranes and letting the solution react for 30 minutes. Blank reading was subtracted to each reading for a clearer representation.*

As expected, filtering the buffer did not contribute to improve the assay's sensitivity but only caused a loss of sensitivity. This is because there is no molecule that needs to be filtered out in PBS 0.05% Tween 20 and the PEEK membrane is just causing losses of enzyme, without beneficial effect. This should not be the case for plasma, where the losses are greatly offset by the exclusion of molecules which drastically decrease the MMP-7 activity.

4.8.3.2   Plasma Sample with 0.1 µm PEEK Filtration

These experiments confirmed what was expected: the MMP-7 was more detectable (Figure 4.40) with respect to the unfiltered plasma assay, with 5 µg/mL being clearly detected and 2 µg/mL showing a very low intensity. However, these results are not yet totally satisfactory: the disturbances are very high due to the fluorescence of plasma: even after subtracting the blank reading, the disturbance intensity is comparable with that of the fluorescence signal given by Mca for the 2 µg/mL reading.
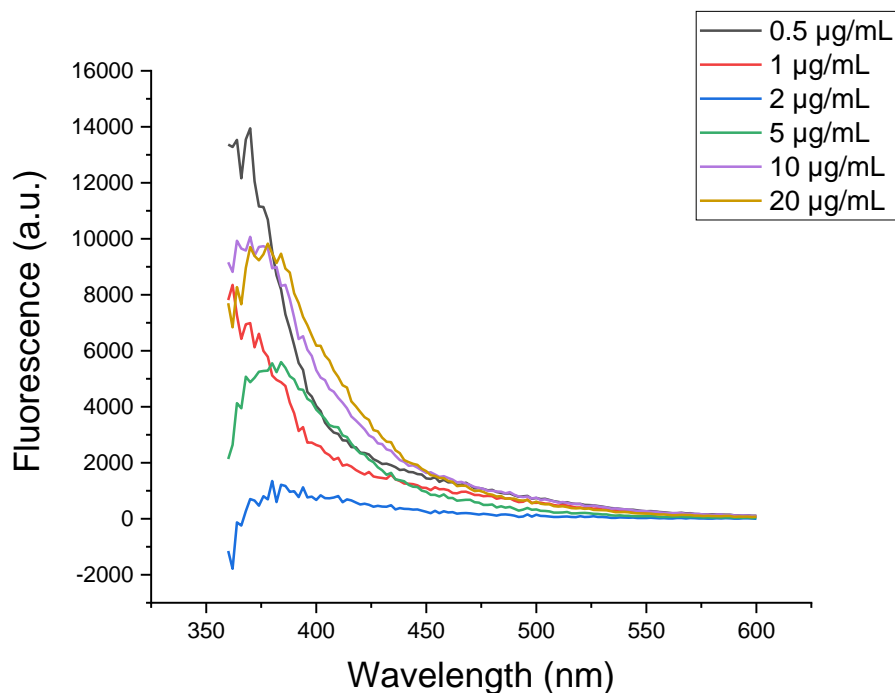
Figure 4.40: *Fluorescence spectra after pulling up the previously filtered solutions of MMP-7 in 10% plasma through the membranes and letting the solution react for 30 minutes. Blank reading was subtracted to each reading for a clearer representation.*

This may be solved just by changing the fluorophore, as suggested in Chapter 5.6.4, but the fluorescence signal can further be improved with the last step of this assay, which involves another filtration.

4.8.3.3   Plasma Sample with 0.1 µm PEEK and 0.3 µm PES Filtration

The solutions obtained with plasma samples were filtered through 0.03 µm PES membrane, to exclude larger plasma molecules interfering with the fluorescence signal and to separate the magnetic beads. Since no disturbance caused by matrix molecules in buffer, this step was carried out only on the diluted plasma samples.
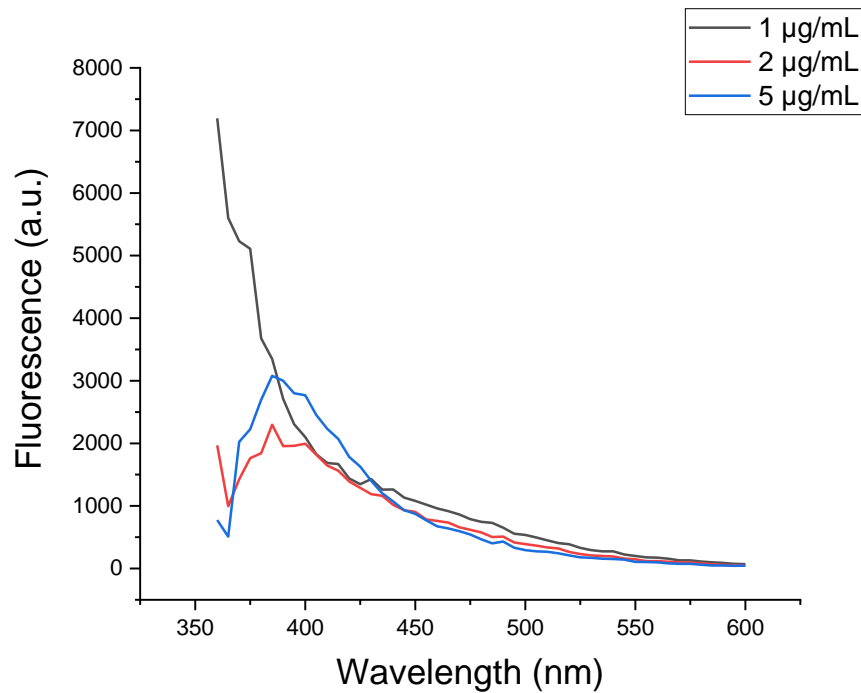
Figure 4.41: *Fluorescence spectra of the plasma sample at different MMP-7 concentrations after filtration through 0.03 µm PES. Blank reading was subtracted to each reading for a clearer representation.*

The filtration resulted effective: as show in Figure 4.41, the disturbances were drastically reduced, and the peaks are easily visible. The limit of detection was decreased from 5 µg/mL MMP-7 in 10% plasma (in solution assay) to 2 µg/mL, which even showed a higher fluorescence intensity with respect to that obtained prior to 0.03 µm PES filtration.

4.9 Selectivity

As reported by Bo Liedberg et al. [138], JR2EC showed a recognition site for Trypsin, causing aggregation of the nanoparticles even in absence of MMP-7.

A brief selectivity experiment was carried out to verify if the current setup, pep0 immobilized on MBs, shows the same selectivity issue. A solution containing a high amount of MMP-7 (5 µg/mL) and one containing a higher amount of Trypsin (50 µg/mL) were added to functionalized beads solution. The results are showed below (Figure 4.42).
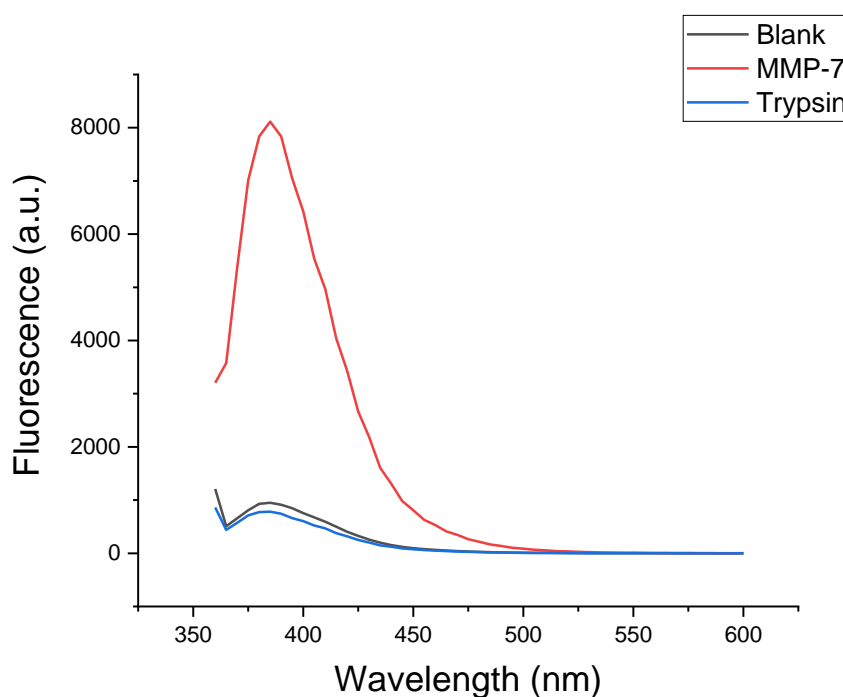
Figure 4.42: *Fluorescence spectra of pep0 functionalized beads after exposure to MMP-7 and Trypsin. Blank reading is reported for comparison.*

The signal given by Trypsin is comparable to that given by the blank reading, while the MMP-7 reading gave significantly higher values, meaning that Trypsin does not cleave the peptide and that the pep0 sequence does not show the same selectivity issue that characterized the previous setup.

4.10 Conclusions

A functional assay for naked eye detection of Matrilysin activity in both PBS and human plasma with pre and post filtration steps and a relatively short incubation time was designed and carried out, simulating the ideal setup shown in Figure 4.1.

The simulated functional assay allowed to significantly improve the detection of MMP-7 with respect to the previous setup: it was possible to detect the enzyme with a limit of detection of 2 μg/mL in 10% diluted plasma, approaching clinically relevant concentrations. In PBS, it was possible to detect 1μg/mL of MMP-7, but the LOD was not established since the membranes were optimized for detection in plasma. Therefore, carrying out the functional assay on PBS would just cause losses of enzyme, without any beneficial effects since PBS does not require filtration to improve MMP-7 activity. For this reason, the in-solution assay was carried out using functionalized beads and without filtration: a limit of detection of 0.25 μg/mL in PBS was established, which is 50 times better than the one obtained with the functionalized gold nanoparticles setup described in Chapter 3.

Since these results were obtained with a 30 minute incubation times, it would be interesting to find out if longer exposure times to the enzyme would further decrease the LOD. Moreover, an optimization of the commercial FRET peptide sequence, together with the optimized reporter molecule, should significantly improve the sensitivity of this assay.

The functionalized beads even showed an improved selectivity, since no signal was reported when exposed to Trypsin, which caused a slight aggregation for the functionalized AuNPs. In conclusion: in addition to being more sensitive, pep0 does not show a recognition site for Trypsin, contrarily to JR2EC.

Chapter 5: Conclusions and Future Outlook

5.1   Summary

This thesis focused on the design of a functional assay for detection of Matrilysin (MMP-7) activity, a metalloproteinase associated to numerous pathological conditions, such as cancer and AIDS.

MMP-7 cleaves proteins and therefore peptides in specific recognition sites, this was exploited to develop a colorimetric and then a fluorometric functional assay, based on two different setups.

The colorimetric assay is an in-solution assay, gold nanoparticles functionalized with JR2EC, a peptide which contains two recognition sites for MMP-7, were used. This molecule bears 5 negative charges, rendering the colloidal solution highly stable. When exposed to this protease, the enzyme cleaves this peptide by catalysing its hydrolysis, lowering its net charge and drastically reducing the colloidal stability of the solution: the nanoparticles aggregate extensively upon exposure to MMP-7 resulting in a localized surface plasmon resonance (LSPR) shift, sufficiently large to be detected by naked eye. The parameters characterizing the in-solution assay were optimized, studying the optimal peptide number immobilized on the beads, the ideal concentration of nanoparticles in solution and comparing two peptide sequences with recognition sites for MMP-7. This assay is characterized by a good robustness, showing activity even after 3 months of storage (at 4 °C) of functionalized nanoparticles. However, it was not possible to obtain a colour change in clinical sample matrices such as plasma and the limit of detection showed in Milli-Q was established at 12.5 µg/mL, a value significantly higher than clinically relevant concentrations (which are approximately 10 ng/mL in plasma).

The fluorometric assay was based on FRET peptides, using fluorophores as reporter molecules, which were immobilized on magnetic beads to improve fluorescence signal in plasma and to be easily used in the syringe setup. This assay was optimized for MMP-7 detection in plasma by including 3 membranes, each with a specific role: one for plasma filtration, one as beads support and the other to separate MBs from the cleaved peptide fragments. A comparative study between a set of membranes with different composition and pores dimension was carried out, establishing the optimal membrane for each step.

The parameters characterizing the functional assay were widely optimized, determining the ideal conditions for MMP-7 detection in solution and replicating them in the syringe setup.

Once all these parameters were optimized, a simulation of the assay was carried out in multiple steps, establishing the LOD in 10% human plasma: after going through the steps of the functional assay, it was possible to detect MMP-7 down to 2 μg/mL in diluted plasma. This value is already lower than the minimum concentration detected using the colorimetric assay using functionalized AuNPs in Milli-Q. The large improvement shown by the FRET peptides immobilized on beads is demonstrated by the experiments in PBS (which has no effect on MMP-7 activity, similarly to Milli-Q): the limit of detection for the in-solution assay was 0.25 μg/mL, which is 50 times lower with respect to the other assay. In this case, the LOD was established carrying out an in-solution assay, since PBS does not require filtration to improve MMP-7 activity and those steps would just cause losses of enzyme.

Before achieving point-of-care application, it would be necessary to carry out more selectivity studies, exposing the enzyme to other substances or enzyme that can be present in human plasma in absence of MMP-7 and verify the absence of fluorescence signal.

Moreover, an optimization of the peptide sequence can further reduce the LOD. This process was briefly carried out and is reported in Appendix, obtaining a peptide which is expected to improve the assay's sensitivity. However this optimization is not complete and was not tested in the proposed setup.

5.2   Future Perspectives

The overall scope of this thesis is to develop a point-of-care that can detect Matrilysin activity in clinical sample matrices such as plasma and saliva. To obtain this, further optimizations of the peptide sequence are needed (starting from the results reported in Appendix) to improve the limit of detection of this functional assay and to finally achieve detection of MMP-7 at clinically relevant concentrations in complex matrices with short incubation times.

In addition, since the setup was tested exposing the functionalized beads only to MMP-7 and Trypsin, more selectivity studies are required, including more substances that can be present in human plasma or saliva and finally excluding the possibilities of false positives.

In this thesis, a simulation of the final functional assay in complex matrices was carried out, obtaining promising results for MMP-7 detection, however, the designed structure was not tested. It is necessary to repeat the assay experiments directly using the final setup, verifying if the optimizations carried out for the simulated assays hold also for the syringe setup, or if the parameters should be reviewed and varied.

Finally, it would be interesting to redesign the recognition molecule to detect also other matrix metalloproteinases, obtaining a set of functional assays able to detect a set of MMPs, achieving early detections for more pathologies or cancer types with improved precision: identifying more matrix metalloproteinases present in the same sample with more assays (or a multifunctional assay) would allow the creation of an array, highlighting the presence of each MMP and giving more precise information about the possible pathologies. Some of these biomarkers are present in higher concentrations in saliva or urine than in plasma [139], therefore, a syringe functional assay, optimized for detection in different clinical matrices could result in a more efficient point of care diagnostics for matrix metalloproteinases, since the LOD necessary for diagnosis would be significantly lowered.

Appendix - Peptide Sequence Optimization

Introduction and Previous Optimizations

The peptide sequence used in Chapter 5 can be optimized to show greater sensitivity and improved kinetics, since the catalytic efficiency of the enzyme depends on the substrate [116]. In a previous study carried out in our laboratory the activity obtained immobilizing the peptide on a surface was found to be drastically inferior with respect to that shown when the peptide was dispersed in solution, as reported in Figure A1.
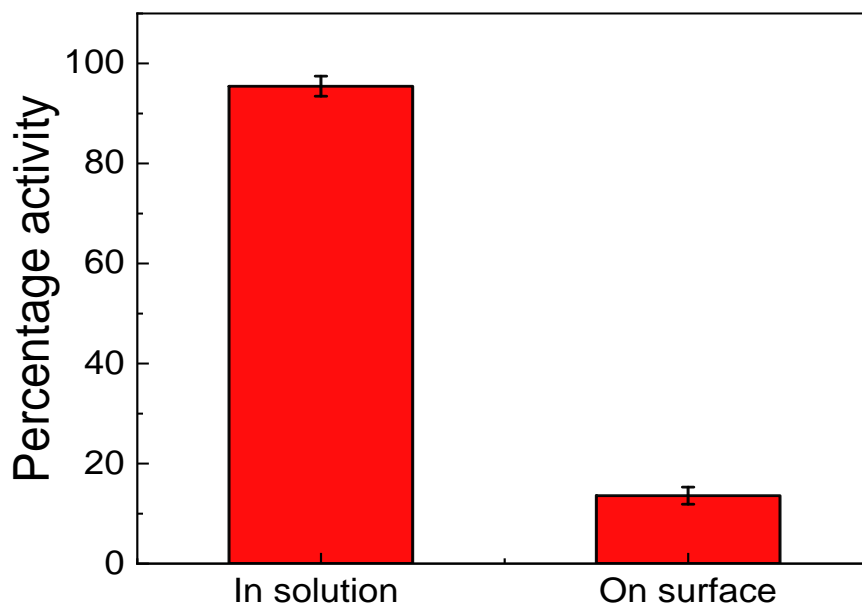
Figure A 1: Comparison of activity shown with peptides dispersed in solution or immobilized on surface. (unpublished data)

This large difference is due to the reduced flexibility that chains show when immobilized on a surface [140]. Moreover, the monolayer of peptide molecules formed on the surface sterically hinders the enzyme from reaching the cleavage site, denying or significantly slowing down the reaction. This behaviour can be of great importance when considering the functional assay setup described in Chapter 5, where the peptide is bound on the 3 μm magnetic beads' surface.

In order to improve this behaviour, "GGS" spacers were incorporated to the peptide sequence. These spacers do not contribute to the hydrolysis reaction but increase the molecule flexibility and distance the cleavage site from the surface, rendering it more accessible for the enzyme. The modified peptide chain was thus modified, obtaining the following sequence:

Mca-KPLG~L-Dpa-AR(GGS)$_{1-3}$K$^{(Me3)}$C-NH$_2$

As represented below (Figure A2), with increasing spacers incorporated, the activity shown for peptide cleavage increased. However, the rate at which this activity grows decreases with increasing spacers added, reaching an estimated saturation value of ~50%.
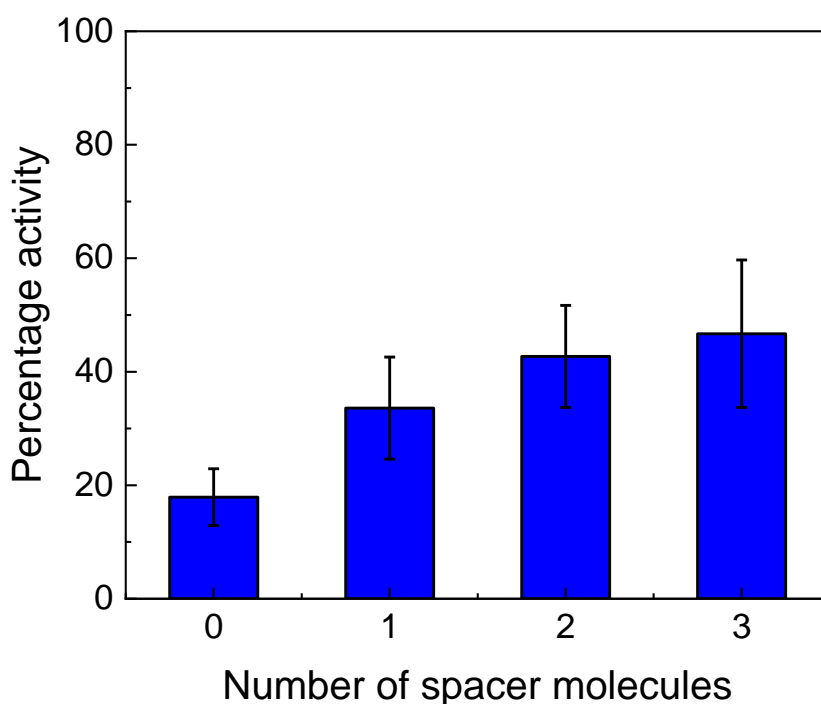
Figure A 2: Increase of activity shown incorporating GGS spacers in the peptide sequence. (unpublished data)

Since it was not possible to reach the same activity levels as those show in experiments in solution, a further optimization of the chain is required. As stated before, the catalytic activity of proteases depends on the peptide sequence, therefore, a set of modified peptide sequences was analysed and compared to the commercial FRET peptide (pep0).

Materials and Instruments

Fluorescence scans and kinetic reading were taken using a Tecan Spark® plate reader.

ThermoFisher Pierce™ Maleimide Activated Plates, Black, 96-Well were used to immobilize peptides on surface and to take readings with Tecan Spark® plate reader.

MMP-7 was synthesized in our laboratory (Centre for Biomimetic Sensor Science), with an estimated activity ten times lower than the commercial Matrilysin.

All the other reagents and solvents were obtained from Sigma-Aldrich and used without further purification.

The peptide sequence compared are:

- Pep0: Mca-KPLG~L-Dpa-ARGK$^{(Me3)}$C-NH$_2$
- PepA: Mca-KPLA~LVARG(DAP)SK$^{(Me3)}$CG
- PepB: Mca-KPLE~LVARG(DAP)SK$^{(Me3)}$CG
- PepC: Mca-KPLQ~LVARG(DAP)SK$^{(Me3)}$CG
- PepD: Mca-KPLS~LVARG(DAP)SK$^{(Me3)}$CG
- PepE: Mca-KPLE~LIARG(DAP)SK$^{(Me3)}$CG

The labelled peptides in the form of powder were weighted and dissolved in Milli-Q, with a concentration of 1mM. For greater accuracy, the concentration of the solutions was double-checked exploiting the absorbance of Mca (Figure A3) and considering that the other components of the solution are transparent.
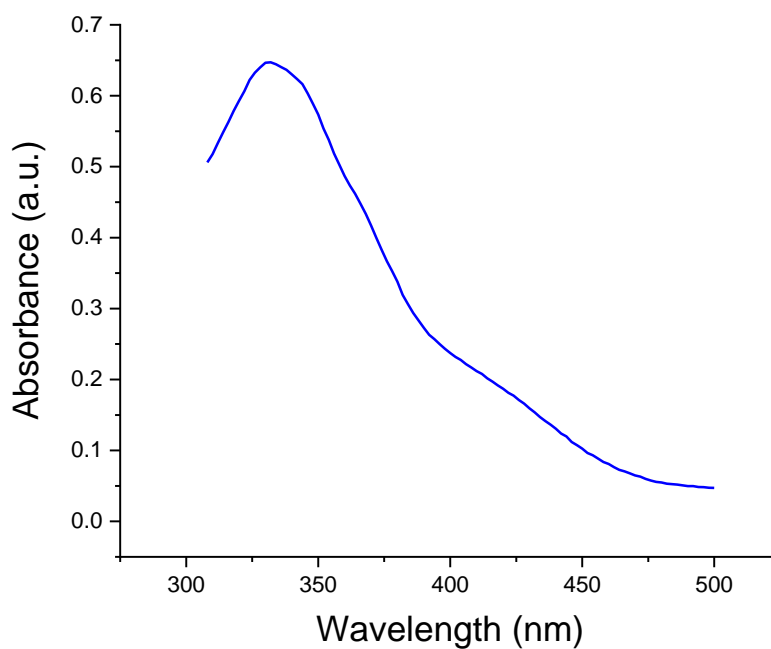
Figure A 3: *Absorbance spectrum of Mca.*

The absorbance of a solution is defined by the Beer Lambert Law as:

$$A = \varepsilon \, l \, c$$

Equation A 1: *Beer-Lambert law. A: absorbance, ε: molar attenuation coefficient, l: optical path length, c: concentration of the attenuating species.*

Considering that every peptide contains the same amount of Mca (1 per molecule), by knowing ε and l, it is possible to calculate the molecules concentration "c" considering the absorbance "A" at 320 nm (maximum absorption wavelength for Mca). After that, the solutions were further diluted, until the absorbance corresponding to 1 mM was reached for each peptide.

Activity in Solution

A preliminary comparison between peptide sequences was carried out, following the protocol established in Chapter 4.3.1: MMP-7 was added at the same time for every peptide solution, letting the solution

react for 3 hours, while recording the fluorescence intensity at 405 nm (excitation wavelength at 320 nm) every 20 seconds.

The kinetics readings were normalized and compared for each peptide. Figure A4 represent the normalized kinetic readings during exposure to 5 µg/mL of MMP-7 for the first 25 minutes.
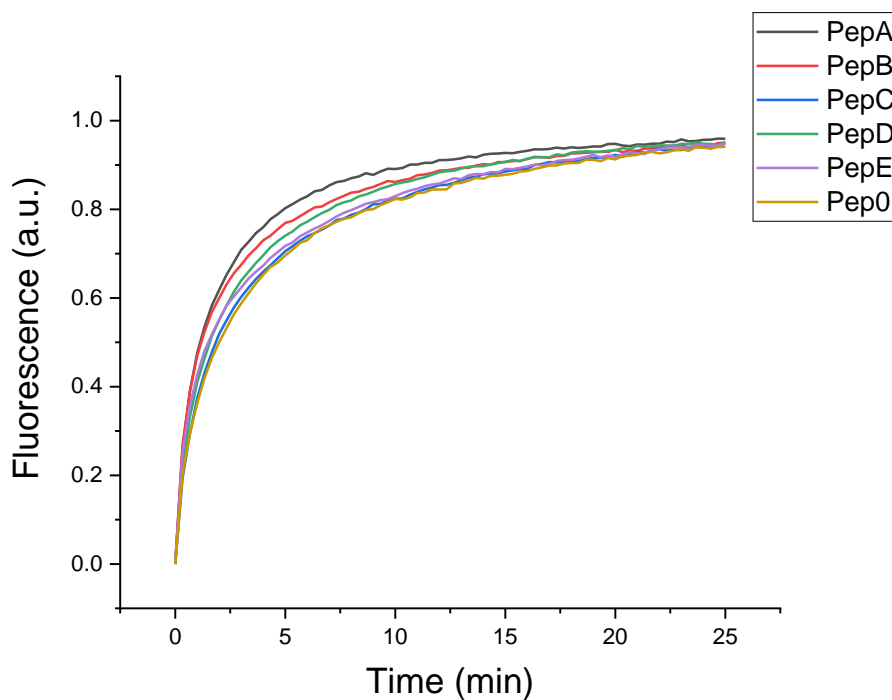
Figure A 4: Kinetics scans of fluorescence intensity over time of the 6 peptide sequences, normalized data.

To understand which peptide cleavage has a faster kinetics it is enough to consider the first part of the graph, in which the fluorescence intensity vs time graph follows a linear trend and find the slope of the linear fit for every peptide (Figure A5). Higher values of slopes correspond to faster reactions, suggesting a more efficient catalytic activity of MMP-7.
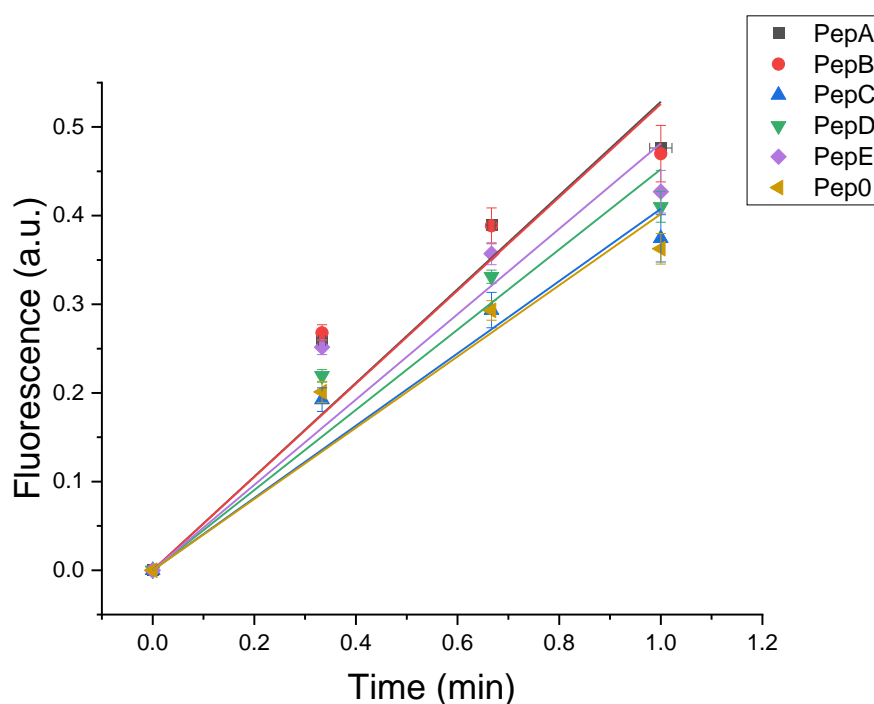
Figure A 5: Linear fit of data from Figure A3 in the first minute of reaction.

The slope values obtained with this procedure are shown in the following table (Table A1):

Peptide sequence	Slope
PepA	0.52848
PepB	0.52588
PepC	0.40767
PepD	0.45231
PepE	0.48138
Pep0	0.40167

Table A 1: Slopes obtained through the linear fit of data from the first minute, at 5 µg/mL of MMP-7.

Four peptides exhibit a faster cleavage rate with respect to the commercial one, with pepC showing a very similar behaviour to that of pep0. In particular, pepA and pepB are the molecules which improve most significantly the catalytic activity on peptide hydrolysis. This result was confirmed by experiments carried out at other MMP-7 concentrations: 1 µg/mL and 2 µg/mL.

However, to assess the improvement of the peptide sequence on the catalytic efficiency, further experiments should be carried out, establishing the catalytic turnover number (k_{cat}), defined as maximum number of chemical conversions of substrate molecules per unit time that an enzyme molecule can execute, and the Michaelis-Menten constant (k_M), defining the affinity between enzyme and substrate, determined by the substrate concentration required to reach half of the maximum reaction velocity (reached at high substrate concentrations) [141]. These experiments could not be completed, for this reason they are not reported in this thesis.

Activity on Surface

In this set of experiments, the peptides were immobilized on a surface, resulting in a monolayer of molecules. In this way, it was possible to evaluate the effect that steric hindrance may have on the substrate activity in the final setup of the assay.

While the catalytic activity in solution only depends on the first neighbour amino acids of the cleavage site, this is not true for peptides bound to a surface:

- Different chain lengths affect the distance of the cleavage site from the surface and from the other end of the molecule.

- Bulky components of the chain can cause steric hindrance, affecting how easily and rapidly the enzyme is be able to reach the cleavage site.

- Steric hindrance and consequently flexibility of the molecule influence its ability to assume the right conformation to fit into the enzyme-substrate complex necessary for cleavage.

The commercial peptide and the new sequences show spacers in different positions; therefore, it will not be possible to directly compare their activity on surface since other variables would play an important role.

For this reason, the following experiments were carried out only on the 5 new peptide sequences (pepA, pepB, pepC, pepD, pepE).

The peptides were immobilized on an activated maleimide plate, similarly to what was done with magnetic beads in Chapter 4.

This process results in a monolayer of peptides bound to the surface, with no fluorescence signal detected prior to MMP-7 exposure. When the enzyme comes into contact with the molecules, the peptides are cleaved: the fragment labelled with Dpa (quencher) remains immobilized on the surface, while the one containing the fluorophore (Mca) is released into the solution. Once Mca is distanced from the quencher, it is possible to detect a fluorescence signal with a maximum at 405 nm.

The protocol followed to immobilize peptides on the maleimide activated plates is the following:

- Wells were washed four times with 300 μL each with Wash Buffer (0.1M sodium phosphate, 0.15M sodium chloride, 0.05% Tween®-20; pH 7.2).

- The peptides solutions were prepared in Binding Buffer (0.1M sodium phosphate, 0.15M sodium chloride, 10 mM EDTA; pH 7.2)

- 100 μL of peptide solution was added to each well and incubated for 2 hours at room temperature.

- Wells were washed again four times with 300 μL of Wash Buffer to remove the unbound peptides.

- A solution of 10 μg/mL cysteine was prepared immediately before use; 100 μL of cysteine solution was added to the wells and incubated for 1 hour.

- Wells were washed four times with 300 μL of Wash Buffer

- The MMP-7 solutions were prepared in Milli-Q and were added to the wells, starting the fluorescence kinetics readings immediately afterwards.

Experiments in solution were carried out in Assay Buffer (20 mM Tris, 10 mM $CaCl_2$, 20 mM $ZnCl_2$, 0.05% Brij), but in this case, this buffer showed a white precipitate on the bottom of the well after the reaction and the fluorescence readings were finished. This is also represented by a decrease in fluorescence intensity after a certain time (Figure A5), which would require some data manipulation to allow a correct mathematical analysis on the peptide behaviour. For this reason, experiments on surface were carried out diluting MMP-7 in Milli-Q instead of Assay Buffer.
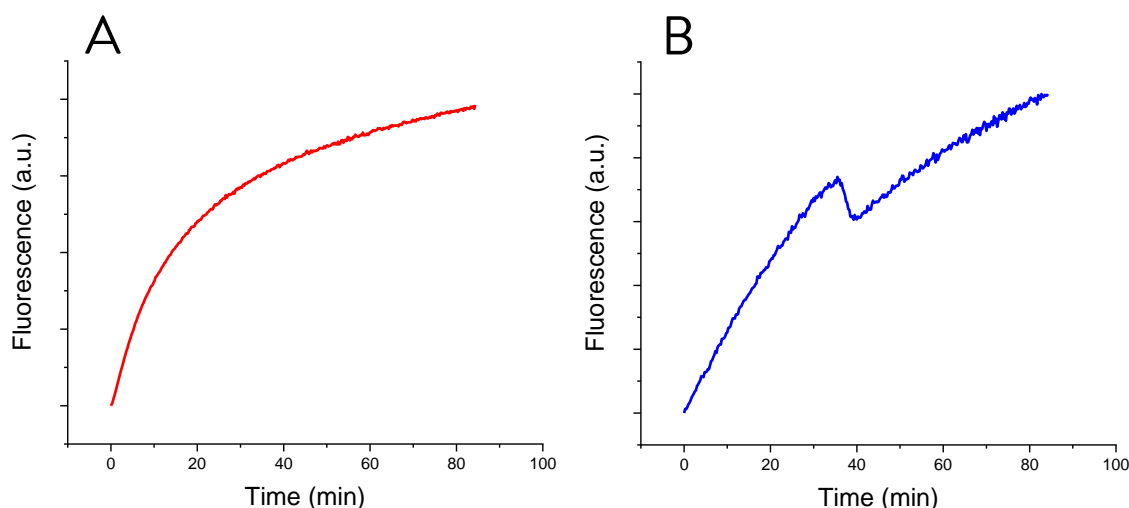
Figure A 6: Fluorescence intensity at 405 nm over time of pep0 during MMP-7 exposure on surface, (A) in Milli-Q and (B) in Assay Buffer.

The most important aspect of every experiment is that it must be repeatable, this is the first step to achieve reliable results: it is necessary to be able to control and fix all the parameters that could influence the results of the experiment, leaving as the only variable of the experiment the parameter that is being studied. In these experiments, the fixed parameters are peptide concentration, enzyme concentration, temperature, total volume, excitation and emission wavelength and others. The experiments in solutions allowed to easily control all these parameters, since the prepared solutions of enzyme and peptide were directly used, without intermediate steps. Experiments on surface, instead, require a further step of optimization to fix the amount of peptide immobilized on the surface, which determines the total amount of peptide reacting with the enzyme: due to the limited time and Brownian motions not all the peptides added to the solutions are immobilized on the plate . This is necessary to guarantee that the results of the peptides comparison only depend on their sequence and not on parameters like peptide quantity that may vary when repeating the experiments.

The easiest way to do this is to saturate the available maleimide binding sites in every experiment, adding an excess of peptides to the solution that reacts with the maleimide plate.

An optimization was carried out to find the minimum concentration of peptide solution (volume is fixed at 100 μL) required to consistently saturate these binding sites, with the following procedure:

- Peptide were immobilized on the surface following the protocol reported previously, using peptide solutions with increasing concentrations.

- A high concentration of MMP-7 (in 100 µL) was added to the wells.

- The fluorescence intensity at 405 nm was measured after the reaction reached saturation, meaning that all the peptides were cleaved.

As described before, each peptide is labelled with one fluorophore (Mca), when the peptide gets cleaved the fragment containing Mca is released in the solution and gives a fluorescence signal when excited. Therefore, the fluorescence intensity at the end of the reaction increases linearly with increasing number of cleaved peptides. This means that immobilizing a higher number of peptides leads to a higher value of fluorescence once all peptides are cleaved.

An increasing concentration of peptides of the solution added to immobilize them on the plate leads to a higher number of peptides bound to the surface, until all the available maleimide sites are occupied. Once the saturation of binding sites is reached, the number of molecules bound cannot increase with higher solution concentrations. Consequently, the fluorescence intensity after 100% of the product is formed reaches a saturation value, since the unbound peptides are washed away before MMP-7 addition.

The fluorescence intensity values turned out to be variable for the lowest concentrations while are approximately constant for 10, 20 µM and higher concentrations: this means that 10 µM is the minimum concentration that allows to consistently saturate all the available immobilization sites. Therefore, it was decided to carry out the experiments on surface using a binding solution with this concentration of peptides, since it allows to obtain repeatable results with reduced losses of peptides.

Finally, the experiments were performed as described in the protocol: the peptides were immobilized on the plate's well surface using 100 µL of 10 µM peptide solution, then 100 µL of MMP-7 was added to the wells at several concentrations. The fluorescence kinetics measurement was started immediately after the addition of the enzyme solution for every peptide. The data was then processed similarly to the experiments in solution.

An example of the resulting processed data, for 2 µg/mL of MMP-7, is reported in Figure A7.
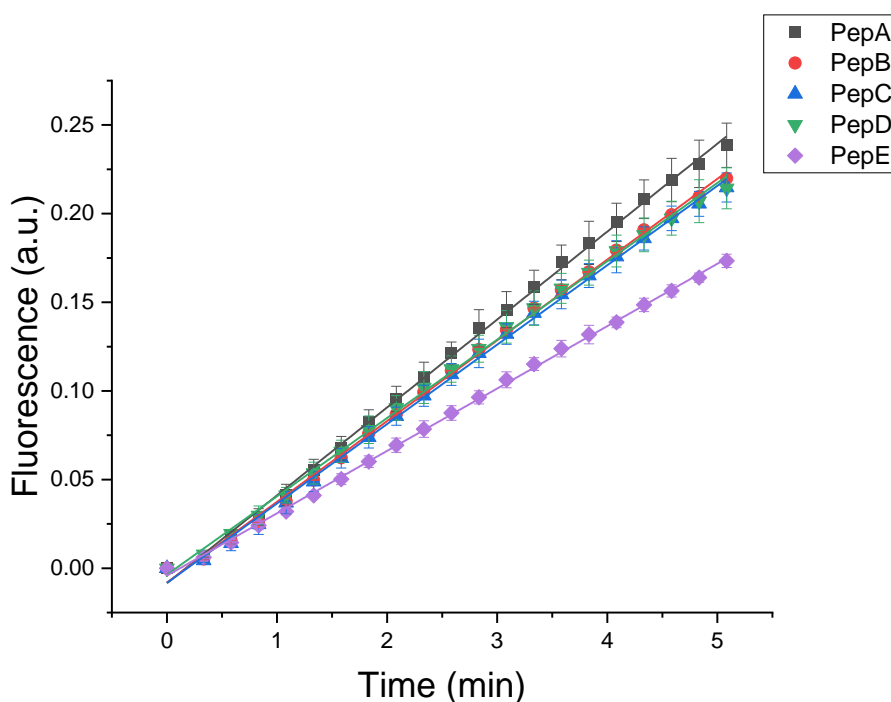
Figure A 7: *Linear fit of fluorescence intensity data over time for the 5 peptide sequences immobilized on surface*

The resulting data from the experiments on surface confirmed that pepA is the most active sequence between the ones analysed and its behaviour is maintained in the new configuration with respect to the other peptides. This is not the case for pepB and pepE, with the latter showing a drastically slower kinetics with respect to the others, suggesting that factors such as the steric hindrance caused by the immobilization on surface has a significant influence on their activity. Further evidence of this is reported in Table A2, representing the slopes for each peptide sequence.

Peptide sequence	Slope
PepA	0.04958
PepB	0.04554
PepC	0.04479
PepD	0.04419
PepE	0.03518

Table A 2: *Slopes obtained through the linear fit of data from the first 5 minutes, at 2 µg/mL of MMP-7.*

Conclusions

The experiments reported show promising results for the optimization of the peptides sequence, that may lead to an improvement of the limit of detection or to a reduction of the incubation time needed to detect MMP-7. However, the experiments reported in this chapter are just a preliminary study: a more complete optimization should be carried out, determining k_{cat} and k_M for each molecule and comparing the peptides on surface ad immobilized on particles. Moreover, it would be interesting to study the effect of the incorporation of "GGS" spacers for each sequence, finally determining which is the ideal peptide to be included in the functional assay.

References

[1]   Douglas Hanahan, Rober A. Weinberg, "The Hallmarks of Cancer," *Cell,* vol. 100, no. 1, pp. 57-70, 2000.

[2]   Lisa J. McCawley , Lynn M. Martisian, "Matrix metalloproteinases: multifunctional contributors to tumour progression," *Molecular Medicine Today,* vol. 6, pp. 149-156, 2000.

[3]   Lisa M. Coussens, Lynn M, Martisian, et al., "Matrix Metalloproteinase Inhibitors and Cancer: Trials and Tribulations," *Science,* vol. 295, no. 5564, pp. 2387-2392, 2002.

[4]   WHO, "Cancer," 12 September 2018. [Online]. Available: https://www.who.int/health-topics/cancer#tab=tab_1. [Accessed 2 June 2020].

[5]   P. Anand, et al., "Cancer is a Preventable Disease that Requires Major Lifestyle Changes," *Pharm Res,* vol. 25, no. 9, p. 2097–2116, 2008.

[6]   Puja Sandbhor Gaikwad, and Rinti Banerjee, "Advances in point-of-care diagnostic devices in cancers," *Analyst,* vol. 143, pp. 1326-1348, 2018.

[7]   Marc A. Bjurlin, Cara J. Nelson, et al., "Characterization of proteolytic activity of proteases," *Biotechnology Letters,* vol. 24, pp. 191-195, 2002.

[8]   Z. Zhao, P. J. Russel, et al., "Application of in-gel protease assay in a biological sample: Characterization and identification of urokinase-type plasminogen activator (uPa) in secreted proteins from a prostate cancer cell line PC-3," *ELECTROPHORESIS,* vol. 25, no. 7-8, pp. 1142-1148, 2004.

[9]   D. Borovsky, D.A. Carlson, et al., "Development of Specific RIA and ELISA to Study Trypsin Modulating Oostatic Factor in Mosquitoes," *Arch Insect Biochem Physiol.,* vol. 21, no. 1, pp. 13-21, 1992.

[10]   Juliet Spencer, Viorica Lopez-Avila, "Methods for Detection of Matrix Metalloproteinases as Biomarkers in Cardiovascular Disease," *Clinical Medicine Insights: Cardiology,* vol. 2, pp. 75-87, 2008.

[11]   Andrew St. John, and Christopher P. Price, "Existing and Emerging Technologies for Point-of-Care Testing," *Clin Biochem Rev.,* vol. 35, no. 3, pp. 155-167, 2014.

[12]   Weian Zhao, Yingfu Li, et al., "Design of Gold Nanoparticle-Based Colorimetric Biosensing Assays," *Chembiochem. ,* vol. 9, no. 15, p. 2363/2371, 2008.

[13]   Matthew E. Stewart, Ralph G. Nuzzo, et al., "Nanostructured Plasmonic Sensors," *Chem. Rev.,* vol. 108, no. 2, pp. 494-521, 2008.

[14]   Juewen Liu, Yi Lu, et al., "Functional Nucleic Acid Sensors," *Chem. Rev.,* vol. 109, no. 5, p. 1948–1998, 2009.

[15]   Andrew D. Ellington, and Jack W. Szostak, "Selection in vitro of single-stranded DNA molecules that fold into specific ligand-binding structures," *Nature,* vol. 355, p. 850–852, 1992.

[16]   Yujun Song, Xiaogang Qu, et al., "Colorimetric Biosensing Using Smart Materials," *Advanced Materials,* vol. 23, no. 37, pp. 4215-1236, 2011.

[17]   Lifang Shi, Zeev Rosenzweig, et al., "Synthesis and Application of Quantum Dots FRET-Based Protease Sensors," *J. Am. Chem. Soc.,* vol. 128, no. 32, pp. 10378-10379, 2006.

[18]   Young-Pil Kim, Hak-Sung Kim, et al., "Energy Transfer-Based Multiplexed Assay of Proteases by Using Gold Nanoparticle and Quantum Dot Conjugates on a Surface," *Anal. Chem.,* vol. 80, no. 12, pp. 4634-4641, 2008.

[19]   Masanari Taniguchi, Toshifumi Akizawa, et al., "MMP-7 Cleaves Amyloid β Fragment Peptides and Copper Ion Inhibits the Degradation," *Biometals,* vol. 30, no. 5, pp. 797-807, 2017.

[20]   Yejiao Shi, Helena Azevedo, et al., "Tuning the matrix metalloproteinase-1 degradability of peptide amphiphile nanofibers through supramolecular engineering," *Biomaterials Science,* vol. 7, pp. 5133-5142, 2019.

[21]   Mílton Cordeiroet, Pedro Viana Baptista, et al., "Gold Nanoparticles for Diagnostics: Advances towards Points of Care," *Diagnostics,* vol. 6, no. 4, p. 43, 2016.

[22]   Andrea Mario, Andrea Mario Rossi, et al., "Rapid and sensitive detection of melamine in milk with gold nanoparticles by Surface Enhanced Raman Scattering," *Food Chemistry,* vol. 159, pp. 250-256, 2014.

[23]   Chia-Chen Chang, Chen-Yu Chen, et al., "Gold Nanoparticle-Based Colorimetric Strategies for Chemical and Biological Sensing Applications," *Nanomaterials,* vol. 9, no. 6, p. 861, 2019.

[24]   K. E. Sapsford, I. L. Medintz, et al., "Fluorescence resonance energy transfer: Concepts, applications and advances," *Minerva Biotecnologica,* vol. 16, no. 4, pp. 253-279, 2004.

[25]   A. M. Alizadeh, S. Farsinejad, et al., "Metastasis review: from bench to bedside," *Tumour Biol.,* vol. 35, pp. 8483-8523, 2014.

[26]   Xiangming Guan, "Cancer metastases: challenges and opportunities," *Acta Pharmaceutica Sinica B,* vol. 5, no. 5, pp. 402-418, 2015.

[27]   D. Maxwell Parkin, "Global cancer statistics in the year 2000," *The Lancet Oncology,* vol. 2, no. 10, p. 596, 2001.

[28]   WHO, "Global Cancer Observatory," World Health Organization, [Online]. Available: https://gco.iarc.fr/. [Accessed 5 June 2020].

[29]   Goodarz Danaei, The Comparative Risk Assessment Collaborating Group, et al., "Causes of cancer in the world: comparative risk assessment of nine behavioural and environmental risk factors," *Lancet,* vol. 366, no. 9499, pp. 1784-1793, 2005.

[30] WHO, "Cancer Today," World Health Organization, [Online]. Available: https://gco.iarc.fr/today/online-analysis-map?v=2018&mode=population&mode_population=continents&population=900&populations=900&key=asr&sex=0&cancer=39&type=0&statistic=5&prevalence=0&population_group=0&ages_group%5B%5D=0&ages_group%5B%5D=14&nb_items=10&gr. [Accessed 20 June 2020].

[31] P. R. Srinivas, S. Srivastava, et al., "Trends in biomarker research for cancer detection," *Lancet Oncol,* vol. 2, no. 11, pp. 698-704, 2001.

[32] Pothur R. Srinivas, Sudhir Srivastava, et al., "Proteomics for Cancer Biomarker Discovery," *Clinical Chemistry,* vol. 48, no. 8, pp. 1160-1169, 2002.

[33] N. Lynn Henry, and Daniel F. Hayes, "Cancer biomarkers," *Molecular Oncology,* vol. 6, no. 2, pp. 140-146, 2012.

[34] Anna Sobiepanek, and Tomasz Kobiela, "Application of biosensors in cancer research," *Review and Research on Cancer Treatment,* vol. 4, no. 1, 2018.

[35] Emanuela Galliera, M. Corsi Romanelli, et al., "Matrix metalloproteinases as biomarkers of disease: updates and new insights," *Clin Chem Lab Med,* vol. 53, no. 3, pp. 349-355, 2015.

[36] H. S. Azzam, E. W. Thompson, et al., "Association of MMP-2 Activation Potential With Metastatic Progression in Human Breast Cancer Cell Lines Independent of MMP-2 Production," *J Natl Cancer Inst,* vol. 85, no. 21, pp. 1758-1764, 1993.

[37] Kai Kessenbrock, Zena Werb, et al., "Matrix Metalloproteinases: Regulators of the Tumor Microenvironment," *Cell,* vol. 141, no. 1, pp. 52-67, 2010.

[38] C. F. Sier, H. W. Verspaget, et al., "Tissue levels of matrix metalloproteinases MMP-2 and MMP-9 are related to the overall survival of patients with gastric carcinoma," *British Journal of Cancer,* vol. 74, no. 3, pp. 413-417, 1996.

[39] Matvey E. Lukashev, and Zena Werb, "ECM signalling: orchestrating cell behaviour and misbehaviour," *CELL BIOLOGY,* vol. 8, pp. 437-441, 1998.

[40] I. Fidler, Molecular biology of cancer: invasion and metastasis, Philadelphia: Lippincott–Raven , 1997, pp. 135-152.

[41] J. M. Whitelock, P. A. Underwood, et al., "The degradation of human endothelial cell-derived perlecan and release of bound basic fibroblast growth factor by stromelysin,collagenase, plasmin, and heparanases," *J Biol Chem*, vol. 271, pp. 10079-10086, 1996.

[42] Lisa J. McCawley, and Lynn M. Matrisian, "Matrix metalloproteinases: they're not just for matrix anymore!," *Cell Biology,* vol. 13, pp. 534-540, 2001.

[43] Irina Massova, Shahriar Mobashery, et al., "Matrix metalloproteinases: structures, evolution, and diversification," *The FASEB Journal,* vol. 12, pp. 1075-1095, 1998.

[44] Maryam G. Rohani, and William C. Parks, "Matrix remodeling by MMPs during wound repair," *Matrix Biology,* Vols. 44-46, pp. 113-121, 2015.

[45] N. Kayagaki, S. Inoue, et al., "Metalloproteinase-mediated release of human Fas ligand," *J Exp Med ,* vol. 182, pp. 1777-1783, 1995.

[46] C. Biswas, K. Nabeshima, et al., "The Human Tumor Cell-Derived Collagenase Stimulatory Factor (Renamed EMMPRIN) Is a Member of the Immunoglobulin Superfamily," *Cancer Res,* vol. 55, no. 2, pp. 434-439, 1995.

[47] V. Volgin, Animal Biotechnology, Academic Press, 2014, pp. 307-325.

[48]   K. Bagwell, Emily Gobin, et al., "A pan-cancer perspective of matrix metalloproteases (MMP) gene expression profile and their diagnostic/prognostic potential," *BMC Cancer,* vol. 19, pp. 581-591, 2019.

[49]   M. Kioi, K. Miyazaki, et al., "Matrilysin (MMP-7) induces homotypic adhesion of human colon cancer cells and enhances their metastatic potential in nude mouse model," *Oncogene,* vol. 22, pp. 8662-8670, 2003.

[50]   Anan H. Said, Guofeng Xie, et al., "The Role of Matrix Metalloproteinases in Colorectal Cancer," *Cancers,* vol. 6, no. 1, p. 366–375, 2014.

[51]   Zhao-Shi Zeng, Jose G. Guillem, et al., "Matrix Metalloproteinase-7 Expression in Colorectal Cancer Liver Metastases," *Clinical Cancer Research*, vol. 8, no. 1, pp. 144-148, 2002.

[52]   "ELISA PRINCIPLE," Boster, [Online]. Available: https://www.bosterbio.com. [Accessed 25 June 2020].

[53]   S. Zucker, C. L. Wu, et al., "Comparison of Techniques for Measurement of gelatinases/type IV Collagenases: Enzyme-Linked Immunoassays Versus Substrate Degradation Assays," *Clin Exp Metastasis,* vol. 12, no. 1, pp. 13-23, 1996.

[54]   Lennart Nilsson, Per Eriksson, ed al., "Increased Plasma Concentration of Matrix metalloproteinase-7 in Patients With Coronary Artery Disease," *Clin Chem,* vol. 52, no. 8, pp. 1522-1527, 2006.

[55]   Tahrin Mahmood, and Ping-Chang Yang, "Western Blot: Technique, Theory, and Trouble Shooting," *N Am J Med Sci,* vol. 4, no. 9, p. 429–434, 2012.

[56]   Patricia A. M. Snoek-van Beurden, and Johannes W. Von den Hoff, "Zymographic Techniques for the Analysis of Matrix Metalloproteinases and Their Inhibitors," *Biotechniques,* vol. 38, no. 1, pp. 73-83, 2005.

[57]   Jennifer Vandooren, Ghislain Opdenakker, et al., "Zymography methods for visualizing hydrolytic enzymes," *Nature Methods,* vol. 10, pp. 211-220, 2013.

[58]   Serena Ricci, Angelina Di Carlo, et al., "Substrate-zymography: a still worthwhile method for gelatinases analysis in biological samples," *Clinical Chemistry and Laboratory Medicine,* vol. 54, no. 8, p. 1281–1290, 2015.

[59]   S. A. Sieber, B. F. Cravatt, et al., "Proteomic profiling of metalloprotease activities with cocktails of active-site probes," *lo,* vol. 2, no. 5, pp. 274-281, 2006.

[60]   James J. Pitt, "Principles and Applications of Liquid Chromatography-Mass Spectrometry in Clinical Biochemistry," *Clin Biochem Rev.,* vol. 30, no. 1, pp. 19-34, 2009.

[61]   Ying Wang, Hulie A. Stenken, et al., "Detection of in Vivo Matrix Metalloproteinase Activity Using Microdialysis Sampling and Liquid Chromatography/Mass Spectrometry," *Anal. Chem.,* vol. 81, no. 24, pp. 9961-9971, 2009.

[62]   Junjie Hu, Huangxian Ju, et al., "Peptide Code-On-A-Microplate for Protease Activity Analysis via MALDI-TOF Mass Spectrometric Quantitation," *Anal Chem,* vol. 8, no. 87, pp. 4409-4414, 2015.

[63]   C. Bremer, C. H. Tung, et al., "Optical Imaging of Matrix metalloproteinase-2 Activity in Tumors: Feasibility Study in a Mouse Model," *Radiology,* vol. 221, no. 2, pp. 523-529, 2001.

[64]   Masatake Sano, Hiroshi Kamimori, et al.,"Assay of Collagenase Activity for Native Triple-Helical Collagen Using Capillary Gel Electrophoresis With Laser-Induced Fluorescence Detection," *J Chromatogr B Analyt Technol Biomed Life Sci,* vol. 809, no. 2, pp. 251-256, 2004.

[65]   Paul Yager, John Gerdes, et al., "Point-of-care Diagnostics for Global Health," *Annu Rev Biomed Eng,* vol. 10, pp. 107-144, 2008.

[66]   S. A. Butler, L. A. Cole, et al., "Detection of Early Pregnancy Forms of Human Chorionic Gonadotropin by Home Pregnancy Test Devices," *Clin Chem,* vol. 47, no. 12, pp. 2131-2136, 2011.

[67]   Brittany A. Rohrman, Rebecca R. Richards-Kortum, et al., "A Lateral Flow Assay for Quantitative Detection of Amplified HIV-1 RNA," *PLoS One,* vol. 7, no. 9, pp. 1-8, 2012.

[68]   Oliver Schnell, Jianping Weng, et al., "Impact of HbA1c Testing at Point of Care on Diabetes Management," *J Diabetes Sci Technol,* vol. 11, no. 3, pp. 611-617, 2017.

[69]   Luc Gervais, Emmanuel Delamarche, et al., "Microfluidic Chips for Point-of-Care Immunodiagnostics," *Advanced Materials,* vol. 24, no. H151-H176, p. 23, 2011.

[70]   Jie Hu, Feng Xu, et al., "Advances in Paper-Based Point-Of-Care Diagnostics," *Biosens Bioelectron,* vol. 54, pp. 585-597, 2014.

[71]   Dong Hwan Choi, Min-Gon Kim, et al., "A dual gold nanoparticle conjugate-based lateral flow assay (LFA)," *Biosensors and Bioelectronics,* vol. 25, pp. 199-2002, 2010.

[72]   Dorin Harpaz, Alfred I. Y. Tok, et al., "Point-of-Care-Testing in Acute Stroke Management: An Unmet Need Ripe for Technological Harvest," *Biosensors,* vol. 7, no. 3, p. 30, 2017.

[73]   Ellen Flávia Moreira Gabriel, Wendell K. T. Coltro, et al., "Enhanced Performance of Colorimetric Biosensing on Paper Microfluidic Platforms Through Chemical Modification and Incorporation of Nanoparticles," *Methods Mol Biol,* vol. 1571, pp. 327-341, 2017.

[74]   H. M. Pan, D. Trau, et al., "Conjugated Polymers for Biosensor Devices," *Comprehensive Biomaterials,* vol. 3, pp. 529-556, 2011.

[75]   H. Kraft, A. B. Holmes, et al., "Electroluminescent Conjugated Polymers - Seeing Polymers in a New Light," *Angewandte Chemie International,* vol. 37, no. 4, pp. 402-428, 1998.

[76]   S. Gunes, N. S. Sariciftci, et al., "Conjugated polymer-based organic solar cells," *Chem Rev,* vol. 107, no. 4, pp. 1324-1338, 2007.

[77]   Kang Won Lee, "Functionalized conjugated polymers for signal amplifying biosensors and sensor arrays," *Material Science,* 2008.

[78]   Hoang-Anh Ho, Mario Lederc, et al., "Colorimetric and Fluorometric Detection of Nucleic Acids Using Cationic Polythiophene Derivatives," *Angewandte Chemie International Edition,* vol. 41, no. 9, pp. 1618-1621, 2002.

[79]   Marie-Pier Plante, Mario Lederc, et al. "Polythiophene biosensor for rapid detection of microbial," *ACS applied materials & interfaces,* vol. 5, no. 11, pp. 4544-4548, 2013.

[80]   M. Béra Abérem, M. Lederc, et al., "Protein Detecting Arrays Based on Cationic," *Advanced materials,* vol. 18, no. 20, pp. 2703-2707, 2006.

[81]   Gaia Rocchitta, Pier Andrea Serra, et al., "Enzyme Biosensors for Biomedical Applications: Strategies for Safeguarding Analytical Performances in Biological Fluids," *Sensors,* vol. 16, no. 6, p. 780, 2016.

[82]   Nanami Suzuki, Koji Sode, et al., "Engineered Glucose Oxidase Capable of Quasi-Direct Electron Transfer after a Quick-and-Easy Modification with a Mediator," *Int. J. Mol. Sci.,* vol. 21, p. 1137, 2020.

[83]   Amin Fatoni, Mekar Dwi Anggraeni, et al., "Low-cost and real-time color detector developments for glucose biosensor," *Sensing and Bio-Sensing Research,* vol. 28, p. 100325, 2020.

[84]   Sujit Kumar Ghosh, and Tarasankar Pal, "Interparticle Coupling Effect on the Surface Plasmon Resonance of Gold Nanoparticles: From Theory to Applications," *Chem. Rev.,* vol. 107, no. 11, pp. 4797-4862, 2007.

[85]   J. Baker-Jarvis, W. A. Kissick, et al., "Improved technique for determining complex permittivity with the transmission/reflection method," *IEEE Transactions on Microwave Theory and Techniques,* vol. 38, no. 8, pp. 1096-1103, 1990.

[86]   Yijun Tang, Jennifer Liang, et al., "Surface Plasmon Resonance: An Introduction to a Surface Spectroscopy Technique," *J Chem Educ,* vol. 87, no. 7, pp. 742-746, 2010.

[87]   BioNavis, "Mathematics of Surface Plasmon Resonance," [Online]. Available: http://www.bionavis.com/en/material-science/technology/mathematics-spr/. [Accessed 15 July 2020].

[88]   U. Kreibig, and M. Vollmer, Optical Properties of Metal Clusters, Berlin: Springer, 1995.

[89]   Lance Kelly, George C. Schatz, et al., "The Optical Properties of Metal Nanoparticles: The Influence of Size, Shape, and Dielectric Environment," *J. Phys. Chem.,* vol. 107, no. 3, pp. 668-677, 2003.

[90]   J. C. Martínez, T. Cordova, et al., "Alternative Metodology for Gold Nanoparticles Diameter Characterization Using PCA Technique and UV-VIS Spectrophotometry," *Nanoscience and Nanotechnology 2012, 2(6): 184-189,* vol. 2, no. 6, pp. 184-189, 2012.

[91]   Robert Elghanian, Chad A. Mirkin, et al., "Selective Colorimetric Detection of Polynucleotides Based on the Distance-Dependent Optical Properties of Gold Nanoparticles," *Science,* vol. 277, no. 5329, pp. 1078-1081, 1997.

[92]   H. Li, and L. Rothberg, "Label-free colorimetric detection of specific sequences in genomic DNA amplified by the polymerase chain reaction," *Journal of the American CHemical Society,* vol. 126, pp. 10958-10961, 2004.

[93]   Sanghak Park, Nokyoung Park, et al., "Reversibly pH-responsive gold nanoparticles and their applications for photothermal cancer therapy," *Scientific Reports,* vol. 9, p. 20180, 2019.

[94]   Li Li, Lihui Mao, et al., "Visual detection of melamine in raw milk using gold nanoparticles," *Food Chemistry,* vol. 122, pp. 895-900, 2010.

[95]   Silly Fabien, Kantorovic Lev, et al., "Melamine structures on the Au(111) surface," *Journal of Physical Chemistry,* vol. 112, no. 30, pp. 11476-11480, 2008.

[96]   Xiaoyang Xu, Chad A. Mirkin, et al., "A Gold-Nanoparticle-Based Real-Time Colorimetric Screening Method for Endonuclease Activity and Inhibition," *Angewandte Chemie International Edition,* vol. 46, no. 19, 2007.

[97]   Z. Zhang, L. Chen, et al., "Fenton-like Reaction-Mediated Etching of Gold Nanorods for Visual Detection of Co2+," *Langmuir,* vol. 31, pp. 643-650, 2015.

[98]   R. de la Rica, and M. M. Stevens, "Plasmonic ELISA for the ultrasensitive detection of disease biomarkers with the naked eye," *Nat Nanotechnol.,* vol. 7, no. 12, pp. 821-824, 2012.

[99]   Y. Zhou, and Z. Ma, "Colorimetric detection of Hg2+ by Au nanoparticles formed by H2O2 reduction of HAuCl4 using Au nanoclusters as the catalyst," *Sens. Actuators B Chem,* vol. 241, pp. 1063-1068, 2017.

[100]   Y. Zhao, Z. Chen, et al., "Colorimetric detection of Hg2+ based on target-mediated growth of gold nanoparticles," *Sens. Actuators B Chem,* vol. 241, pp. 262-267, 2017.

[101]   Jinhao Gao, Bing Xu, et al., "Multifunctional Magnetic Nanoparticles: Design, Synthesis, and Biomedical Applications," *Acc. Chem. Res. 2009, 42, 8, 1097–1107,* vol. 42, no. 8, pp. 1097-1107, 2009.

[102]   Jin Xie, Shouheng Sun, et al., "Ultrasmall c(RGDyK)-Coated Fe3O4 Nanoparticles and Their Specific Targeting to Integrin αvβ3-Rich Tumor Cells," *J. Am. Chem. Soc.,* vol. 130, no. 24, p. 7542–7543, 2008.

[103]   Fengli Qu, Minghui Yang, et al., "Colorimetric platform for visual detection of cancer biomarker based on intrinsic peroxidase activity of graphene oxide," *Biosensors and Bioelectronics,* vol. 26, no. 9, pp. 3927-3931, 2011.

[104]   Keith J. Albert, and David R. Walt, "High-Speed Fluorescence Detection of Explosives-like Vapors," *Anal. Chem.,* vol. 72, no. 9, pp. 1947-1955, 2000.

[105]   Xiaoyan Wang, Lingxin Chen, et al., "Molecular Imprinting Based Hybrid Ratiometric Fluorescence Sensor for the Visual Determination of Bovine Hemoglobin," *ACS Sens.,* vol. 3, no. 2, pp. 378-385, 2018.

[106]   Bernhard Hochreiter, Johannes A. Schmid, et al., "Fluorescent Proteins as Genetically Encoded FRET Biosensors in Life Sciences," *Sensors,* vol. 15, no. 10, pp. 26281-26314, 2015.

[107]   Xiaojing Zhang, Yin Lu, et al., "Förster resonance energy transfer (FRET)-based biosensors for biological applications," *Biosensors and Bioelectronics,* vol. 138, p. 111314, 2019.

[108]   Niko Hildebrandt, Igor L. Medintz, et al., "Energy Transfer with Semiconductor Quantum Dot Bioconjugates: A Versatile Platform for Biosensing, Energy Harvesting, and Other Developing Applications," *Chem. Rev.,* vol. 117, no. 2, pp. 536-711, 2017.

[109]   R. C. Stringer, S. A. Grant, et al., "Quantum Dot-Based Biosensor for Detection of Human Cardiac Troponin I Using a Liquid-Core Waveguide," *IEEE Sensors Journal,* vol. 8, no. 3, pp. 295-300, 2008.

[110]   Jungmi Lee, Joon Myong Song, et al. "Peptide substrate-based inkjet printing high-throughput MMP-9 anticancer assay using fluorescence resonance energy transfer (FRET)," *Sensors and Actuators B: Chemical,* vol. 256, pp. 1093-1099, 2018.

[111]   I. W. Hamley, Introduction to peptide science, Hoboken: CPI group, 2020.

[112]   P. Katsoyannis, "Peptide synthesis and protein structure," *J. Polym. Sci. Polym. Chem.*, vol. 49, no. 151, pp. 51-74, 1961.

[113]   Ayub Karimzadeh, Miguel de la Guardia, et al., "Peptide based biosensors," *TrAC Trends in Analytical Chemistry*, vol. 107, pp. 1-20, 2018.

[114]   Q. Liu, B. J. Boyd, et al., "Peptide-based biosensors," *Talanta*, vol. 136, pp. 114-127, 2015.

[115]   J. M. Berg, J. L. Tymoczko, L. Stryer, Biochemistry, New York: W H Freeman, 2002.

[116]   Sarah E. Wood, Milan Mrksich, et al. "A Bottom-Up Proteomic Approach to Identify Substrate Specificity of Outer-Membrane Protease OmpT," *Angewandte Chemie*, vol. 56, no. 52, pp. 16417-16676, 2017.

[117]   S. Grahn, H. D. Jakubke, et al., "Design and Synthesis of Fluorogenic Trypsin Peptide Substrates Based on Resonance Energy Transfer," *Analytical Biochemistry*, vol. 265, no. 2, pp. 225-231, 1998.

[118]   James J. Schmidt, and Robert G. Stafford, "Fluorigenic Substrates for the Protease Activities of Botulinum Neurotoxins, Serotypes A, B, and F," *Applied and Environmental Microbiology*, vol. 69, no. 1, pp. 297-303, 2003.

[119]   Daniel Aili, Bo Liedberg, et al. "Assembly of Polypeptide-Functionalized Gold Nanoparticles through a Heteroassociation- and Folding-Dependent Bridging," *Nano Lett*, vol. 8, no. 8, pp. 2473-2478, 2008.

[120]   Peng Chen, Bo Liedberg, et al., "Peptide functionalized gold nanoparticles for colorimetric detection of matrilysin (MMP-7) activity," *Nanoscale*, vol. 5, p. 8973, 2013.

[121]   J. Kimling, A. Plech, et al., "Turkevich Method for Gold Nanoparticle Synthesis Revisited," *J. Phys. Chem. B*, vol. 110, no. 32, p. 15700–15707, 2006.

[122]   Peng Chen, Bo Liedberg, et al., "Nanoplasmonic Sensing from the Human Vision Perspective," *Analytical Chemistry,* vol. 90, no. 7, pp. 4916-4924, 2018.

[123]   Peng Chen, Hua Zhang, et al., "Assembly of Graphene Oxide and Au0.7Ag0.3 Alloy Nanoparticles on SiO2: A New Raman Substrate with Ultrahigh Signal-to-Background Ratio," *J. Phys. Chem. C,* vol. 115, no. 49, p. 24080–24084, 2011.

[124]   Julian Crespo, Katerina Soulantica, et al., "Synthesis and plasmonic properties of monodisperse Au–Ag alloy nanoparticles of different compositions from a single-source organometallic precursor," *J. Mater. Chem. C,* vol. 2, no. 16, pp. 2975-2984, 2014.

[125]   Li Sun, Yue Jin Shan, et al., "A composition and size controllable approach for Au-Ag alloy nanoparticles," *Nanoscale Res Lett.,* vol. 7, no. 1, p. 225, 2012.

[126]   Petr Slepicka, Vadav Svorcik, et al., "Methods of Gold and Silver Nanoparticles Preparation," *Materials,* vol. 13, no. 1, p. 1, 2020.

[127]   Xiaogang Xue, Zhang Lin, et al., "Crystal Growth by Oriented Attachment: Kinetic Models and Control Factors," *CrystEngComm,* vol. 16, no. 8, pp. 1419-1429, 2014.

[128]   Giridhar Madras, and Benjamin J. McCoy, "Temperature effects on the transition from nucleation and growth to Ostwald ripening," *Chemical Engineering Science,* vol. 59, no. 13, pp. 2753-2765, 2004.

[129]   M. Ferrari, Nanobiotechnology of Biomimetic Membranes, Springer Science & Business Media, 2007.

[130]   Cecilia Fernández-Ponce, Rocìo Litràn, et al., "Influence of size and surface capping on photoluminescence and cytotoxicity of gold nanoparticles," *Journal of Nanoparticle Research,* vol. 20, p. 305, 2018.

[131] Grażyna Ewa Będkowska, Slawomir Lawicki, et al., "Plasma levels of MMP-7 and TIMP-1 in laboratory diagnostics and differentiation of selected histological types of epithelial ovarian cancers," *J Ovarian Res. 2017; 10: 39.*, vol. 10, p. 39, 2017.

[132] Rajesh Babu Sekar, and Ammasi Periasamy, "Fluorescence resonance energy transfer (FRET) microscopy imaging of live cell protein localizations," *J Cell Biol,* vol. 160, no. 5, pp. 629-633, 2003.

[133] Masataka Yoshino, and Keiko Murakami, "Analysis of the substrate inhibition of complete and partial types," *SpringerPlus,* vol. 4, p. 292, 2015.

[134] Judith M. Neugebauer, "Detergents: An overview," *Methods in Enzymology,* vol. 182, pp. 239-253, 1990.

[135] L. Mocé-Llivina, M. Muniesa, et al., "Comparison of polyvinylidene fluoride and polyether sulfone membranes in filtering viral suspensions," *Journal of Virological Methods,* vol. 109, no. 1, pp. 99-101, 2003.

[136] J. Lakowicz, Principles of Fluorescence Spectroscopy, 2nd Ed., New York, London, Moscow, Dordrecht: Kluwer Academic/Plenum, 1999.

[137] R. Farinotti, G. Mahuzier, et al. "4-Bromomethyl-6,7-dimethoxycoumarin as a fluorescent label for carboxylic acids in chromatographic detection," *J. Chromatography,* vol. 269, pp. 81-90, 1983.

[138] Garima Goyal, Bo Liedberg, et al. "Protease functional assay on membrane," *Sensors and Actuators B: Chemical,* vol. 305, p. 127442, 2020.

[139] M. Vočka, L. Petruzelka, et al., "Serum levels of TIMP-1 and MMP-7 as potential biomarkers in patients with metastatic colorectal cancer," *The International Journal of Biological Markers,* vol. 34, no. 3, pp. 292-301, 2019.

[140]   Vladimir Y. Torbeev, Stephen B. H. Kenta, et al., "Protein conformational dynamics in the mechanism of HIV-1 protease catalysis," *Proc Natl Acad Sci U S A*, vol. 108, no. 52, pp. 20982-20987, 2011.

[141]   I. Segel, Encyclopedia of Biological Chemistry (Second Edition), 2013.